Determination of optimal separation well distance for Single Borehole ATES systems in the Netherlands, implementing an axisymmetric numerical model

Delft University of Technology, faculty of Civil Engineering and Geoscience

Maria Xynogalou, MSc candidate

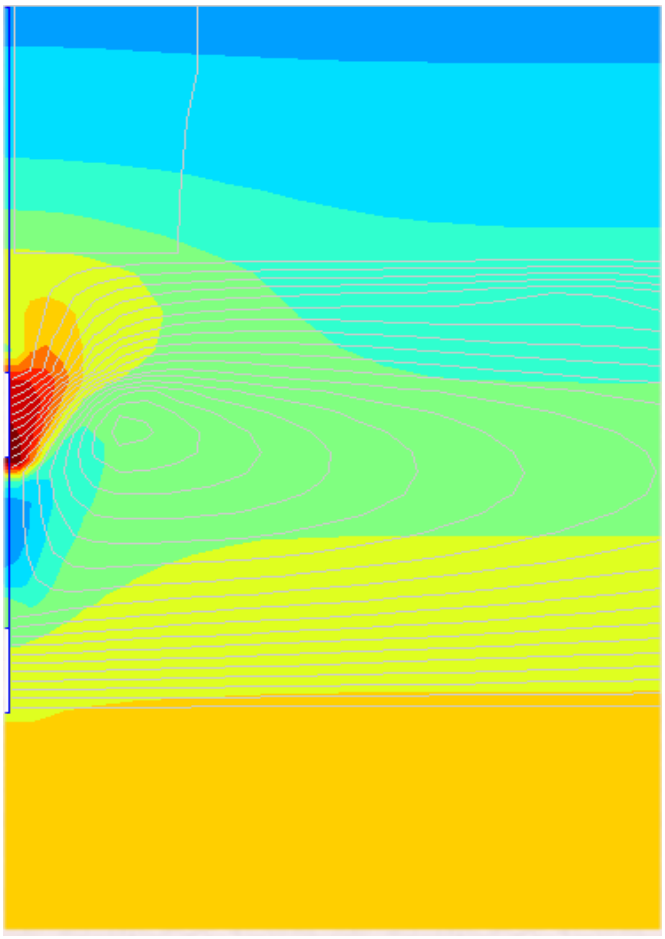

September, 2015

COLOPHON

Thesis title:	Determination of optimal well distance for Single borehole ATES systems in the Netherlands, implementing an axisymmetric numerical model
Date:	30/09/2015
Author:	Maria Xynogalou
	mxynogalou@gmail.com
Student number:	4179374
University:	Delft University of Technology (TU Delft)
Faculty:	Civil Engineering and Geosciences
Specialization:	Geohydrology
Graduation committee:	Prof. dr. ir. T.N. Olsthoorn (TU Delft)
	Ir. J.M. Bloemendal (TU Delft)
	M. Afanasyev, Msc (TU Delft)
	Dr. Ir. Mark Bakker (TU Delft)
	Ing. Wil van den Heuvel (Installect)

Installect Baak
Rozenstraat 11
7223 KA Baak
The Netherlands
Tel: +31 (0) 57 54 41 187
http://www.installect.nl/

Delft University of Technology
Faculty of Civil Engineering and Geosciences
Stevinweg 1
2628 CN Delft
The Netherlands
Tel: +31 (0) 15 27 85 440
www.tudelft.nl

Cover Figure: The figure on the front page shows a vertical cross-section through an axi-symmetrical model simulating an SB-ATES system with salinity induced density difference, which involves that common circular streamlines. The columns indicate temperatures. Notice that SB-ATES systems with density flows were not analyzed in this thesis.

ACKNOWLEDGMENTS

This report details research carried out as the final requirement for completion of the Master Program in Water Management, a program of Delft University of Technology. The research focused on the determination of the optimal well screen distance for the single borehole aquifer thermal energy storage (ATES) systems with the implementation of an axiasymmetric numerical model that was developed in MATLAB environment.

Completion of this thesis was only made possible with the help of many people who shared their experience, knowledge and encouragement. Firstly, I would like to thank Prof. Dr. Ir. Theo N. Olsthoorn for helping me with the numerical model. Secondly, I would like to thank my supervisor Ir. Martin J. Bloemendal for involving me with the project and sharing his knowledge throughout this study. I sincerely appreciate the evaluation made by Ir. Michael Afanasyev and Ing. Wil van den Heuvel from Installect Company, who graciously provided the required field data used in this work. Finally, I would like to thank Dr. Ir. Mark Bakker for participating in the committee of my MSc Thesis.

Finally, I would like to thank my family, my closest friends, Vangelis and Ioanna who provided exceptional encouragement and personal support to pursue this degree throughout this difficult period.

Maria Xynogalou

ABSTRACT

Aquifer thermal energy storage (ATES) is a growing technology in the Netherlands. There are two kinds of ATES configurations the doublet and the single borehole ATES (SB-ATES) layout. The limited subsurface space in combination with the lower construction cost and the lower performance of the SB-ATES lead to the need to optimize their design. This master thesis focuses on gaining a better insight in the processes that occur around this configuration. Specifically, how anisotropy influences the efficiency of the design and what the optimal distance between filter screens is, in order to limit the interference between the screens, as it has a negative impact on system performance. To meet these two objectives, an axisymmetric numerical model was developed in a MATLAB environment, using MODFLOW and MT3DMS or SEAWAT groundwater flow and transport simulators.

The simulation of heat advection was conducted applying the finite different method (FD method), it was the only method compatible with axial symmetric models that produced consistent results. As the FD method is subjected to numerical dispersion, three different grid resolutions were tested that were the 0.25, 0.50 and 1.00 m, respectively. The finest grid was decided to be used in the elaboration, as it gave the most accurate results compared to larger thickness width grid cells.

Capacity test and borehole profile data were used to calibrate the overall vertical anisotropy of the case-studies. The capacity test allowed the calibration of one hydraulic parameter, for which the overall vertical anisotropy was chosen. The Kozeny-Carmen equation was used to calculate the hydraulic conductivity of each soil layer. This overall vertical anisotropy even though was estimated roughly, can be used to determine the presence of overlooked clay layers during the drilling of the borehole (anisotropy <<2) or whether high permeable layers are between the screens (anisotropy >>10).

A sensitivity analysis was applied to estimate the optimum distance between the filter screens. Three different types of SB-ATES, called GT15xx, GT20xx and GT25xx, were examined separately. The numbers indicate the installed pump capacity in m^3/h while their mean and representative screen lengths are 5, 7 and 10m respectively. For the sensitivity analysis, three discharge fractions, Qfrac, were tested with values 0,25, 0.50 and 1.00 and three anisotropy values of 2, 5 and 10, these values are representative for sandy soils. The simulation time was 5 years, which was sufficient to the recommended efficiencies. The results showed that the maximum efficiency is practical independent of system type. The optimum separation distance for an anisotropy of 2 is respectively, 25, 30 and 35 m for Qfrac 0.25, 0.50 and 1.00.

The evaluation of the sensitivity analysis was conducted, using real-scale case-studies and taking into account the distribution of conductivities along the layers. The available 18 case-studies were

examined in terms of efficiency; it was found that a thin resistance layer between the screens, like a clay or peat layer, influences positively the performance of SB-ATES systems. On the other hands, when there is a high conductive zone between the screens, the efficiency drops.

Finally, it was found that temperature induced differences in density and viscosity have a negligible effect on SB-ATES systems, at least with injection temperature differences between warm and cold wells up to 12^0C.

CONTENTS

NOMENCLATURE

Symbol	Units	Description
K	$[m^3/d]$	Hydraulic conductivity
K_x	$[m^3/d]$	Horizontal hydraulic conductivity
K_z	$[m^3/d]$	Vertical hydraulic conductivity
K_{xe}	$[m^3/d]$	Average horizontal hydraulic conductivity
K_{ze}	$[m^3/d]$	Average vertical hydraulic conductivity
μ	[kg/(m s)]	Dynamic viscosity
κ	m^2	Intrinsic permeability
ρ_w	$[kg/m^3]$	Water density
g	$[m/s^2]$	Gravitation acceleration
Q	[m/d]	Specific discharge
Q_{inj}	[m/d]	Injection discharge
Q_{ext}	[m/d]	Extraction discharge
S_b	$[m^{-1}]$	Specific storativity
b	[m]	Thickness of the aquifer
d_i	[m]	Thickness of the soil layers
S	[-]	Storativity
q_x	$[W/m^2]$	Heat flux
k	[W/(mK)]	Thermal conductivity
n	[-]	Porosity
T	$[^0C]$	temerature
ΔT	$[^0C]$	Temperature difference between warm and cold well
r_w	[m]	Well radius
A	$[m^2]$	Well surface
h	[m]	Water head
P	[W]	Required capacity
c_p	[kJ/(kg ^{0}C]	Heat capacity of water
L	[m]	Filter screen length
H	[m]	Filter screens distance

CHAPTER 1

1. Introduction to Aquifer Thermal Energy Storage Systems

Aquifer thermal energy storage (ATES) is an open-loop geothermal technology, aiming at seasonal storage of thermal energy in the form of cold and/or warm water in an aquifer. ATES technology is interesting, as it offers a cost-effective sustainable way to save energy through seasonal storage, can limit the consumption of fossil fuels and reduce CO_2 emissions. For these reasons, ATES application is rapidly growing in the Netherlands. At the moment, more than 1000 ATES systems operate and it is predicted that by the end of 2020 the number of active systems will have increased by 200% [3]. Since the technology is still relative new, there is a need to optimize their subsurface configuration. Different configurations of ATES are applied worldwide that can be divided into multiple and single borehole systems [3].

This master thesis deals with the optimization of Single Borehole ATES (SB-ATES) systems. It focuses on the minimization of thermal energy losses due to vertical circuit flows between the filter screens that are placed above each other in a single borehole within the same aquifer. The thesis is conducted by Delft University of Technology in partnership with Installect Advies b.v, which is specialized in supplying SB-ATES systems in the Netherlands (http://www.installect.nl/).

This first chapter introduces the content of this study and includes a brief overview of the design of ATES and their operation.

1.1. OVERVIEW OF ATES SYSTEMS

Single borehole aquifer thermal energy storage (SB-ATES) is a growing technology. It is based on seasonal storage of thermal energy in an aquifer using two screens installed above each other in the same borehole and within the same aquifer [25]. This technology has been applied in the Netherlands for about 20 years [3]. The technology is being officially fostered as a means to reduce carbon dioxide emissions by replacing conventional ways of heating and cooling based on fossil fuels [5]. The different types of thermal energy storage systems exist, which can be divided into two main categories, namely open and closed-loop systems, according to their distinct well or well-screen configurations; the most commonly used layouts are illustrated in Fig. 1. 1. This thesis deals specifically with open systems that have their warm and cold screen installed within a single borehole and inside the same aquifer.

Open systems, contrary to closed ones, pump water from an aquifer between their so-called “warm” and “cold” screen. Closed systems do not exchange water with the aquifer, and are further ignored in this thesis.

There are two main open ATES techniques, unidirectional and bidirectional, depending on the flow. Unidirectional systems abstract and discharge the groundwater in one direction and are used for either heating or cooling but not both; the water is pumped always in the same direction. Bidirectional systems on the contrary, pump groundwater in both directions; the flow is reversed every season; these bidirectional systems provide the ability for heating in winter and cooling in summer using the thermal energy stored in the previous season [5]. ATES systems are bidirectional systems.

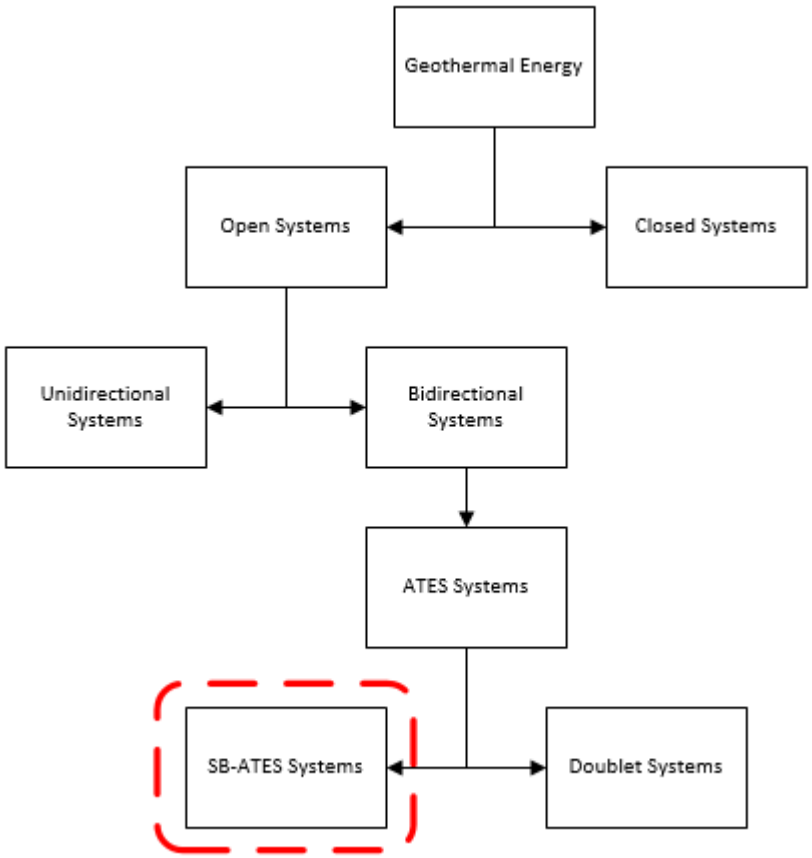

Fig. 1. 1: Schematization of thermal energy storage systems

ATES systems can have different well or screen configurations. The most common one is a so-called doublet system. This kind of layout uses at least two different wells, one for injection and one for pumping. These wells are installed at a sufficient distance from each other to prevent

thermal interaction, which would reduce their thermal efficiency. The two wells are conveniently called “cold” and “warm” well, depending on the water temperature they inject and extract with respect to that of the natural groundwater. During summer, cold water is extracted from the “cold”

well for cooling purposes, while heated water is injected into the “warm” well for storage until the next winter. During winter, the flow is reversed. Then stored heated water is extracted from the warm well and cold water is injected in the cold well for storage till the next summer.

Another configuration is characterized by placing the two screens above each other in the same borehole, using vertical instead of horizontal separation to prevent interaction. These systems are called SB-ATES systems and are the topic of this thesis. In a SB-ATES system [3] the deep filter screen generally operates as the “cold” well in the doublet system while the shallow filter screen operates as the “warm” one to prevent interaction due to density differences between the warm and the cold water.

1.2. CURRENT TECHNOLOGY OVERVIEW OF ATES SYSTEMS

Fig. 1. 2 illustrates an SB-ATES system, where the red and blue areas schematically illustrate the areas of influence of the “warm” and “cold” water respectively [2].

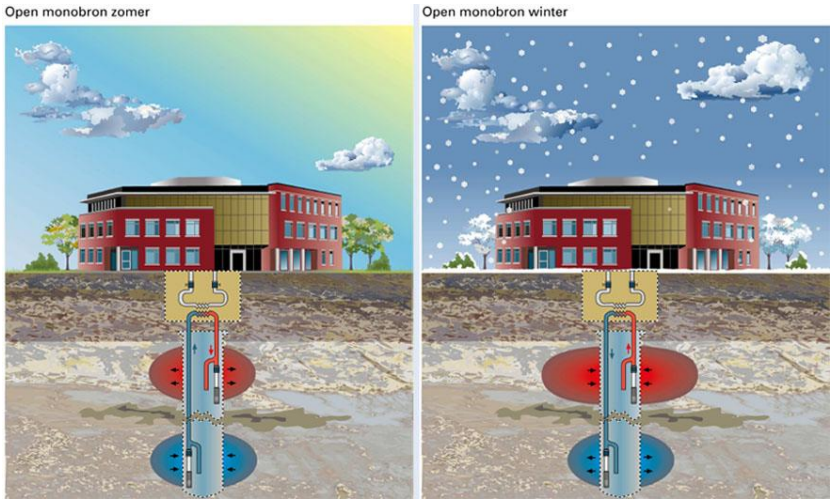

Fig. 1. 2: SB-ATES system configuration

An SB-ATES should provide cold water in summer and warm water during winter. The somewhat less dense warm water is stored above the cold water to prevent mixing. A most important problem with such a configuration is the risk of short-circuit flows between cold and warm screen. This risk is reduced by maintaining a certain minimum vertical separation between the two screens in the borehole. This separation is especially required when there is no aquitard or any other hydraulically resistant layer between the two filter screens to actively prevent short-circuit flows. Generally this is the case, as the permitting provincial authorities require the two screens to

be within the same aquifer to prevent hydraulic effects of the injection and extraction in the wider surroundings of an ATES system.

In a SB-ATES system such as the one illustrated in Fig. 1. 3, the water from one screen flows through a heat exchanger in the attached building and then back into the other screen. The flow direction is reversed every season. A heat pump is generally required to further raise the temperature off the heat exchanger to values required for heating the connected building and also lowering the return temperature to be injected into the cold screen [17] so that the water from that screen can be used to cool the building during the next summer.

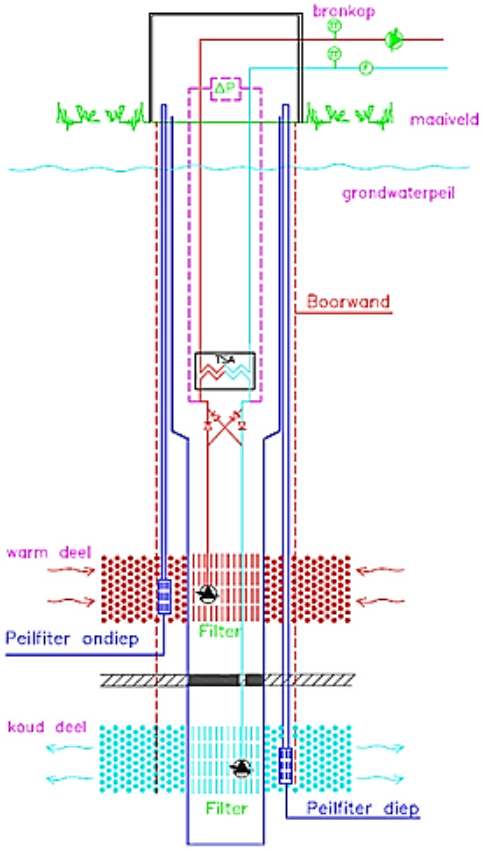

Fig. 1. 3: Vertical cross section of a BS-ATES

1.3. THE REQURIED SCREEN DISTANCE OF ATES SYSTEMS

The Dutch guidelines for ATES-system designs [35] require a minimum distance between the screens of a doublet of three times the so-called thermal radius. These guidelines do not provide rules for SB-ATES systems. Thermal radius refers to that of the maximum extent of the bubble of the warm and or cold water stored around the filter screens. Basically, it is the radius of thermal influence and computed by equation 4. 5. However, the SB-ATES systems considered in this thesis have vertically spaced filter screens, for which no guidelines exist, and for which the

thermal radius defined by the NEOV does not apply. Nevertheless, a sufficient vertical separation is required to minimize short-circuit flows between the warm and cold screen. The determination of this required separation is the subject of this thesis.

1.4. FACTORS THAT INFLUENCE THE PERFORMANCE OF SB-ATES SYSTEMS

In this section, the most important factors or parameters that influence the thermal performance of SB-ATES systems are presented. These factors are separated into three groups. The first group relates to the geology and hydrology of the site. The second group comprise the factors that relate to the design of the SB-ATES system. The last group are operational factors that influence the system.

Table 1. 1 presents the most important parameters that influence the thermal performance of ATES systems. Some of them are evaluated in this thesis in terms of their impact on the system's thermal efficiency. Aquifer parameters characterize site characteristics, design parameters characterize system layout, while operational parameters influence the performance through the way the system is operated.

Table 1. 1: Factors that influence the performance of ATES systems [19, 31]

Aquifer parameters	Design parameters	Operational parameters
• Aquifer-aquitard configuration of the subsurface • The distribution of the horizontal hydraulic conductivity of the sub layers of the aquifer in which the screens are installed • Vertical anisotropy of these layers, i.e. the ration of the horizontal over the vertical hydraulic conductivities of these layers • Depth of the aquifers • Thickness of the aquifers and aquitards • Thermal properties of the layers • Porosity of the layers • Water density • Water viscosity • Clogging properties of the groundwater, formation of well skin	• Pump capacity • Position of the screens • Distance between the filter screens • Screen length • Well skin	• Operational capacity (season-average flow rate) • Operation schedule • Injected temperatures and whether varying or not

The parameters that characterize the subsurface play an important role in the design of the location of an ATES system, its depth, potential capacity, screen length and screen position. The screen depth depends on the depth of the present aquifers and aquitards and any other layers with vertical hydraulic resistance.

The aquifer aquitard configuration of the subsurface is important to the extent that sufficient aquifer thickness is necessary to install the two screens above each other and include the required separation. But it is also important to have a sufficiently thick cover layer on top of the aquifer to prevent too much thermal exchange with the atmosphere and possible infrastructures like cellars and subsurface parking lots. Given the reach of thermal conduction over one years of about 20 m, 20-25 m would be considered as a minimum screen depth.

The average horizontal hydraulic conductivity of the aquifer with the screens has no influence on the flow, which is completely determined by the equal injection and extraction of the screens; only the distribution of the horizontal conductivities of the sublayers within the aquifer matters. We will test the effects in chapter 7. The vertical anisotropy of the aquifer and of the sublayers within the aquifer matters as this determines the shape and extent of the stored warm and cold bubbles. An overall anisotropiy value is calibrated using the data obtained from the capacity test that is carried out on both screens after their installation.

The storativity is not important for ATES systems because both screens always operate at the same but opposite rates, which virtually eliminates any non-stationary and areal hydraulic effects as long as the screens are in the same aquifer, as is required by the permitting authorities.

Porosity is definitely important together with the thermal properties of the aquifer, but for the Dutch situation in which ATES systems are always applied in clastic unconsolidated fluviatile sediments, these properties vary little, so that without further information they are considered constant with a porosity of 0.35 [-] as representative for all layers.

Thermal properties of the subsurface are important, which are the thermal conductivity of the aquifer and its heat capacity. Both parameters are determined by both the thermal properties of the grains and that of the water and, therefore, are also dependent on porosity. In this thesis, these properties are considered constant and the same for all subsurface layers, as is the case for porosity.

The water density depends both temperature and the presence of dissolved salts. The model that we use in this thesis (SEAWAT) can take the viscosity into account as it varies with water temperature and the density as it varies with temperature and dissolved solutes but we ignored it in the analysis of the required screen separation (in Chapter 7, examination of their impact on the SB-ATES systems can be found). Density variations due to differences of groundwater salinities

are ignored in this MSc report altogether. Chapter 3 includes a more detailed examination of these parameters.

Essential design parameters are the location of the screens with respect to the top and the bottom of the aquifer, screen length, and the separation distance between them.

The most important operational parameter is the season-average injection and abstraction rate, as they determine the maximum extent of the warm and cold bubble, and, therefore, the risk of their mutual interaction and short-circuit flows. Bubbles that become too large in the subsurface will cause the thermal efficiencies to attain negative values because then the cold screen will extract warm water from the large warm bubble and the warm screen will extract cold water from the large cold bubble. Therefore, there is always a minimum separation between the screens in relation to the total volume injected during a season to be attained in order to guarantee satisfactory thermal efficiencies. For doublet systems, their thermal radius characterizes this separation. A similar characterization may be setup for SB-systems.

The operating schedule or operating regime, that is, the variation during the seasons, between the seasons and between successive years will also influence the performance of the system at least to some extent. Some of this influence is due to processes that continue and operate separate from the actual operation like the impact of density flows, viscosity and, especially, ambient groundwater flow. These factors have a large effect the longer the available time irrespective of the actual operation. In this thesis ambient flow is ignored as it is believed not to impact the required screen separation at least much. The same is true for the actual regime during the seasons.

The injected and extracted temperatures themselves have no impact on the thermal performance other than through their effect on viscosity and density, which will be verified with an example in chapter 7.

1.5. THERMAL LOSSES

Thermal energy losses reduce the energy performance of SB-ATES systems. These losses can be divided into, heat losses due to advective heat transport (convection), to heat conduction and due to mutual interference between the screens, i.e. by short-circuit flows.

Heat Convection. Convective heat causes losses into zones with groundwater flowing at lower velocities and with different temperatures. This includes conduction into zones within the aquifer with lower permeabilities as well as in overlying and underlying aquitards. This heat flown into adjacent zones by conduction can only be recovered to a very limited extent when the stored water is extracted in the next season. These processes result from an increase in entropy over time. Hydraulic dispersion adds a little to this conduction and diffusion is negligible to the effects

of conduction. Convective heat losses are also due to ambient groundwater flow as part of the water and its heat advected downstream can be recovered upon subsequent extraction. Some convection may occur due to temperature caused density differences between the warm and the cold bubbles. But this effect is negligible for the small temperature differences of up to about 14 degrees applied in ATES systems. The effect can be computed using SEAWAT (chapter 7).

Interference. One type of interference is the contact zone between the warm and the cold bubble. Conduction in this zone leads to canceling out the temperature rise of the warm bubble with the temperature fall in the cold bubble leading to a net loss of heat and cold and, therefore, reduces the overall thermal efficiency. This is what is meant by mutual interaction or interference. If the injected volumes are so large compared to the separation between the screens, then warm water may even enter the cold screen and vice versa. This is what short-circuiting means and which must be prevented. However, due to the heat capacity of the grains, the extent of the bubble is smaller than the actual space that the injected water occupies in the pores. Therefore, the exchange of heat between water and grains reduces the thermal volume by a factor called the retardation, which is generally about 2 in the Dutch circumstances.

As it was mentioned above, the criterion to judge the performance of the ATES systems is the overall thermal efficiency computed over two successive seasons for the warm and the cold screen separately.

1.6. THESIS OUTLINE

Fig. 1. 4 illustrates a flow chart of the thesis outline.

- An introduction of ATES systems (Chapter 1)
- The thesis objectives and the general approach followed (Chapter 2).
- The theoretical background (Chapter 3)
- The presentation of the study cases and the assessment tools that were used (Chapter 4)
- The results from the calibration of hydrological parameters, applying Kozeny- Carmen equation in combination with a numerical model (Chapter 5)
- The results from the Flow and Transport Model which was developed and the optimization of the SB-ATES systems (Chapter 6)
- The model evaluation (Chapter 7)
- The conclusions and recommendations (Chapter 8)

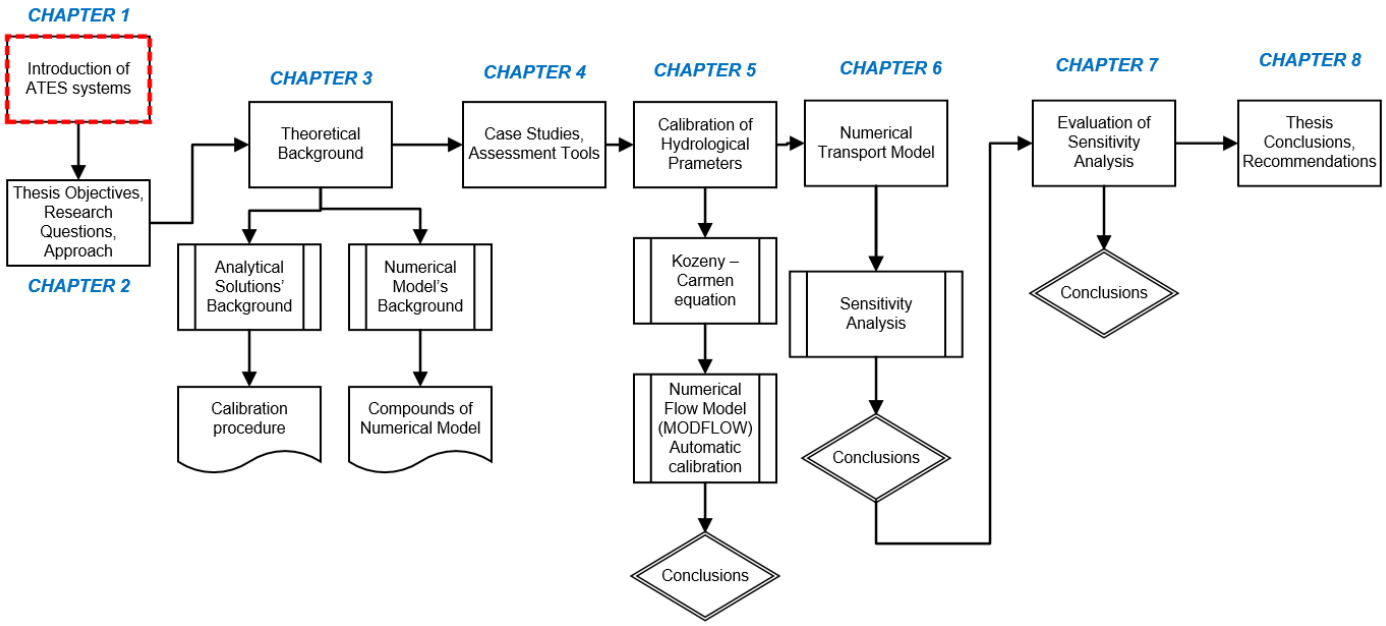

Fig. 1. 4: Thesis Outline

1.7. SUMMARY

Different configurations of ATES are discussed focusing on the SB-ATES design. The factors that influence their performance are identified and categorized, as aquifer design and operational parameters. Furthermore, the possible physical processes are mentioned that can impact system performance. This work seeks criteria to minimize the interference of the screens of SB-ATES systems by optimizing their vertical separation. Finally, the outline of this thesis is presented.

CHAPTER 2

2. Statement of the Problem

The thermal performance of an SB-ATES system is generally lower than that of a doublet based ATES system [3]. This is due to vertical interference and possibly short-circuit flows caused by the generally small separation between the screens that are installed above each another in the same borehole. Drilling cost and risk of reduced efficiency requires optimization of screen lengths, their placement and their vertical separation. The design procedure takes into account the subsurface and aquifer properties. Currently, experience is the most important factor.

The purpose of this thesis is to come up with design rules to minimize energy losses by short-circuit flows and interference in SB-ATES systems. The two main objectives are:

- To gain insight in the flows around the well screens in SB-ATES systems
- To design optimal screen position and separation given an actual aquifer and measurements obtained from drilling the borehole and practical well-capacity tests

2.1. RESEARCH QUESTIONS

To approach the objectives, two research questions and three sub-questions are posed next, which are answered in the subsequence chapters.

1. *Which factors affect the performance of an SB-ATES configuration and in what way?*

The examined parameters are listed below

1. Anisotropy
2. Pumping rate and screen average operational pumping rate
3. Screen lengths and screen position
4. Screen separation

The effects that these factors have on the performance of the SB-ATES system are assessed through modeling.

Vertical anisotropy and the season-average flow (total injected volume) are the predominant parameters influencing the performance of an SB-ATES system. The pumping rate was selected for assessment, as it strongly determines interference and the risk of short-circuit flows between the screens.

a. *How does vertical anisotropy influence the performance of an SB-ATES system and affect short-circuit flows between the screens? Are the currently applied screen separations adequate?*

Vertical conductivity is currently essentially based on rule-of-thumb methodology [2, 19, 22]. Different ratios of horizontal hydraulic conductivity and vertical hydraulic conductivity are considered and examined for their influence on the efficiency of an SB-ATES system (chapters 6 and 7).

The *1a sub-question* aims at deriving an optimal way to calculate the relevant soil parameters necessary for the design.

b. *How does horizontal and vertical conductivity between the screens affect the performance of an SB-ATES system?*

In SB-ATES systems, there is generally no aquitard between the two screens. Regulations currently demand the two screens to be within the same aquifer. Therefore, resistant layers are generally not present between the screens of an SB-ATES system. Nevertheless the performance of SB-ATES systems will benefit from strong vertical anisotropy of the aquifer material and even from thin layers between the two vertically spaced screens.

c. *How does soil heterogeneity affect the efficiency of an SB-ATES system?*

The soil heterogeneity may be considered random in space or more as aquifers consisting of many sublayers with different conductivities. The latter is certainly a dominant, ubiquitous, geological or sedimentary phenomenon that has to be considered in the analysis. This is done in chapter 6 and especially in chapter 7.

Spatial inhomogeneities are ignored, because inhomogeneities are less dominant than the sublayers, the impact of random inhomogeneities may be simulated, at least to some extent, by hydraulic dispersion and because all models that are implemented in this elaboration, are axisymmetric flow and transport models. Such models cannot handle spatially random conductivities, but conductivity may be varied between horizontal layers.

2. *What is the optimal vertical distance between the screens with respect to the performance of an SB-ATES configuration?*

Several distances between the filter screens are examined in the sensitivity analysis in chapter 6 and then tested with actual cases in chapter 7 to allow deriving at an optimal vertical screen separation.

2.2. APPROACH

The behavior and thermal efficiency of an SB-ATES system at the time of design is analyzed as a function of subsurface property values using an axisymmetric flow and transport model based on MODFLOW, MT3DMS and SEAWAT. This model makes it possible to gain the required insights in what extend, the thermal efficiency of SB-ATES systems is affected on the short and the long run.

The model was managed in mfLab, a MATLAB environment that controls MODFLOW, MT3DMS and SEAWAT codes for flow and transport modeling. Initially, hydraulic conductivity of the layers, which was encountered during drilling of the borehole, was estimated by applying the Kozeny-Carmen equation on the grain sizes determined or estimated from the soil samples (Chapter 3). An overall vertical anisotropy was optimized afterwards in a calibration phase (chapter 5). A mean vertical anisotropy was thus found for each actual case together with the horizontal conductivity.

Chapter 5 includes the results of this elaboration.

Paragraph 2.1 gives the factors that were assessed in the sensitivity analysis done in Chapter 6 They are: system capacity/type, season-average flow (i.e. pump capacity times factor Qfrac), overall anisotropy, and screen separation. The factors were examined using a homogeneous aquifer while non-homogeneous aquifers were tested in chapter 7 using the layer distribution of all 18 available actual cases. The computed thermal efficiency after 5 years of operation was used for the assessment. Simulation times for up to 30 years have been simulated, but 5 years was enough to reach the final efficiency, so that all simulations in chapters 6 and 7 were broken off after 5 years, taking the last computed efficiency as the overall performance criterion in all evaluations.

Thermal efficiency was deemed generally acceptable if it has a value of at least 70%, but 65% may be a better criterion for smaller systems for which 70% may be hard to achieve. Chapter 7 illustrates the computed thermal performance for the actual systems/cases for 3 values of anisotropy (2, 5 and 10) and for 3 values of the factor Qfrac (0.25, 0.50 and 1.00) that relates the season-average flow to that of the installed pump of the different standard systems (GT15xx GT20xx and GT25xx, where the number refers to the installed pump capacity in m3/h). More information, regarding the configurations, can be found in chapter 4.

Chapter 8 given the conclusions of this work and recommendations for future research.

Geometry of the case-studies:

All case-studies consider vertically downward of at least a cover layer, an aquifer with the screens and a confining layer. The cover layers is confining and at least about 24 m thick as the permitting authorities do not allow ATES systems in unconfined aquifers for several reasons, technical, social-economic and ecological.

The depth of the aquifer and the underlying confining layer is mostly not obtainable from the borehole that terminates at some preset depth. Of course, one could obtain an estimate of the actual depths using the national geological database REGIS at TNO, but this was not done in this Thesis. When the depth of the aquifer was unknown, we assumed another 10 to 25 m of aquifer material below the screen until the underlying confining layer. The conductivity of this lower aquifer zone was taken equal to that of the lowest aquifer layer reached by the borehole.

In the analysis, the top screen is placed immediately below the cover layer and the bottom screen at the required or designed separation below it. This was done for all cases as it is generally observed to be the case when comparing actual screen positions with the top of the aquifer.

To set an aquifer depth we chose a fixed value for the sensitivity analysis in chapter 6 that is equal to maximum depth from the set of available actual cases, which was 70 m. For the test with the actual cases in chapter 7, we set the bottom of the aquifer at 25 m below the bottom of the lower screen, as the lower screen is generally not at the bottom of the aquifer.

The thermal efficiency of the upper screen with its top against the bottom of the cover layer and the lower screen with its bottom above the top of the underlying confining layer will be different as the lower bubble of cold water has more space in the aquifer than the upper bubble of warm water. Therefore, both the efficiencies of the lower and the upper screen are always presented. As the simulations show, this difference is generally very small.

Assessment of the parameters:

- *Vertical anisotropy*

There exist several rules of thumb to estimate anisotropy of aquifers. Commonly the vertical anisotropy of aquifers is simply assumed to be between 2 and 10. The lowest value of 2 is suitable as the overall vertical conductivity of a pack of isotropic horizontal layers with different conductivities is always smaller than the average horizontal conductivity. This is due to vertical flow passing the pack in series while horizontal flow does so in parallel. All the case-studies consist on sandy soils, thus the vertical anisotropy is expected to be between 2 and 10. Values 2, 5 and 10 were used in the sensitivity analysis in chapter 6, while actual values were attempted to be determined by calibration using the data from the capacity test that is always done on newly installed system (chapter 5).

- *Pumping rate*

The extent of the actual bubbles of warm and cold water, i.e. the season-averaged pumping rate, highly influences the efficiency of the ATES systems, especially when their screen separation is

small. The actual cases made available by Installect and used in this study, belong to three standard types that are indicated by their name that starts with GT and a number that refers to the capacity of the installed pump in m3/h (GT15xx, GT20xx and GT25xx). It was clear from the analysis of the actual cases that running such systems on their nominal capacity during a whole season often leads to large interference and short circuiting between the screens. Therefore, a factor Qfrac was introduced that relates the actual season capacity to the nominal pump capacity. This factor must be lower than one. We evaluated the systems for Qfrac, which is 0.25, 0.50 and 1.00, in chapters 6 and 7.

- *Screen lengths*

The screen lengths of the actual cases differ, but are similar for each of the three system types GT15xx, GT20xx and GT25xx. The average screen length for each type, which was 5, 7 and 10 m respectively, were fixed for each type in the sensitivity analysis of chapter 6. The tests with the actual cases in chapter 7 used the actual screen lengths pertaining to each individual case.

- *Screen separation*

To assess the screen separation the largest value was first obtained form the actual cases, which was less than 5 times the system-specific screen length of 5, 7 and 10 m for the systems GT15xx, GT20xx and GT25xx respectively. To cover this range in the sensitivity analysis in chapter 6, we used 5 separations equal to 1, 2, 3, 4, and 5 times the screen length of each system type. That is 5, 10, 15, 20 and 25 m for the GT15xx, 7, 14, 21, 28 and 35 m for the GT20xx and 10, 20, 30, 40 and 50 m for the GT25xx.

CHAPTER 3

3. Theoretical Background

This chapter presents the theoretical background of the physical processes relevant for SB-ATES systems and provides the theory of an axially symmetric numerical model and the numerical tools that were used in this work.

The used analytical solutions that were used for the calibration of the case studies are also included.

The physical processes associated with SB-ATES systems are the flow in porous media, heat transport by advection, diffusion and dispersion, conduction and convection.

3.1. NUMERICAL MODELS USED

The two major classes of numerical methods to solve the groundwater flow and transport equations are the finite-difference and finite element methods. The difference between these two methods is that the former approximates the first derivatives in the partial differential equation while the latter integrates the partial differential equation over elements. The finite difference method is conceptually and mathematically easier to develop and (perhaps) more commonly used [29]. The numerical models used this thesis are based on finite differences. This is true for the flow model MODFLOW and partly for the transport model MT3DMS and SEAWAT. The transport model uses finite differences to simulate dispersion and diffusion (and conduction) but may use different techniques to simulate advection. The non-finite difference methods to simulate advection aim to reduce or even to eliminate numerical dispersion by taking a Lagrange approach, i.e. moving along with the flow during a time step. As it turned out we were not able to obtain consistent results with any of the Lagrange type methods in the MT3D model with our axisymmetric setup and, therefore, had to revert to the finite difference method to compute advection. This required to test several grid refinements to limit to the extent possible the numerical dispersion. The transport of chemicals and heat can be equally well simulated with MT3DMS and SEAWAT, but only if temperature induced viscosity and density as well as salinity caused density differences are ignored. If not, SEAWAT must be used, which interacts with MODFLOW on a time-step by time-step basis and allows updating these temperature dependent parameters during the simulation, whereas MT3DMS does not.

3.2. FLOW IN POROUS MEDIA

The flow in a porous medium is characterized by three significant parameters: the intrinsic permeability, the porosity and the viscosity and sometimes also the density of the fluid [1, 9].

The Intrinsic Permeability is a property of the porous medium alone measuring of the generic ability of the medium to transmit a fluid with yet unspecified fluid viscosity and density. Permeability facilitates seepage between the two screens of an SB-ATES system.

The flow through a porous medium is driven by Darcy's law:

$$\vec{q} = \frac{K}{\mu}\nabla(p - \rho\vec{g}) \qquad 3.1$$

Where K [L^2] is the permeability tensor, a 3x3 matrix holding the permeability values for the different spatial directions. This tensor is diagonal if the coordinate axes are parallel to the main axes of the permeability tensor. In practice, depending on the geology, i.e. in sediments or sedimentary rock, these main axes correspond often with the vertical and horizontal directions. Further, μ [$F/L^2/(L/T)/L$] (Ns/m^2 in ISO) is the fluid viscosity, p [F/L^2] is fluid pressure and, $\vec{g}$ [F/M] the gravity vector and ρ [M/L^3] fluid density.

This relation shows that properties of the medium, i.e. K and that of the fluid, i.e. μ and ρ are completely separated by the definition of permeability.

We may then express the flow through the porous medium by:

$$\vec{q} = \frac{\kappa_x}{\mu}\frac{\partial \mathrm{p}}{\partial x} \qquad 3.2$$

$$\vec{q} = \frac{\kappa_y}{\mu}\frac{\partial \mathrm{p}}{\partial y} \qquad 3.3$$

$$\vec{q} = \frac{\kappa_z}{\mu}\frac{\partial(p - \rho g)}{\partial z} \qquad 3.4$$

The density difference between water around the "warm screen" is and that around the "cold screen" may generate extra flows that may impact the thermal efficiency of the ATES system. Density-driven flows may also occur as a consequence of spatially varying concentrations of dissolved solids as when operating in water with spatially varying salinities. [1].

Contrary to oil-reservoir engineers, groundwater hydrologists favor using the hydraulic conductivity *k* [L/T] over intrinsic permeability. This allows a somewhat simpler expression of Darcy's law and the use of familiar hydraulic heads:

$$q_x = -k_x \frac{\partial \varphi}{\partial x} \quad 3.5$$

$$\mathrm{q_y} = -\mathrm{k_y} \frac{\partial \varphi}{\partial \mathrm{y}} \quad 3.6$$

$$q_z = -k_z \frac{\partial (\varphi + \delta)}{\partial z} \quad 3.7$$

This is obtained by expressing the pressure in hydraulic head and elevation

$$p = \rho g(\varphi - z) \quad 3.8$$

The hydraulic conductivity becomes:

$$k = \rho g \frac{\kappa}{\mu} \quad 3.9$$

Porosity, ϵ, is the spatial fraction of the volume of voids, V_{pore}, [m^3] in a given bulk volume of the porous medium, V_{bulk}, [m^3].

$$\epsilon = \frac{V_{pore}}{V_{bulk}} = \frac{V_{bulk} - V_{matrix}}{V_{bulk}} \quad 3.10$$

Where V_{matrix} is the volume of solid particles composing the material matrix [m^3] [9].

3.2.1. Heat Transfer

Heat in a porous medium is transferred by a) thermal conduction b) heat convection and c) thermal radiation. Conduction and convection will be explained below. Radiation deals with the transfer of thermal energy by electromagnetic radiation, which is of negligible importance inside porous media [23], but could be relevant as boundary condition at ground surface.

3.2.2. Conduction

Thermal conduction is driven by temperature gradient induced by the stored warm and cold water without regarding flow. The heat flux q_x [E/L^2/T] by conduction is described by Fourier's law and presented in equation 3. 5:

$$q_x = -\lambda \frac{\partial T}{\partial x} \quad 3.11$$

And likewise the equation 3. 11 takes the same form for the flux into the other two directions *y* and *z*.

This shows that the heat flux depends on the combined bulk heat conductivity of the medium λ_s and the pore water, λ_w. With porosity ε this bulk heat conductivity can be expressed as:

$$\lambda = \epsilon\lambda_w + (1-\epsilon)\lambda_s \quad 3.12$$

Changes in subsoil temperature always involve the combined, i.e. bulk heat capacity of the medium and the pore water. With $\rho_w c_w$ the heat capacity of water and $\rho_s c_s$ that of the grains, we can express the bulk heat capacity of the pore medium [E/L^3/K] as:

$$\rho c = \epsilon\rho_w c_w + (1-\epsilon)\rho_s c_s \quad 3.13$$

The volumetric heat capacity refers to the ability of the aquifer to store thermal energy while undergoing a temperature change [4, 23].

In general, thermal conduction occurs at the molecular level driven only with a temperature gradient.

3.2.3. Convection with retardation

Convection is the transfer of heat driven by fluid movement. It combines advection and conduction on the pore scale, i.e. heat exchange between moving pore water and fixed grains. This exchange causes a delay (retardation) of the heat transfer relative to that of the pore water. The retardation is the total bulk heat capacity divided by the heat capacity of the water in the pores, which actually convects the heat:

$$R = \frac{\epsilon\rho_w c_w + (1-\epsilon)\rho_s c_s}{\epsilon\rho_w c_w} \quad 3.14$$

The retardation factor (R) [-] in Dutch fluviatile aquifers is in the order of 2.0.

Convective heat transfer is also subject to the density differences cased by the injection and extraction of water with varying temperatures and maybe salinities [23].

3.3. ANALYTICAL SOLUTIONS FOR THE CALIBRATION OF GEOLOGICAL PARAMETERS

The horizontal and vertical conductivities of the aquifer are essential parameter for groundwater flow. While an overall estimate of them may be obtained from pumping tests, such tests cannot reveal the differences within the aquifer caused, for instance by sedimentation processes at the time that the layers were deposited. Nevertheless, such conductivity variations will or at least can be of importance for the thermal efficiency of ATES systems. Most of the cases provided by Installect for this study, contain grain size values determined from samples taken about every meter during drilling. While still coarse, this information may be used to at least gain some feeling for the vertical variation of hydraulic conductivity within the aquifer. Of course, a single grain size per sample cannot give any information about soil structure and, therefore, about vertical anisotropy. The most we can obtain from it is a general idea about the overall hydraulic conductivity for each of the mixed samples, namely by applying the well-known Kozeny-Carmen equation (Bear, 1970),

which combines porosity and effective grain size and viscosity. It is unknown whether the given grain sizes provide an effective grain size, nor do we have

information about porosity of the layers for the provided cases. Therefore, we have to stick with the general idea about the porosity of Dutch aquifers of about 35% (T.N. Olsthoorn, oral information).

Kozeny-Carmen equation. The Kozeny-Carmen equation was developed to estimate the hydraulic conductivity of clastic soil samples [1], combining relevant properties of the medium (effective grain size and porosity) and the water (viscosity and density). It can essentially be derived from the flow in a single pore and introducing the concept of porosity:

$$K = \frac{\rho_w \cdot g}{\mu} \cdot \frac{\epsilon^3}{(1-\epsilon)^2} \cdot \frac{d_m^2}{180} \qquad 3.15$$

Where K is the hydraulic conductivity [m^3/d], ρ_w is the density of water [kg/m^3], g is the acceleration of gravity [N/kg], μ the dynamic viscosity [Ns/m^2], ϵ the porosity [-] and d_m is a represented grain size [m].

Estimating average hydraulic conductivities based on Darcy's law. In the Netherlands, we exclusively deal with essentially horizontally structured sediments, i.e. sandwiched formations. Therefore, we regard horizontal flow in an aquifer as a parallel flow within many stacked layers of possibly different conductivity and vertical flow as a flow that passes these layers in series. This leads to a different formula for the upscaling of the horizontal conductivities of these layers to that of an aquifer on the one hand and that for the upscaling of vertical flow through aquifers or aquitards on the other. The equivalent, i.e. upscaled average vertical (K_{xe}) and horizontal (K_{ze}) conductivities are directly derived based from Darcy's law, yielding [8]:

$$K_{xe} = \frac{\sum(K_{xi} \cdot d_i)}{\sum d_i} \qquad 3.16$$

$$K_{ze} = \frac{\sum d_i}{\sum d_i / K_{zi}} \qquad 3.17$$

Where $K_{xi}$and K_{zi} are the conductivities in *x* and *z* axes direction and d_i is the thickness of the layer [9]. These equations are used when converting a set of horizontal sub-layers into a single one with average properties.

3.4. RECIPROCITY PRINCIPLE

The reciprocity principle was proven mathematically by Bruggeman (1999). According to this principle, pumping with a discharge Q at an arbitrary point A causes the same drawdown in an arbitrary point B as the drawdown that pumping with that same rate in point B causes in point A [3]. This principle has direct consequences for the interpretation of the capacity tests carried out on every newly installed SB-ATES system because the drawdown in screen B due to pumping

screen A is exactly the same as the drawdown in screen A when pumping at the same rate in screen B. Hence, the principle predicts that the capacity test on screen A yields the same results as the capacity test on screen B, which we will verify in chapter 5. As a consequence the two capacity tests done on every system only yield a single result. And because the steady state situation is reached in seconds to a few minutes due to the short distance between the screens the measurements taken at different times during the one hour that the test lasts, all yield the same value. Hence the two capacity tests done on each SB-ATES system only yield a single numerical value, i.e. the drawdown after say 60 minutes to use for any calibration. In fact, the capacity tests only yield information to estimate an overall anisotropy from. Which is little information, which, however may still be useful in combination with the conductivity distribution as will be shown in chapters 4 and 7.

Fig. 3. 1 presents a qualitative schematization of the reciprocity principle. The locations of *A* and *B* are indicated. The drawdown, H_A in *A* location, when the pumping is conducted in *B* location is the same as the drawdown H_B in *B* location when pumping is conducted in *A* location such that ($Q = Q_A = Q_B$). Hence:

$$\left(\mathrm{H}_{\mathrm{A\_pumping\ at\ A\ with\ discharge\ Q}}\right)_t = \left(\mathrm{H}_{\mathrm{B\_pumping\ at\ B\ with\ discharge\ Q}}\right)_t$$

and

$$\left(\mathrm{H}_{\mathrm{B\_pumping\ at\ A\ with\ discharge\ Q}}\right)_t = \left(\mathrm{H}_{\mathrm{A\_pumping\ at\ B\ with\ discharge\ Q}}\right)_t$$

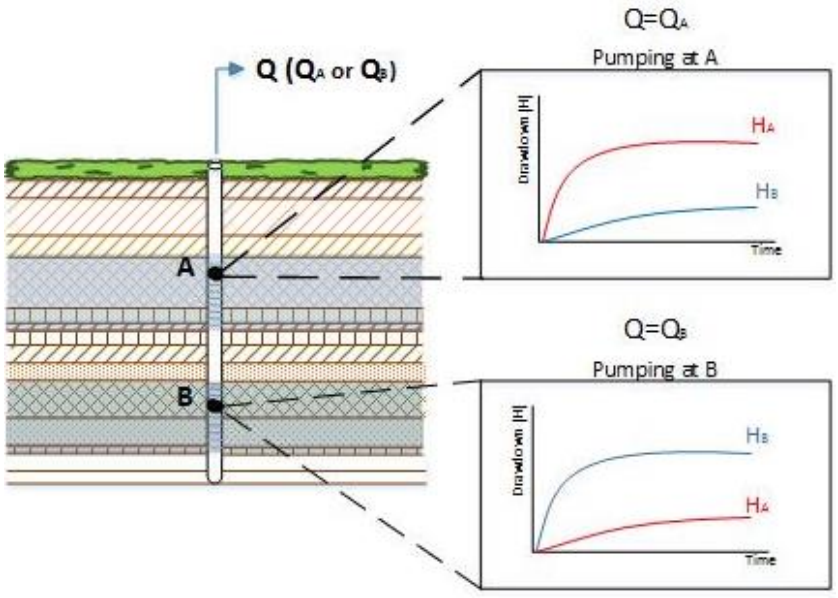

Fig. 3. 1: Qualitative schematization of reciprocity principle, the discharge equals to $Q = Q_A = Q_B$

3.5. PROCEDURE TO CALIBRATE HYDRAULIC PROPERTIES

In an early stage, we used an analytical multi-layer model to calibrate the capacity tests after it was verified that it is possible to be used an equivalent finite difference configuration directly which is implemented in Matlab and presented as tool in mfLab. Because the numerical model turned to be more flexible, especially, in the mfLab environment, and because its setup integrates smoothly with MODFLOW and the transport models MT3DMS and SEAWAT, we dropped the analytical flow model in further evaluations. The analytical model is, therefore, not described in this thesis.

A numerical model was developed in Matlab to automatically calibrate the overall vertical anisotropy of each of the available cases obtained from Installect Advies for this study. Only the hydraulic conductivities could be independently derived from the available data, i.e. one estimated grain-size value for about every meter during drilling. The Kozeny-Carmen equation (equation 3. 15) was used for this purpose and accepted despite all its uncertainties. Two capacity tests were also available for each case, each consisting of pumping one of the two screens for approximately one hour and registering the drawdown in the pumped and opposite screens at about 5 time instances. These capacity tests provided only one single value. This is the drawdown in either test in one screen after 60 minute pumping in the other. Only this value is suitable for use in a calibration. Therefore only one parameter may be optimized against this value, for which we choose the overall vertical anisotropy.

We will use the capacity tests to demonstrate the reciprocity principle. It also allows verification of the outcome of the first test by the second as a check. We further use the capacity test to calibrate an average anisotropy for each case, to the extent that it was possible with the available data.

This calibration was implemented in Matlab using a finite difference model also implemented in Matlab. The calibration then determines the overall vertical anisotropy of the aquifer automatically using nonlinear optimization with the *lsqnonlin* function provided by Matlab. A more extensive description of the calibration procedure can be found in Chapter 5. Fig. 3. 2 presents a flow chart of the steps that were followed to derive the soil hydraulic properties.

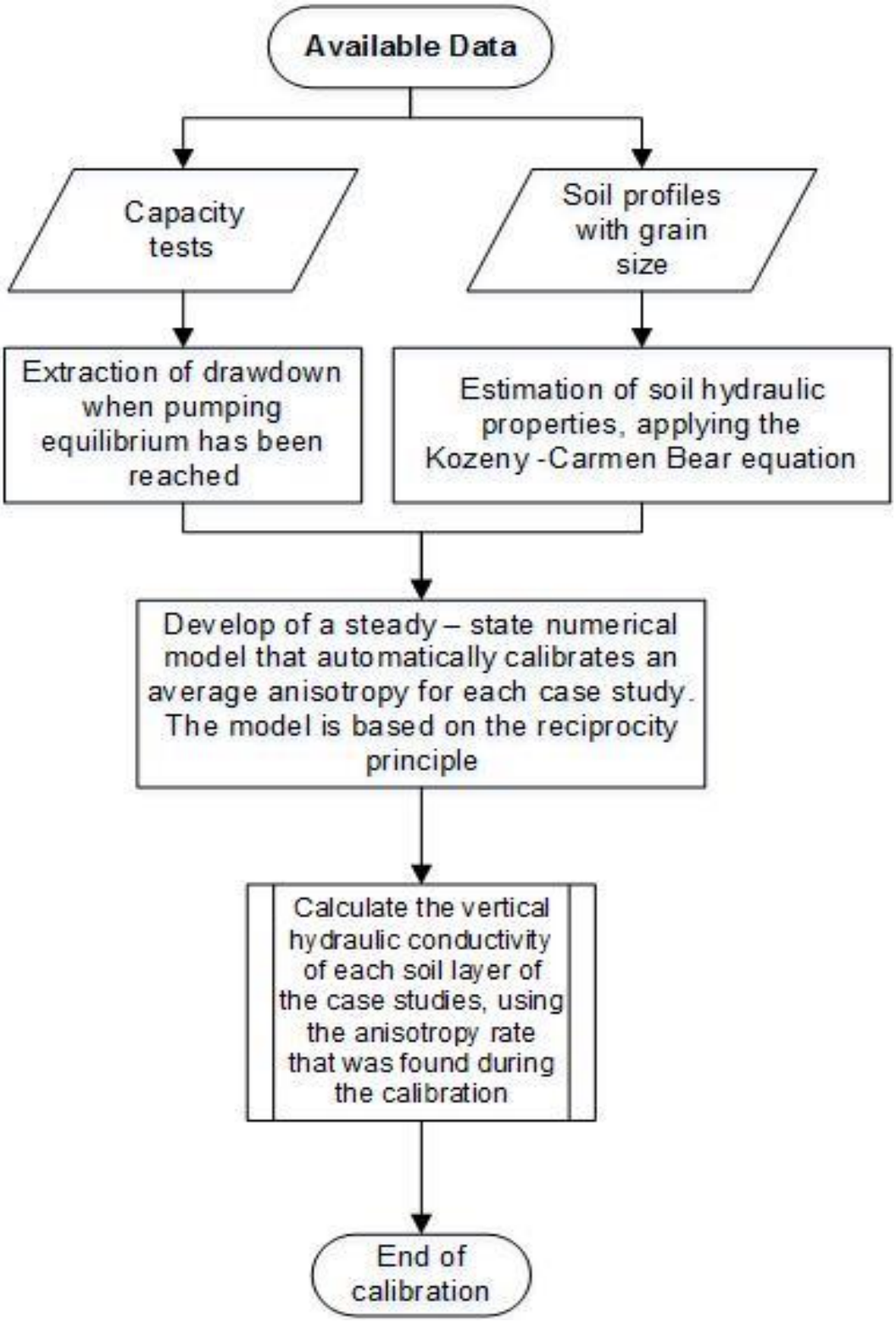

Fig. 3. 2: Flow Chart with the steps for finding the soil hydraulic properties

3.6. MODELING TOOLS

The simulations in chapter 6 and 7 were carried out with MODFLOW and MT3DMS and partly SEAWAT codes, in MATLAB environment, using mfLab. This mfLab adapts the input such that the mentioned codes simulate an axisymmetric model. In fact, for the sensitivity analysis it simulated 135 axisymmetric models simultaneously and also reads back the results and provides their visualization. The theory behind the usage of radial symmetry is that when the regional hydraulic gradient is absent and the groundwater flows to an extraction or away from an injection well, radial symmetry occurs [22].

An axisymmetric model was preferred over a three dimensional one, a 3D modelling would require much longer running times, with almost the same accuracy [22]. Additionally, the use of the axisymmetric approach in the estimation of hydraulic parameters from capacity tests is commonly used in the past, due to its lower computational complexity [19, 22]. Thus an analysis of a cross section model is enough to evaluate the performance of the SB-ATES systems.

The numerical model used further in this study are based on the open-source codes MODFLOW and SEAWAT provided by the USGS [21]. Through mfLab, we will use these codes in axisymmetric modes exclusively [22]. Hence our models will always simulate axisymmetric flows around one or more vertically spaced well screens. It also implies that inhomogeneities are limited to vertical layering and that we cannot deal with ambient groundwater flow. On the other hand, axisymmetric models are efficient and can be very detailed near the well, which 3D models fail to do because of computer limitations. Running a MODFLOW and SEAWAT model in axisymmetric mode can be entirely achieved by appropriately defining its input parameters as described by Langevin (2008) [22] and is fully incorporated in the mfLab toolbox.

MODFLOW uses a block-centered discretization, thus the head and the hydraulic conductance are calculated in the center of each grid cell based on the finite difference form of the continuity equation and by averaging transmissivity values between adjacent cells. Logarithmic averaging of conductivities in horizontally adjacent cells has been verified to give the correct head distribution for a linear variation transmissivity. This averaging can be chosen when applying the Layer Property Flow (LPF) packages of MODFLOW, These packages include the logarithmic inter-block transmissivity weighting option, which calculates accurate hydraulic conductivities for axially symmetric models. This weighting option is assigned by the LAYAVG flag and equals 2 [22].

3.6.1. MODFLOW

MODFLOW 2005 was used.

The flow balance of a cell is derived by applying the continuity equation, assuming that the groundwater density is constant, and described by equation 3.18 [21].

$$Q_i = S_s \frac{\Delta h}{\Delta t} \Delta V \quad 3.18$$

Where Q_i is the flow rate into the cell [m^3 /d], S_s stands for the specific storativity in the finite difference formulation [-], ΔV represents the volume of the cell [m^3], Δh is the drawdown over a time interval of length Δt.

Based on Darcy's law, the rate of water flow through a porous media can be described by equation 3.19:

$$q_i = -K_{ij} \frac{\partial h}{\partial x_j} \quad 3.19$$

Where q_i is the specific discharge [m/d], $K_{ij}$the hydraulic conductivity [[m/d] and h the hydraulic head [m].

Thus, by combining the equations 3. 18 and 3. 19, a general groundwater flow in Cartesian tensor notation can be derived (equation 3. 20) in the cases where nonhomogeneous anisotropy and transient flow are present.

$$\frac{\partial}{\partial x_j}\left(K_{ij} \frac{\partial h}{\partial x_j}\right) = S_s \frac{\partial h}{\partial t} + W \quad 3.20$$

Where S_s stands for the specific storage, t is the time and W the volumetric flux per unit volume (takes positive values for outflows and negative values for inflows) while x_j stands the Cartesian coordinate's axis [28].

3.6.2. MT3DMS

MT3DMS package is used to simulate three dimension transport models, including advection, dispersion, sorption, as well as, biological and geochemical reactions that may occur in the groundwater. Equation 3. 21 describes mass transport and expresses the change rate of concentration in terms of dispersion and advection.

$$\left(1 + \frac{\rho_b K_d}{\epsilon}\right) \frac{\partial(\epsilon C)}{\partial t} = \nabla\left[\epsilon\left(D_m + \alpha \frac{q}{\epsilon}\right) \cdot \nabla C\right] - \nabla(\mathrm{q}C) - q_s' C_s \quad 3.21$$

Where ρ_b stands for the bulk density [kg/m^3], K_d is the distribution coefficient [m^3/kg], ϵ the porosity [-], C the concentration [kg/m^3], D_m is the molecular diffusion coefficient [m^2/d], α the dispersivity tensor [m], q_s' the specific discharge of sink or sources [m/d] and C_s is the sink or source concentration [kg/m^3]. To convert the mass-transport equation to calculate heat transport the two mathematical expressions are made equivalent to each other. Fourier's law which describes the heat transport is mathematical similar to the Fick's First law of diffusion. Fourier's law states that the negative temperature gradient is proportional to the heat flow, meaning that the amount of energy that flows through a particular surface per unit area and time, is:

$$\varphi_q = -\lambda \nabla T \qquad 3.22$$

Where φ_q stands for the local heat flux [W/m^2], λ for the thermal conductivity of the material [W/mC^0] and T for the temperature [C^0].On the other hand, Fick's First law states that the negative gradient of concentration is proportional to the diffusion flux which is the amount of substance flowing through a particular surface per unit time and area and can be describe by the equation 3.23.

$$\varphi_m = -D_m \nabla C \qquad 3.23$$

Where φ_m stands for the diffusion mass flux [kg/md]

Two key factors are taken into consideration in the conversion of mass transport to heat transport, the diffusion of heat, which is conduction and is ruled by the diffusion coefficient, and the use of the sorption characteristics of the heat transport, which is the exchange between pore transport by the water and the exchange of heat between the water and the pores that causes a retardation factors.

Regarding the diffusion coefficient, it is always the ratio between the easiness of flow over the storage. In the case of heat, this transfers to the ratio of the bulk heat conductivity coefficient and the bulk heat storage, which can be described by:

$$D = \frac{\lambda_b}{(\rho c)_b} = \frac{\varepsilon_w \lambda_w + (1-\varepsilon_s)\lambda_s}{\varepsilon_w \rho_w \lambda_w + (1-\varepsilon_s)\rho_s c_s} \qquad 3.24$$

Where the index *b* stands for bulk, i.e. the pore space including water and solids, where the indices *w* and *s* refer to water and solids respectively.

The sorption characteristics of the heat transport cause a retardation that is about 2 in the case of heat transport through clastic sediments. MT3DMS used its reaction package RCT to deal with sorption. This package requires definition of the coefficients SP1 and SP2 and RC1 and RC2 to deal with reactions, or different sorption processes, between water and solids. Because the exchange between water and grains is a linear process, it was implemented linear sorption to deal with this. This requires only the coefficient SP1 which set to 0.000212. Linear sorption is defined as the total amount of species over the transported amount of species, the ratio is the retardation factor. Linear sorption only requires one coefficient, the distribution coefficient, *K*, for which MT3DMS used SP1.

Retardation due to linear sorption of a chemical is:

$$R = \frac{\epsilon c + \rho_s \sigma}{\epsilon c} \qquad 3.25$$

Where σ stands for the mass of species sorbed to 1kg of solids.

From laboratory experimentation the mass of species can be described by the equation 3.26

$$\sigma = K_d c \tag{3.26}$$

With K_d the distribution coefficient.

Thus, from equations 3. 25 and 3. 26 can be derived that:

$$R = \frac{\epsilon c + \rho_s K_d c}{\epsilon c} = 1 + \frac{\rho_s K_d}{\epsilon} \tag{3.27}$$

Where $\frac{\rho_s K_d}{\varepsilon}$ is the ratio of the absorbed mass over the dissolved mass. To include heat transfer in the equation 3. 21, we may write the retardation as the total heat per unit of space volume over the heat in the convecting water, the heat transported by advection:

$$R = \frac{\epsilon \rho_w c_w T + (1-\epsilon)\rho_s c_s T}{\epsilon \rho_w c_w T} = 1 + \left(\frac{1-\epsilon}{\epsilon}\right)\frac{\rho_s c_s}{\rho_w c_w} \tag{3.28}$$

Where $\rho_w c_w$ and $\rho_s c_s$ are the volumetric unit heat capacities of the water and solids respectively. The right term of the equation is the ratio of total heat stored in the solids over the total heat stored in the water. Thus, the distribution coefficient in the case of heat transport takes the following form:

$$\frac{\rho_s K_d}{\epsilon} = \left(\frac{1-\epsilon}{\epsilon}\right)\frac{\rho_s c_s}{\rho_w c_w} \Rightarrow K_d = \left(\frac{1-\epsilon}{\rho_w}\right)\frac{c_s}{c_w} \tag{3.29}$$

The heat transport equation can be written as:

$$\left(1 + \frac{1-\epsilon}{\epsilon}\frac{\rho_s}{\rho_w}\frac{c_s}{c_w}\right)\frac{\partial(\epsilon T)}{\partial t} = \nabla\left[\epsilon\left(\frac{k_{Tbulk}}{\varepsilon \rho_w c_w} + a\frac{q}{\epsilon}\right)\cdot \nabla T\right] - \nabla(\mathrm{q}T) - q_s' T_s \tag{3.30}$$

Where ρ_s stands for the density of the solid [kg/m^3], c_s is the specific heat capacity of the solid [J/kg^{0}C], c_w is the specific heat capacity of the water [J/kg^{0}C], k_{Tbulk} the bulk thermal conductivity of the aquifer material [W/m^2] and T_s is the sink or source temperature [^{0}C].

By comparing the equations 3. 21 and 3. 30, it can be seen that the retardation factor depends on other parameters while the diffusion parameter has been replaced by conduction. Thus, some parameters in the equation 3.30 can be written as:

$$K_d = \frac{c_s}{\rho_w c_w} \tag{3.31}$$

$$D_{m\_temp} = \frac{k_{Tbulk}}{\epsilon \rho_w c_w} \tag{3.32}$$

$$\rho_b = \rho_s(1-\epsilon) \tag{3.33}$$

Then replacing the equations 3. 31 - 3. 33 into equation 3. 30:

$$\left(1+\frac{\rho_b K_d}{\epsilon}\right)\frac{\partial(\epsilon T)}{\partial t}=\nabla\left[\varepsilon\left(D_{m\_temp}+a\frac{q}{\epsilon}\right)\cdot\nabla T\right]-\nabla(\mathrm{q}T)-q_s' T_s \quad 3.34$$

Where D_{m_temp} is the thermal conduction term [m²/d] and K_d the thermal distribution factor [m³/kg]. The equation 3. 34 can be seen that is equivalent with the equation 3. 21.

3.6.3. SEAWAT

SEAWAT package combines MODFLOW and MT3DMS packages and simulates three dimension at problems with variable density and transient flow in porous media [4, 19]. It solves the coupled flow and solute transport equation. SEAWAT takes into account variable density flow, due to temperature differences [19]. The flow equation includes the variable water density and viscosity. It is presented in equation 3. 35:

$$\nabla\left[\rho\frac{\mu_0}{\mu}K_0\left(\nabla h_0+\frac{\rho-\rho_0}{\rho_0}\nabla z\right)\right]=\rho S_{s,0}\frac{\partial h_0}{\partial t}+\epsilon\frac{\partial\rho}{\partial C}\frac{\partial C}{\partial t}-\rho_s q'_s \quad 3.35$$

ρ stands for the water density [kg/m³], μ_0 is the dynamic viscosity at the reference concentration and temperature and μ the dynamic viscosity [Ns/m²], K_0 the hydraulic conductivity tensor of material saturated with the reference fluid [m/d], h_0 is the measured hydraulic head in terms of the reference fluid at a specific concentration and temperature [m], ρ_0 is the water density at a reference concentration and temperature [kg/m³], z is the elevation [m], $S_{s,0}$ is the specific storage coeficient, t is time [d] and ρ_s the density of the source /sink [kg/m³].

3.6.4. Numerical model components

This paragraph includes the components of the numerical model. These are the model grid, the objects that were used in the model as well as its boundary conditions. Additionally, reference on the simulation time-step is given.

3.6.4.1. Grid Selection

The grid is axisymmetric with the horizontal coordinate, *r*, the distance to the center of the well. To obtain sufficiently detail near the well and to prevent effects from outer boundaries, the width of the ring-shaped cells increases gradually with distance. The function sinespace is used to force a more gradual column size increase than would be obtained with a logarithmic series:

```
xGr = sinespace(0,500,201,pi/50,pi/2);% Grid object in x direction, Matlab
```

This yields grid column widths of which the first 6 are:

```
0.2652    0.2934    0.3216    0.3498    0.3780    0.4062 …
```

The r in this model runs from 0 to 500 m and has 201 points. The cell sizes increase according to a portion of the sine function, here between pi/50 and pi/2, which implies that the cells near the outer boundaries have about equal widths.

The coarse models have used the same function with 0 and 500 m limits but only a lower number of points, i.e. 101 for the 0.5 m resolution grid and 51 for the 1.00 m resolution grid. These coarser grids also have their aquifer model layers increased in thickness to 0.5 and 1.0 m respectively. In total, the finest model has 16 times as many cells as the coarsest and would required about 250 times more computation time.

The vertical subdivision of the grid is made sufficient detail to accurately model sublayers and areas with concentrated streamlines i.e. near the ends of the screens. The coarsest has 1 m layers and so a 5 m screen is divided over 5 model layers. In the finest model, this screen would be divided over 20 model layers.

The axisymmetric grid occupies only one model row. A figure of the grid (Fig. 3. 2) shows a constant row thickness however, but this is purely technical. The row thickness for MODFLOW and MT3DMS/SEAWAT is actually always 1 m, but the parameters that are proportional to $2 \cdot \pi \cdot r$ are multiplied by $2 \cdot \pi \cdot r$ by mfLab before generating the input files for MODFLOW and MT3DMS/SEAWAT.

Notice that the model layers that are part of the confining layers at the top and at the bottom of the model always have a thickness of 5 m to reduce the overall computation time.

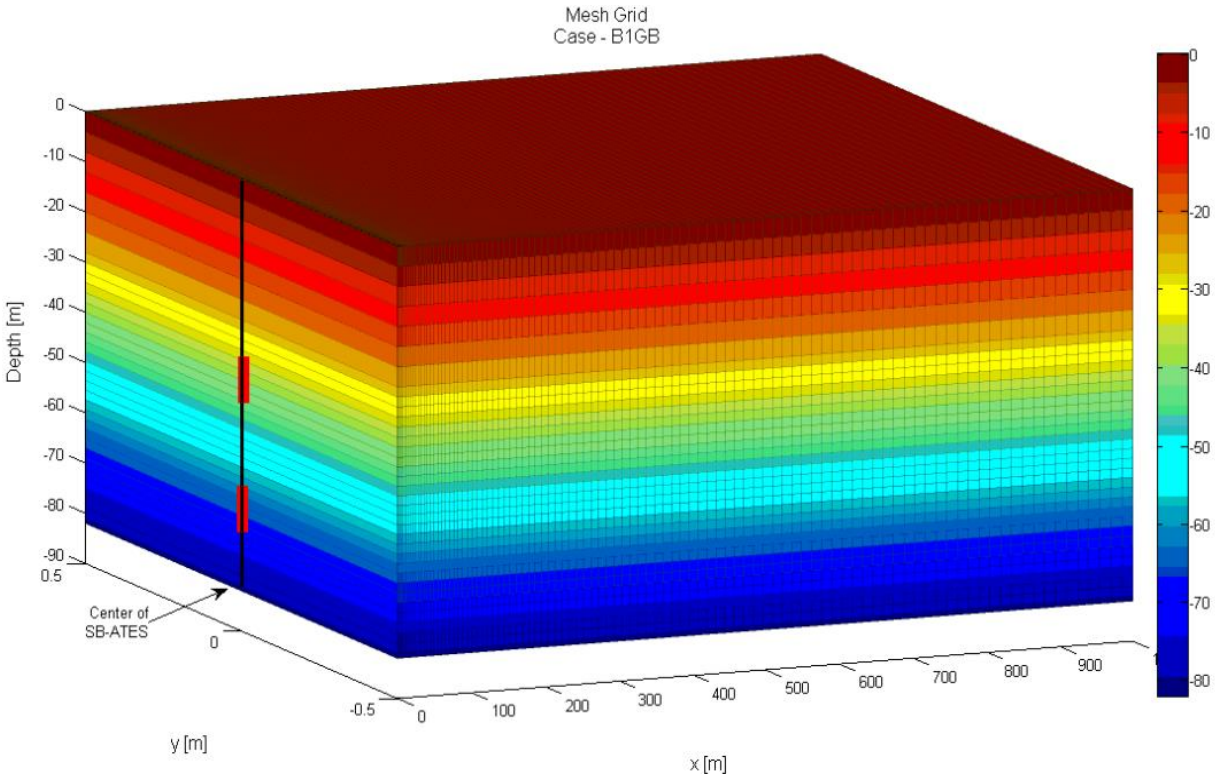

Fig. 3. 3: Mesh Grid for the case of B1GB (Gemeentehuis Boxtel) with one cell in the y direction (axial symmetry). Notice that the model has only one row, which is drawn here as running from y= -0.5 m to y=0.5 m. Conceptually, the row thickness in the axisymmetric grid is to be considered as $dy = 2\pi r$.

3.6.4.2. Time step and solution technique

Time steps are relevant when computing transport of flow and heat. A time step of 1d was chosen from the user perspective, but the transport time step is further automatically reduced to fulfill the requirement that transport should be less than the size of the cell within one time-step anywhere in the model. This limit is specified by the Courant number being set to 1.0 or less [4]. Additionally, the accuracy also depends on the solution technique, in this work, the FD solution method was used as it was the only advection computation method in MT3DMS/SEAWAT that gave consistent results when it was applied in the axisymmetric model. To increase the accuracy of the model two refined grids were also used on with 0.50 m resolution and one with 0.25 m resolution. The Courant number does not play any role in the advection computation by means of the FD technique,

3.6.4.3. Well Skin

A well skin is caused by clogging of the borehole and causes a jump in head between the screen, the gravel pack and further out in the formation.

A well-developed well, however, has a reduced resistance around its screen due to the gravel pack, which, in the Netherlands, is installed artificially and which in other countries with coarser and more heterogeneous sands may be automatically obtained by the well development procedure in which fines surrounding the well are removed by intense pumping. For this reason, it was decided to be assigned to the cells where the screens are present high conductivity of 500m/d. Well skin is not considered in this thesis as it has no effect on thermal efficiency it only determined hydraulic losses and required screen maintenance.

3.6.4.4. Well objects in the Grid

Well Object. MODFLOW's WELL package is applied to implement wells [21]. The well screens extend beyond one node, thus the calculation of discharge at each node of the grid is conducted based on equation 3. 36:

$$Q_{i,j,k} = T_{ijk} \frac{Q}{T_{sum}} \qquad 3.36$$

Where $Q_{i,j,k}$ is the discharge at each grid cell [m^3/d], $T_{i,jk}$ the transmissivity at the grid cell [m^2/d], Q stands for the pumping rate [m^3/d], while T_{sum} is the summation of the transmissivities of all cells that the well screen intersects [m^2/d].

3.6.4.5. Boundary Conditions

Head-boundary conditions. The selection of suitable boundary conditions is critical for every model. The head boundaries are specified to the model with the IBOUND array which has one value for each model cell. When $IBOUND_{i,j,k}>0$, the grid cell with coordinates (i,j,k) has a variable, computed head. $IBOUND_{i,j,k}=0$ tells that cell i,j,k is inactive, i.e. it is considered outside the active

model domain and is ignored completely as if non-existent. $IBOUND_{i,j,k}<0$ tells MODFLOW that the cell has a constant head and that it maintains its initial value during the simulation.

Only the cells at the outer boundary of the axisymmetric model are assigned fixed heads. The distance from the well for these cells is 500 m, far enough to prevent any influence near the well where the thermal storage takes place and where heads are measurably changed.

In the case of the multi-model (see paragraph 3.6.5) each row of the 3D grid may represent one complete axisymmetric model. A row of inactive cells is introduced between two such axisymmetric models to prevent interference between them.

Concentration and Temperature Boundary Conditions for heat transport. $ICBUND_{i,j,k}$ is the array of the Basic transport package (MT3DMS) that introduces the concentration and or temperature boundary conditions. For $ICBUND_{i,j,k} >0$ indicates that the cell has a variable concentration, when $ICBUND_{i,j,k} =0$ means that the cell is inactive while for $ICBUND_{i,j,k}<0$ the cell has a constant concentration. The concentration boundaries were assigned in the same manner as the head boundaries, i.e. cells with variable head have also variable concentration cells with constant head have also constant concentration, while to prevent the interference between the different scenarios in the Multi-Model (paragraph 3.5.5), a layer with inactive cells was introduced into the model.

3.6.5. Multi-Model verification

A multi- model was created to solve simultaneously the different scenarios that are presented in Chapter 6. The multi-model solves a larger number of axially symmetric or flat models simultaneously by implementing each one in separate row of a 3D grid. To separate the models both hydraulically and thermally (chemically), an insulating row with both IBOUND=0 and ICBUND=0 is placed between each pair of models.

Problems arise with the stability of the solution. Neither the MOC nor TVD advection computation methods yielded stable, plausible results; only FD did. This implies that the implementation through mflab is correct, but that MT3DMS itself suffers from instability for ours specific model setup and, thus MOC and TVD, provide useless results.

Several steps were taken to find a more stable outcome with the TVD method.

1) PERCEL, the Courant number, was set to 0.5, i.e. lower than 1.0, limiting the maximum allowed transport distance during one transport step in terms of the size of the cells.
2) The casing of the wells was made inactive. Only the screens are active. This corresponds to reality.
3) The VK inside the well screens was set to zero, which forces the injected water horizontally out of the first column into the rest of the model.

4) The size of the cells near the well does not change abruptly. The first cell size is about 1.1 m, and this value slowly grows with increasing column number. The *sinespace* function of *mfLab* is used to obtain a smooth distribution of column cell sizes.
5) The iteration scheme of CGC solver used by MT3DMS was set to 10 outer and 20 inner iterations to allow coefficients to be updated during the transport step computations. This especially affects updating of the dispersion coefficients, which were put to the right-hand side of the transport equation using the parameter NCRS=0.
6) The computation accuracy, i.e. CCLOSE was set more stringently to10^{-5}.
7) The ISOLVE flag was assigned a value of 3,
8) The FD method was used as it was more stable than the TDV method.
9) To increase the accuracy of the FD method a grid refined first by a factor 2 to 0.5 m in both the vertical and horizontal direction and later with another factor 2 to 0.25 m.
10) Setting confined layers at the top and the bottom by assigning the IBOUND and ICBUND equals to 0 for those layers

All these measures could net solve the instability of the TVD method, while the FD method always yielded consistent results which were exactly the same for the lower and the top screen as expected in this test model setup. Therefore the FD method had to be used in the further analyses in chapters 6 and 7. The end conclusions are based on simulations that were all done with the highest (25 m) grid resolution, where all aquifer layers were 0.25 m thick and all confining layers 5 m and were the columns near the well are also about 0.25 m wide, slowly increasing with distance using mfLab's sinespace function.

3.7. SUMMARY

This chapter presents the theoretical background of this thesis. In more detail, the analytical solutions that were used during the calibration are listed, as well as the numerical tools that were applied during the elaboration. Specifically, the Kozeny – Carmen Bear equation and the reciprocity principle were used during the calibration of the case studies. The elaboration was carried out using an axisymmetric flow and transport numerical model, by implementing MODFLOW and SEAWAT packages.

CHAPTER 4

4. Case-Studies

This chapter illustrates the actual cases that were provided by Installect and that are analyzed and assessed in this Thesis. It deals with the specifications of the examined wells, together with the assumptions and the calculations applied to assess the thermal performance of the SB-ATES systems.

4.1. LOCATION AND GEOLOGY OF SB-ATES SYSTEMS

Installect provided data for the 18 SB-ATES that were selected for this Thesis. The data pertaining to each of these cases are bound together in the Soil- Profile Textbook.

Fig. 4. *1* shows the locations of these mono-wells. They are in Amsterdam, near Utrecht, in Hertogenbosch, Apeldoorn, Alkmaar, Almere, Amersfoort, Tilburg, Eindhoven, Deurne, Meppel and Groningen, essentially from all over the Netherlands. The set of cases, therefore, is considered representative for the country.

Fig. 4. 1: Location of case studies

Table 4. 1: Available case-studies

Location	Borehole code	Dutch geographical coordinates
Utrecht Leidsche Rijn	GT15ULR	207240 381855
Kantoorpand Vathorst Amersfoort	GT25VA	156000 462000
Goosens te Veghel	GT25GV	165534 401466
Tuinen van Bergen	GT25TB	109054 519627
Gementehuis Boxtel	B1GB (GT20)	150791 399938
VMBO West Gronongen	GT20VWG	231050 581759
Ursulinen Grubbenvorst	GT20UG	207269 381842
Wageningen	GT20WA	265809 463781
Pierter Zand College	GT15PZC	190294 507640
De Schiphorst te Meppel	GT20SM	211178 522800
Kropman Utrecht	GT15KU	133995 453115
Rabobank Houten	GT25RH	140525 447765
De Meern	GT15M	131758 399380
Centraal College te Utrecht	GT20CCU	137527 454824
Poort van Veghel	GT25PV	163710 401115
La Nuova Bella Donna Buiten	GT25NBDA	118725 480853
Kpa te Almaar	GT25-2KPA	113412 515392
Fortis Woerden	GT20WW	119745 398733
Keizerskroon	GT10KEIZ	-
Hondsheuvels Eindhoven	GM10HE	162348 384871
Businesspark gebouw te Apeldoorn	GT20BA	194222 465957
Apollolaan te Amsterdam	GT40AA	119749 484816
Minithermic Werkplaats	GTmini	174837 387178
City Theater Amsterdam	GT20CTA	120730 486286
TBS kliniek te Almere Buiten	GT25TBS	150840 490667
Avondozon Apeldoorn	GM121/2D	194512 468366

The cases for this study were selected based on three criteria:

1. The soil profile had to be sufficiently detailed and include a sufficient description of the layers with an estimation of their effective grain size.
2. Capacity tests had to be available, done under constant pumping
3. Only fresh water is involved with each case. Those with brackish groundwater were eliminated.

All of the selected cases have confining layers near the surface, with a sandy aquifer below, in which the screens are installed. The sub-layers encountered during drilling of the wells have been characterized with an estimation of their grain-size, using a sand ruler. Generally one soil sample was taken for every meter depth. Layers within the aquifer have grain sizes between 0.2 and 0.9 mm, which are characteristic for the fluviatile Pleistocene formations in the country (Oral information T.N.Olsthoorn, 2015). These fluviatile aquifers are used for drinking-water production and to serve ATES systems even if they are not in the same location.

The grain sizes provided are most often estimated by the driller in the field, generally by comparing the grains of a small sample with a sand ruler that has a set of fixed-sized grain samples to compare with. Clearly, the obtained grain-size values are only a coarse attempt to characterize layer properties, as they disregard details of the true grain-size distribution, let alone their actual packing configuration in the undisturbed formation. This causes a substantial uncertainty with respect to any hydraulic values determined from such grain sizes. The Kozeny -Carmen equation that was used to compute those conductivities, requires an “effective” grain size diameter which should correspond to the 10% of the sample. There is no information with respect to the representative estimation of the grain sizes. Having said that, these grain sizes are the only concrete independent information that we have on the properties of the encountered layers; therefore we have to deal with its limitations. Of course it is possible to refer to other information about the properties of the subsurface, like pumping tests and the REGIS national database, but that was not done for this Thesis.

For the estimation of the conductivities, we used a fixed porosity value of 35%. This assumption was made, as this value is considered representative for sandy soils in the Netherlands and has been applied in similar projects [3].

4.2. TECHNICAL SPECIFICATIONS OF THE INSTALLECT SB-ATES SYSTEMS

This thesis investigates three standard types of SB-ATES systems which are installed by the Installect Advies, The notations GT15, GT20 and GT25 that were found in all the provided data, are an indication for the configuration type and its design. In these code names, the two numbers

in the name indicate the pump capacity pertaining to each configuration, in m3/h, while the specifications of these systems are presented in Table 4. 2

Table 4. 2: Technical specifications of SB-ATES systems [26, 27] The first two letters, GT, stand for "Geo Thermic", while the number that follows (15, 20 or 25) refers to the maximum pump capacity in m^3/h. The final letters of each case name are a mnemonic of the location of the borehole or the name of the project.

	GT15	GT20	GT25
Cooling capacity at full load [kW], $\Delta T=10^0C$	175	233.3	291.7
Payload [kW], $\Delta T=5^0C$	87.5	116.7	135.8
Groundwater flow [m^3'h]	2.5-15	2.5-20	2-25
Pump motor power [kW]	5.5	3.7	5.5
Nominal pump motor power [kW]	3.3	2.7	3.7
Maximum pressure on the well [bar]	6	6	6
Standard heat pump's pressure [bar]	4	4	4

Appendix A gives the design specifications for the cases.

Appendix B presents the capacity tests.

In Soil-Profile Textbook, the cross sections of the cases are presented.

Fig. 4. 2 on the left illustrates the configuration of the analyzed SB-ATES cases. Notice that the two screens and the separation between them are all part of the same aquifer. Below the bottom of the lower screen there may be part of the aquifer or a confining layer the depth of which is unknown because the borehole is not deep enough to tell. A confining layer is always present below the aquifer, but at which depth it starts is unknown from the drilling. Regarding the GT15xx cases, a mean filter length of 5 m is used, for the GT20xx cases a length of 7 m while for the cases GT25xx a mean length of 10 m is applied. These values are the rounded averages of the actual screen lengths used in the respective types over the 18 cases in our database.

Fig. 4. 2 on the right shows the depths of these cases on a percentage scale.

There seems to be no specific pattern regarding the length of the screens and the separation distance between them. It also seems that the separation is mostly determined by the thickness of the available aquifer (Appendix C). The top and the deep screens are located on the top and sometimes at the bottom of the aquifer as it can be seen in Appendix C. The actual screen length surely depends on the system type GT15xx, GT20xx and GT25xx, but also seems to be determined

in-situ, based on the actual conditions determined during drilling in combination with the actual thickness of the aquifer. The bottom screen is further determined by the required separation, if the bottom of the aquifer is not reached earlier. Permeability of the aquifer will also play a role, as finer grained aquifers would require longer screens to reach the same capacity. Nevertheless, the bandwidth of screen length over all samples is larger than that over the three categories, leading to the characteristic screen length for each category, i.e. type of system with values 5, 7 and 10 m as said in the previous paragraph.

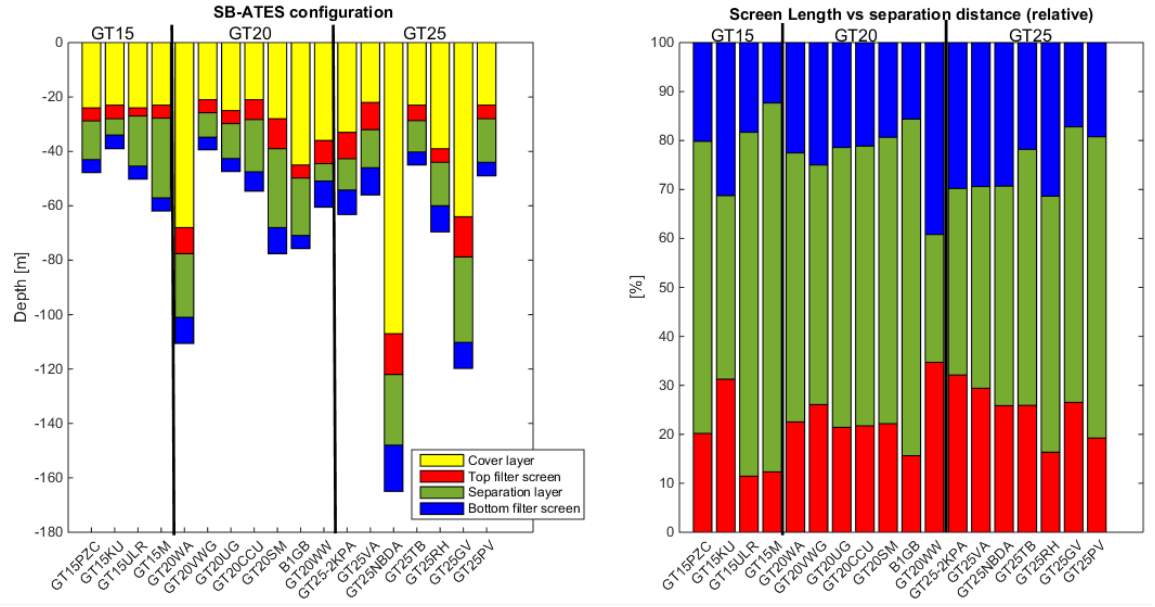

Fig. 4. 2: Screen lengths versus separation distance

4.3. OPERATIONAL SCHEDULE

We have no representative operational schedules for the actual cases, for this reason we are going to use constant monthly pumping discharge for the simulation period of 5 years. As it was discussed in paragraph 2.2, a discharge fraction factor, Qfrac, is introduced to the models with values of 0.25, 0.50 and 1.00. This factor relates the nominal capacity of the pump with the seasonal capacity of the systems. The systems GT15xx, GT20xx and GT25xx have a full capacity of 15, 20 and 25m^3/h respectively. Thus, for the GT15xx system, operational rates of 90m^3/d, 180m^3/d and 360m^3/d are examined, for the GT20xx pumping rates of 120, 240 and 480m^3/d while for the GT25xx rates of 150, 300 and 600m^3/d are used as an input in the models. It should be noted that the use of the cold and warm well is the same throughout the season, i.e. 6 months the cold well operates and the rest of the months the warm well. Specifically, from September to March, warm stored water is extracted while from April to August, the cold well is used. We used monthly pumping rates, as this complies with the obligation of ATES owners to register monthly values. Literature [3] determined the operational schedule by simulation heating when the actual outside temperature drops below

5^0C and cooling when it rises above 15^0C. In spring and autumn, cooling and heating can take place within the same month depending on the use and insulation of the served building. The

months with the highest uncertainty are April and September, as both cooling and heating occurred [3].

The season-average pumping discharge (Q in m^3/d) is computed according to equation 4. 1. The flow required to store or extract thermal energy power of P [W] in one season equals with:

$$Q = \frac{P}{c_p \cdot \rho \cdot \Delta T} \tag{4.1}$$

Where *P* is the required seasonal capacity [W], c_p the heat capacity of the water [kJ/(kg ^{0}C], ρ the water density [kg/m^3], and ΔT the temperature difference [^{0}C].

Additionally, the design also defines the maximum allowed pumping discharge. One reason to limit this in practice is to prevent the screen clogging. We commonly named the flow *Q* infiltration discharge in this study as others have done [3].

Different empirical formulas are in use for the allowable capacity for injection and extraction wells [3]:

For injection wells:

$$Q_{inj} = 1000 \cdot \left(\frac{K}{150}\right)^{0.6} \cdot \sqrt{\frac{v_v}{2 \cdot MFI \cdot u_{eq}}} \cdot A \tag{4.2}$$

For extraction wells [3]:

$$Q_{ext} = \frac{K}{12} \cdot A \tag{4.3}$$

Where Q_{inj} stands for the injection discharge [m^3/h], *K* is the (mean) horizontal hydraulic conductivity [m/h], *A* the well surface [m^2], v_v the specific clogging speed, which is commonly set equal to 0.1 [m/year], MFI is the "Membrane Filter Index [s/l^2]. It determined the clogging potential of water by filtering it under constant pressure fall of 2.0 bars through a 5 cm diameter membrane filter with 0.45 micrometer pores and is then normalized to a water temperature of 10C to eliminate the effect of viscosity. Its dimension seems strange at first, but it expresses the number of seconds it takes to pass an extra liter through the filter under the prescribed conditions. This MFI is or should be constant in time for constant water quality, as every subsequent liter would build up an additional layer of particles on the filter with the same properties, thus s/liter per liter passed. A value of 2.0 is generally chosen as required quality (i.e. particle content) for these types of wells. The MFI should be measured in practice.

Finally, the evaluation of the so-called thermal radius is often of limited importance for SB-ATES systems, because filter screens are configured above each other and, therefore, tend to impact neighboring wells much less than ordinary ATES doublets do.

The thermal radius of doublet wells is computed by comparing the total seasonally injected heat with the space it occupies in the subsurface around the well, or rather between the infiltrating and extracting well during one season. The required distance between the wells of a doublet is three times this thermal radius r_{th} according to current permits.

With V the total volume injected during one season, ϵ porosity and $\rho_w c_w$ and $\rho_s c_s$ the volumetric heat capacities of water and solids respectively, and H the effective thickness of the injected volume, the thermal radius thus follows from:

$$V\rho_w c_w = H(\epsilon\rho_w c_w + (1-\epsilon)\rho_s c_s)\pi {r_{th}}^2 \tag{4.4}$$

Equation 4. 4 leads to:

$$r_{th} = \sqrt{\frac{V}{H\pi}\frac{\rho_w c_w}{(\epsilon\rho_w c_w + (1-\epsilon)\rho_s c_s)}} = \sqrt{\frac{V}{\epsilon H\pi}\frac{\epsilon\rho_w c_w}{(\epsilon\rho_w c_w + (1-\epsilon)\rho_s c_s)}} = \sqrt{\frac{V}{\pi\epsilon HR}} \tag{4.5}$$

Where R is the so-called retardation, the factor that the thermal front is delayed relative to the injected water.

For SB-ATES systems, we may define another thermal radius assuming half spherical flow from the top and bottom of the screens assuming they hit the top and the bottom of the aquifer.

$$V\rho_w c_w = (\epsilon\rho_w c_w + (1-\epsilon)\rho_s c_s)\frac{2}{3}\pi {r_{th}}^3 \tag{4.6}$$

$$r_{th} = \sqrt[3]{\frac{3V}{2\pi}\frac{\rho_w c_w}{(\epsilon\rho_w c_w + (1-\epsilon)\rho_s c_s)}} = \sqrt[3]{\frac{3V}{2\pi\epsilon R}} \tag{4.7}$$

Which is easy to estimate and gives an impression of the radius of the bubbles. If the aquifer is anisotropic then the coordinates must be transformed so that the thermal radius in *r*-direction will be different from that in *z*-direction. A vertical anisotropy yields wider and thinner bubbles, lower anisotropy values leads to a larger vertical conductivity and as a result the water escapes to neighboring layers making the bubbles thinner. The opposite result has when the vertical anisotropy takes large values, in this case the vertical conductivity is low and as a consequence more water flows horizontally in the layer making the bubbles wider.

4.4. ASSUMPTIONS FOR THE REPRESENTATION OF THE CASE-STUDIES

The following assumptions were made to allow building a successful model:

1. The model for all cases consists conceptually of three geologic layers, the cover layer, the aquifer layer, where the screens are located and the semi-confined bottom layer which is present at some distance below the deep screen. The actual model, however, has a large number of model layers that subdivide the previous geologic layers to make sure the computations are accurate. Details about the grids were given in chapter 3.
2. The developed model assumes radial symmetry. A cross sectional model is converted to axially symmetric model by the mfLab toolkit by automatically adapting the input fed into the finite difference codes.
3. Due to the choice of using only axisymmetric models, ambient groundwater flow cannot be taken in account.
4. Brackish water is not present
5. The operation schedule as defined above, with monthly constant injection and extraction rates, are taken the same in all simulated years.
6. The systems are simulated for a 5 year period. Simulation periods of up to 30 years have been used, but it turned out that 5 years were sufficient to reach a final thermal efficiency.
7. The configuration operates with a constant temperature difference of mostly 8^0C between the cold and warm wells.
8. The diameter of the wells is 800mm. In the model the well always is in the first column of the model grid. The size of that columns equals the well radius that was actually used. This depends on the grid resolution, for which 1.0, 0.50 and 0.25 m were used. However, this choice does not affect the thermal efficiency of the wells.
9. The required capacity of the systems would be calculated based on equation 4. 2, assuming a water heat capacity of 4.18 kJ/ (kg ^{0}C) and a water density of 994.2 kg/m^3. After discussing the available information we used the nominal capacity as implied by the system type and multiplied it by the factor Qfrac to obtain season-average injection and extraction flows. The Qfrac factors used were 0.25, 0.50 and 1.0. Aberrant situations may be interpolated.
10. For the simulations, a porosity of 0.35 was assumed for all the cases, the thermal conductivity for water is 0.58W/m^{0}C and for sand solids 1.76 W/m^{0}C, the dispersion was considered equal to 0.5 and diffusion coefficients equal to 0.1242.

4.5. PERFORMANCE ASSESSMENT

The performance of the SB-ATES systems is solely based on the achieved thermal efficiency, given the pre-defined operational schedule. Operational problems due to clogging, irregular outdoor temperatures, weather variations from year to year and even influences of climate change over for instance a 30 year simulation period are left out of the considerations, because in this study, we are only interested in the optimization of the separation distance between the well screens of SB-ATES systems.

4.5.1. Energy analysis, thermal efficiencies

There are different ways to calculate the energy efficiency of an ATES system.

One out of two basic approaches focuses on the amount of energy a building can use and the amount of energy that the building can obtain from its ATES system. The other basic approach focuses on the wells instead of the building as the main point of interest. It is then determined how much energy is injected and extracted from the subsurface, and energy efficiency is computed accordingly mostly over one complete year [3, 15].

Building perspective. The equations 4. 8 and 4. 9 describe the energy that is delivered to and from the building [3, 15]. Integration if taken over one or more seasons:

$$E_s^b = \int Q_s \cdot \rho \cdot c_p \cdot (T_e^{warm}(t) - T_{in}^{cold}(t)) \cdot dt \quad 4.8$$

$$E_c^b = \int Q_c \cdot \rho \cdot c_p \cdot (T_{in}^{warm}(t) - T_e^{cold}(t)) \cdot dt \quad 4.9$$

Where E_c^b and E_s^b stand for the charged energy and the supply energy from and to building in [J] respectively. Q_c and Q_s are the charged and supply discharged energy in [m^3/d], ρ is the water density [kg/m^3], c_p is the specific heat capacity of the water [J/kg/^{0}C]; T_e^{warm} and T_e^{cold} are the extraction temperatures from the warm and the cold filter screen respectively in [^{0}C], T_{in}^{cold} and T_{in}^{warm} are the injected temperatures of the cold and warm filter screens respectively and dt is the model time step [d].

Well perspective. Concerning the well's point of view, the energy efficiency of the supplied and charged well screen can be estimated respectively by the equations 4. 10 and 4. 11 [3].

$$E_c^w = \int Q_{in} \cdot \rho \cdot c_p \cdot (T_{in}(t) - T_o(t)) \cdot dt \quad 4.10$$

$$E_s^w = \int Q_{out} \cdot \rho \cdot c_p \cdot (T_{out}(t) - T_0(t)) \cdot dt \quad 4.11$$

In which E_c^w and E_s^w stand for the charged and supplied energy to and from the well respectively [J], T_{in} is the temperature of the injected water [^{0}C], T_{out} is that of the extracted water and T_0 is the temperature of the groundwater [^{0}C] and is taken as a reference temperature.

It should, however be noticed that any other than the groundwater temperature may be taken as reference, because ATES systems will alter the groundwater temperature in their surroundings to their mean temperature on the long run. This temperature then becomes a choice that is optimized by the designer of the ATES system, and may be higher or lower than the average temperature of the original natural groundwater before ATES was installed. Therefore, this reference temperature should not be always set equal to the original groundwater temperature.

4.5.2. Thermal Efficiency of ATES systems

The thermal efficiency of the system based on the energy analysis is the ratio of the amount of supplied to over injected i.e. charged energy, relative to some reference temperature for which the initial groundwater temperature may be taken depending on the choice of the designer [3]. The efficiency expression is:

$$\eta_E = \frac{E_s^{b,w}}{E_c^{b,w}} \qquad 4.12$$

Based on the sensitivity analysis (Chapter 6), a value of 0.65 may more useful for smaller systems that generally have a somewhat lower efficiency.

4.6. SUMMARY

This chapter presents the case-studies that were used in this study based on which the model is designed. The operational schedule which is applied in the elaboration was presented. The assumptions underlying the model were specified and some quantities often encountered with ATES systems were defined. Finally, the energy performance was defined, including a minimum acceptable efficiency of 65%, to allow comparison between scenarios which are examined in subsequent chapters.

CHAPTER 5

5. Calibration – Hydrological Parameters

The horizontal conductivities of the various layers for the considered real-world cases were estimated by applying the Kozeny-Carmen equation and a fixed porosity of 35% on the reported grain sizes that were determined during drilling. However, the vertical conductivities are unknown, yet are essential to determine the efficiency of SB-ATES systems. In this chapter, we optimize the mean vertical anisotropy, i.e. the horizontal over vertical conductivity, for all aquifer layers of each case by automatic calibration. The amount of information that is available from the capacity tests is extremely limited, in fact, only the drawdown after 60 min is independently available because drawdown measurements at earlier times yield the same information. Furthermore, because of the reciprocity principle, the capacity test at the second screen does not add any extra information to that on the first screen. This conclusion is fundamental. The drawdown inside the pumping screen only gives information about the skin at the borehole or in the gravel pack, but this information is not used in this thesis, because it is irrelevant for the thermal efficiency of the SB-ATES systems.

Because of the above, we have for each system only one independent measurement from the capacity tests. Therefore, per SB-ATES system, only one parameter can be calibrated with the available information. The average vertical anisotropy was chosen as the parameter to calibrate as it is the most important hydraulic parameter for the energy efficiency of SB-ATES systems. The reason is that vertical anisotropy determines the potential for short-circuits between the two screens.

This overall vertical anisotropy was calibrated using a numerical axisymmetrical finite-difference model available in the mfLab environment; it is similar to MODFLOW. The model was made realistic by applying the conductivities of the layers as determined from the borehole grain sizes. This chapter reports the calibration and presents the obtained results:

- The calibration was conducted automatically. The reciprocity principle makes use of the upper screen drawdown equivalent of the lower screen drawdown as was explained in paragraph 3. 4. Hence, only one of the two capacity tests was calibrated.
- The model inputs were the horizontal conductivities as derived by the Kozeny-Carmen equation using the grain sizes from the soil profile data collected during the drilling of the borehole for each case.

For each SB-ATES system, a capacity test is available on both the shallow and the deep screen. The measurements show that the drawdown is already almost steady state after first head

measurement at 15 minutes, so only the last measured drawdown, at 60 min, was used in the calibration. The reciprocity principle implies that the capacity test on the shallow well screen whose drawdown is measured in the deep screen yields exactly the same information as the capacity test carried out on the deep screen with the drawdown measured in the shallow screen. Hence, the second capacity tests does not add any information with respect to hydraulic parameters of the aquifer. This is shown on the hand of the actual data in Appendix B.

Because of this behavior of the measurements, only steady-state simulations were used, both to verify the reciprocity principle and to determine the vertical anisotropy through calibration.

5.1. AUTOMATIC CALIBRATION OF THE AXI-SYMMETRIC NUMERICAL FLOW MODEL

Soil profile **d**ata with a recorded “average” grain size for distinct layers that were obtained by sampling during drilling, were made available by Installect. These grain sizes were used to estimate the hydraulic horizontal conductivities of distinct layers using the Kozeny-Carmen equation (paragraph 3. 2). These values can be found in Soil-Profile Textbook.

It is important to realize that the accuracy of the estimated hydraulic conductivities may be low because the Kozeny-Carmen equation ignores shape and roughness of the grains, while also porosity is uncertain, yet playing an important role in it. We nevertheless apply Kozeny-Carmen as our best possible proxy to the hydraulic horizontal conductivities of layered aquifers.

Because we only have a single numerical value in each case to calibrate onto, i.e. the drawdown of the capacity test after one hour of pumping, we can calibrate one and only one parameter for each of the cases. For this, we chose the most sensitive parameter for which we have no independent data, the average vertical anisotropy for all the layers combined.

The numerical model is applied to take into account details, such as partial penetration of the well screens, heterogeneity and refined modeling around the screen ends by using a finer grid. The calibration of the numerical model was done by optimizing the overall anisotropy by minimizing the difference between the measured and computed drawdown of one of the capacity tests after 60 minutes for each case. Thus, the horizontal hydraulic conductivities estimated by Kozeny-Carmen were not changed during the calibration; only the overall vertical conductivity was optimized.

The graphs in Appendix C show for each project the estimated horizontal conductivities for the layers encountered during drilling, together with the position of the screens. Very low conductivities indicate clay layers. Fig. 5 1 shows that in most cases the top screen is installed immediately below a clay layer directly, the so-called cover layer. Several cases also show a clay layer directly below the deep screen, like Fig. 5 2. Only in some of the cases, a low conductivity layer is present between the screens (B1GB, GT15KU, GT15PZC, GT20SM and GT25PV); most cases have no resistant

layer between the upper and lower screen. This implies that the screens are essentially in the same aquifer, which is also a policy of the permitting authorities. Fig. 5 1 and Fig. 5 2 show two examples.

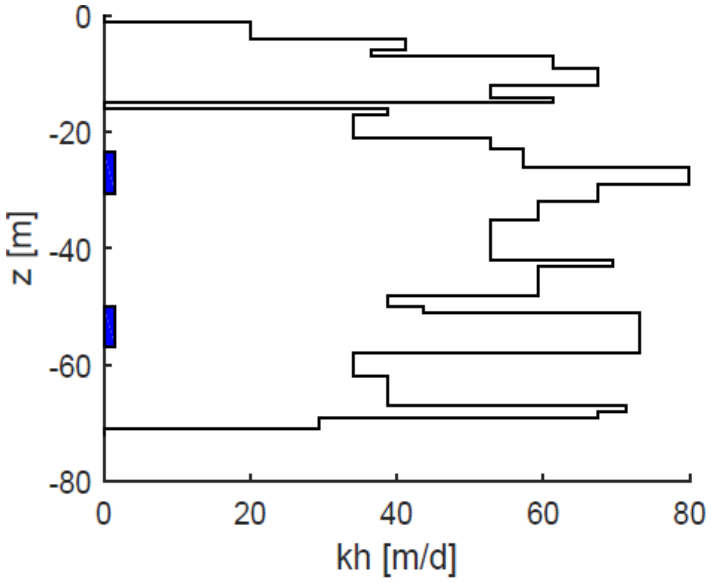

Fig. 5 1: Case GT20SM horizontal conductivity versa depth when the drawdown is 0.02m (Q=25m3/h)

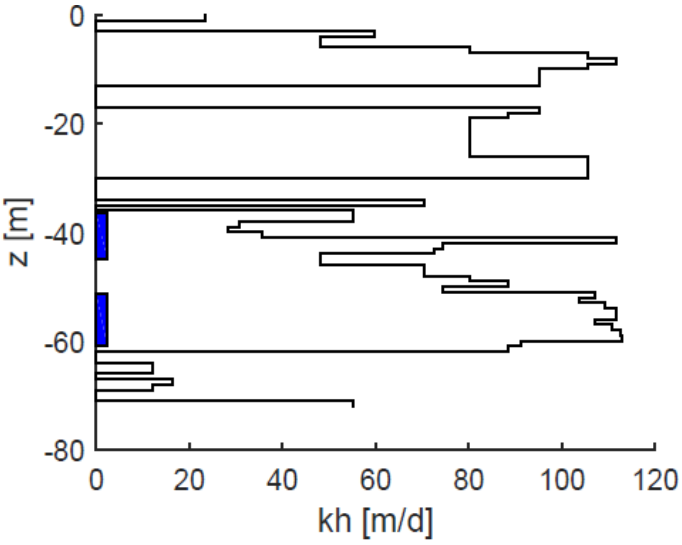

Fig. 5 2: Case GT20UG horizontal conductivity versa depth when the drawdown is 0.39m (Q=25m3/h)

In the actual aquifer, the layers will have a vertical conductivity that is different from the horizontal one. The ratio K_h/K_v is known as vertical anisotropy. Because we can optimize only one parameter, we optimize only the overall vertical anisotropy, i.e. we assume that the ratio of vertical to horizontal

conductivity is the same for all the layers of the aquifer, which, of course, is a very crude approximation of reality, to that we have to check its validity afterwards.

Thus, the automatically calibrated overall vertical anisotropies are listed in **Error! Reference source not found.**. The "Exitflag" in this table indicates which of the cases were difficult to calibrate by the non-linear optimization function in Matlab that was used for the purpose (lsqnonlin); when the "Exitflag" equals 1, the calibration finished without difficulty. When the "Exitflag" equaled 2, the system did not completely converge and, therefore, the obtained vertical anisotropy value is uncertain. The cases with "Exitflag" equaling 2 were eliminated from further elaboration, because the calibration was considered not accurate enough.

Table 5. 1: Calibrated anisotropies

Case study	Anisotropy	Discharge Q [m3/d]	Measured 60 min drawdown [m]	Computed drawdown [m]	Exitflag
B1GB	1.60	600	0.06	0.06	1
GT15KU	37.5	600	0.08	0.08	1
GT15M	2.90	600	0.14	0.14	1
GT15PZC	111	600	0.01	0.01	1
GT15ULR	0.36	600	0.11	0.11	1
GT20CCU	0.023	600	0.12	0.12	1
GT20SM	226	600	0.02	0.02	1
GT20UG	0.014	600	0.39	0.58	2
GT20VWG	10	600	0.03	0.06	1
GT20WA	3.1E-06	600	0.09	0.10	2
GT20WW	0.53	600	0.13	0.13	1
GT25-2KPA	10	600	0	0	1
GT25GV	6.67	600	0.14	0.14	1
GT25NBDA	7.96	600	0.01	0.01	1
GT25PV	0.011	600	0.07	0.07	1
GT25RH	0.00033	600	0.42	0.67	2
GT25TB	0.56	600	0.06	0.06	1
GT25VA	3313	600	0	0	1

It can be seen that the average anisotropy in Table 5. 1 for the most of the cases is not within the presumed probable range of 2 to 10 for sandy layers. Some cases have a higher to much higher anisotropy than 10. We explain this by assuming that in these cases there are some thin clay lenses or layers present that have been overlooked during the drilling. This situation will be encountered in practice quite regularly as, such thin layers will generally not be visible in the samples taken during the rotary drilling methods applied. Such layers are probably less important for the design of SB-ATES systems as they will generally raise their thermal efficiency, which we will check later in chapter 7. Other cases, however, show an anisotropy that is much lower than

1.0, which is physically impossible with horizontal layers as encountered in the aquifers of the cases. However, all the cases with lower than 1.0 anisotropy show a layer between the screens that has been attributed a low conductivity by the Kozeny-Carmen equation, as if it was a clay or loam layer. If in reality this is not a low-conductivity layer but actually sandy, at least on a scale that is relevant for this analysis, then the measured drawdown obtained in the capacity tests is too low for the situation with the presumed clay layer; the calibration tries to compensate this by raising the vertical conductivity of all the layers through reducing the anisotropy. Hence these low values.

Because the Konzeny-Carmen derived conductivities are the only independent information next to the capacity-test drawdown, we have to accept these conductivities as the best initial guess. However, it is certain that the values are not correct for every layer. In the end, they were computed from hand-estimated grain sizes, which may be far off in some cases, especially when fine-grained sediments are concerned. In conclusion, the cases with too-low anisotropies are deemed low due to too low conductivities of some layers in the profile, which subsequently dominate the flow in the model, but not in reality.

From the above it follows that is allowed to “correct” these low-conductivity layers within the aquifer for the cases with these lower than 1.0 anisotropies. The question is then to what value to change the conductivity of these low-conductivity layers? From various possibilities we choose to take the average of the conductivities of the layer directly above and below the low-conductivity layer, after which these cases were recalibrated for an improved vertical conductivity value, the results of which are in table 5. 2. The resulting anisotropies now vary from 2 to 10 for all these recalibrated cases. This range is expected, as it is commonly used as a rule of thumb for the calculation of the vertical hydraulic conductivity.

Table 5. 2: Calibrated vertical anisotropy after an interlaced clay layer in the cases that initially had calibrated anisotropy lower than 1.0

Case study	Anisotropy	Reciprocity input drawdown [m]	Computed drawdown [m]	Exitflag
B1GB	9.47	0.06	0.059997	1
GT15ULR	7.61	0.11	0.110001	1
GT20CCU	5.74	0.12	0.019942	1
GT20WW	2.1	0.13	0.129957	1
GT25PV	5.57	0.07	0.069991	1
GT25TB	4.3	0.06	0.060059	1

The previous paragraphs show that physically realistic anisotropies may be estimated from the available data. But also, that the actual values will be uncertain because only one overall value may be determined based on the available amount of information (one drawdown value per case and the Kozeny-Carmen derived conductivities) and the uncertainty to express the conductivity of

any layer by a grain-size estimate from muddy samples during coarse open-hole rotary drilling, in which many a thin layer will remain unseen. Another source of uncertainty is no doubt the sensitivity of the Kozeny-Carmen equation for porosity, while no field estimates of porosity are available. And, finally, that the actual vertical anisotropy will be different for each of the layers comprising the aquifer.

It is, therefore, that the optimization of the vertical separation between the two screens of the SB-ATES systems will be estimated using a sensitivity analysis on a well-determined representative aquifer system, while the results will be tested on the data for the actual cases to verify the practical usefulness of the results (in chapter 7).

How useful are then the capacity tests for the estimation of hydraulic parameters? Although these test provide little detailed information, it can show that there is a high resistance between the two screens or not. This allows judging whether some interlaced clay layers or clay lenses went unseen by the samples taken during drilling or if an interlaced clay layer that was noticed during drilling actually provides a significant vertical resistance or not. This information by itself is valuable and a check on the conductivity values obtained from applying the Kozeny-Carmen equation on the registered grain sizes. In fact, for a sandy aquifer, any estimated anisotropy lower than 1 and higher than 10 should be considered a warning that something is not consistent with the estimated horizontal conductivity distribution.

5.2. CONCLUSIONS

The reciprocity principle is fundamental, and makes that the second capacity test carried out on every newly installed SB-ATES system does not add new information to the first, except for the skin at the well face, but skin does not affect thermal efficiency.

This chapter showed that calibration is limited to only one parameter value per case due to the extremely limited information (one capacity-test drawdown value) to base the calibration on. Therefore, only the most sensitive parameter, i.e. the overall vertical anisotropy was calibrated by matching the model with the capacity-test drawdown value, while assuming the Kozeny-Carmen derived conductivities were assumed correct. Anisotropy values larger than 10 for the sandy aquifers were then deemed to be caused by thin clay lenses or layers that are undiscovered in the muddy samples of the applied rotary drilling, while the physically impossible values lower than 1.0 were deemed due to interlaced clay layers in the drilling profile that actually behave as sandy layers, i.e. being lenses or due to unrepresentative grain sizes registered during drilling. When such layers, mostly only one per case, was adapted to sand, an anisotropy in the feasible range between 2 and 10 was obtained.

The high uncertainty of the Kozeny-Carmen derived conductivities is not important by itself as the thermal efficiency is independent on the average hydraulic conductivity. This fact will be utilized in the sensitivity analysis of chapter 7. The impact of the distribution of the horizontal conductivities on the thermal efficiencies will be tested in the same chapter as well.

Regarding the location of the screens, no relation was found between the cases. However, in all the cases, there was a clay layer on top of the shallow screen. Thus, it was assumed that the top of the shallow screen is immediately below the bottom of the cover layer. In some of the cases, a second clay layer was also present below the deep screen and consequently it was assumed that both filter screens are located in the same aquifer. For most cases the depth of the aquifer is unknown from the borehole.

Due to the lack of information concerning the vertical conductivity, an acceptable anisotropy range for sandy aquifers is presumed between 2 and 10. Values greater than 10 can be explained when a clay layer might be overlooked. When the anisotropy takes very small values, it can be the result of a horizontal conductivity overestimation in one or more layers. Thus, it is suggested grain size samples to be collected in short distance during the drilling.

CHAPTER 6

6. Sensitivity Analysis

In Chapter 6 a sensitivity analysis was conducted, examining various parameters that can influence the performance of the SB-ATES systems. The parameters that were investigated are the vertical anisotropy, the operational capacity and the separation screen distance. The aim of this analysis is to optimize the separation screen distance of warm and cold well for the SB-ATES systems in terms of efficiency. An axial symmetric model was developed for this purpose using MODFLOW and MT3DMS, in MATLAB environment. Initially, the model is verified for axially symmetry, and afterwards a 3D grid is developed in order to handle the different models of the sensitivity analysis simultaneously, as each row of the grid is occupied by one axial-symmetric model. The steps that are followed for the sensitivity analysis are the following:

1. Presentation of the sensitivity analysis (paragraph 6. 1) and the axial symmetric model (paragraph 6. 2)
2. Investigation of the grid resolution (paragraph 6. 3)
3. Verification of the model's axial symmetry (paragraph 6. 4)
4. Setup of the sensitivity analysis (paragraph 6. 5)
5. Results of the sensitivity analysis (paragraph 6. 6)
6. Conclusions (paragraph 6. 7)

6.1. INTRODUCTION OF THE SENSITIVITY ANALYSIS

This chapter covers the sensitivity analysis and may be considered the most important chapter of the thesis. It's called sensitivity analysis because we will simulate the three SB-ATES systems in a standardized, yet representative geohydrological context, and do this for a range of parameter values that most determine the thermal efficiency of an SB-ATES system. The main objective is to obtain curves of thermal efficiency versus screen separation for the three system types, i.e. GT15xx, GT20xx and GT25xx, and within each type for three vertical anisotropies and three operational schemes. The latter is simplified to three values of the factor Qfrac that relates the installed nominal capacity of each of the systems, i.e. 15, 20 and 25 m3/h to the seasonal average value applied in reality. These Qfrac factors are chosen to be 0.25, 0.50 and 1.00. The injection and extraction will be constant in time but injection and extraction screens switch after every season; a season lasts exactly half a year and, therefore both the winter season and summer season are of equal lengths. The result will be 9 figures, each combining one value of anisotropy and one value of Qfrac. Within each of these figure there will be three sets of two graphs showing thermal efficiency versus screen separation. Each set belongs to one of the system types. For each of the system types there is a separate graph for the efficiency of the warm screen and one for that of the cold screen. These figures comprise the full scope of the results of the sensitivity analysis and can be used to read the required screen separation for each type for each of the three anisotropies and each of the three operational modes, i.e. their Qfrac value. In conclusion,

we are not using the derivative of the efficiency versus each of the parameters as is normally the result of the sensitivity analysis, but the efficiency itself. The derivatives can be extracted from the results but do not supply useful additional information to answer the question at hand. Nevertheless we call this procedure a sensitivity analysis as it simulates the SB-ATES systems for a range of values for each of the chosen parameters. A detailed description of the setup and analysis is given further down in this chapter.

We will simulate the SB-ATES system with an axially symmetric model using MODFLOW and MT3DMS. The axisymmetry is guaranteed by the mfLab environment that generates MODFLOW and MT3DMS input that will simulate an axisymmetric model in a row of the 3D finite difference grid. Because one such model occupies only one row in the 3D grids of these codes, we can simulate as many axisymmetric models simultaneously as required for the sensitivity analysis. To prevent mutual influence between these models in the same grid, we use one grid row of inactive cells between each pair of rows that contain a model.

We will first verify the model by simulating an SB-ATES system that is vertically symmetrical. This system has a cover layer at the top, a confining layer at the bottom and an aquifer in between with the top screen immediately below the cover layer and the bottom screen immediately above the confining layer at the bottom. Without viscosity and density effects, the efficiency of the warm top screen and the cold bottom screen must approach to the same efficiency over time. We will investigate the different methods to compute the advection by MT3DMS as this turns out to be critical. We end up with using the finite difference method as the only one that yields consistent and plausible results. However, the FD method is highly sensitive to numerical dispersion. This forced us to experiment with more refined grids, ending with a resolution of 0,25 m for the thickness of the aquifer layer and the cells near the well. We carried out the sensitivity analysis with three model resolutions, 1.00m (our original model), 0.50 m (the in-between resolution) and 0.25 m the finest resolution, which we also based our conclusions on.

The sensitivity analysis was done with a standardized subsurface. We chose the same cover layer, sufficiently thick to prevent interference from ground surface. We further chose a confining layer at the bottom of the same thickness as the cover layer. The thickness of the aquifer in between was chosen equal to the largest aquifer thickness deduced from all the actual case studies that were provided by Installect for this MSc study, i.e. 70 m. Cover layer, aquifer and confining layer at the bottom of our geohydrological system are all homogeneous but with a given anisotropy. The conductivity of the layers was chosen a priori as an overall average over all actual systems because the conductivity as such does not affect the results, only the vertical distribution of conductivities of the sublayers in the system has such an effect, together with the anisotropy (which may also differ per sublayer). Therefore, we cannot verify the impact of this distribution of conductivities within this sensitivity analyses. However, we will test the generality of the obtained results in the chapter 7, by comparing the efficiencies of the 18 actual systems with those obtained in the sensitivity analysis and discussing our interpretation of deviating results.

6.2. FLOW AND TRANSPORT NUMERICAL MODEL

An axially symmetric model was chosen over a full 3D model because of its simpler applicability than a full 3D model, but more importantly because the simulation time of a full 3D-flow and transport model is several orders of magnitude larger and would make a sensitivity analyses essentially impossible [4, 32].

Because the main scope of this work is to investigate the necessary separation between the two screens of an SB-ATES system in the same aquifer we consider, the ambient groundwater flow to be zero, which is also a requirement for application of the axisymmetric model.

This model can deal with an arbitrary number of sublayers, each with its own horizontal and vertical conductivity, but it cannot really cope with random spatial inhomogeneities, as the subsurface of the axially symmetric model must be the same all around the well. Therefore we ignore spatial inhomogeneities other than layering, its inclusion through hydrodynamic and numerical dispersion.

The boundary conditions of the model applied in this thesis is always a fixed head at the outside of the model, which was chosen to be 500 m, with no fixed heads at the top and the bottom of the model. The same boundary conditions were applied for the transport model. The boundary at 500 m distance is sufficient to not affect the flow near the well where the seasonal storage takes place. The so-called near field of the two screens is about the thickness of the aquifer, i.e. 70 m. The boundary condition at the well screens is a fixed flow condition, while the vertical conductivity inside the screens was set to a high value of 500 m/d to limit head difference within each screen. The first column is assumed to match the well's borehole. Therefore, the cells of the first column outside the screen were set to inactive as to represent the casing of the well, which is impervious.

The simulations were all done in steady-state, but the flow switches at the end of every season. The steady state simulation is sufficient because the flow that is caused by the screens, which always pump the same but opposite amount is steady within a few minutes due to the low elasticity of the subsurface. Over a season, therefore, flow transients are completely negligible, which allows for a steady-state simulation.

Simulations have been carried out for up to 30 years, but the results showed that a final efficiency was already obtained within 5 years. Therefore all further analyses, including the sensitivity analysis were done with a simulation period of five years; the final efficiency, i.e. that after five years was used for further analysis and interpretation.

The said thermal energy efficiency of the two screens was used to assess the results [23, 32]. Often the aquifer reaches below the bottom screen, while the top screen touches more or less the overlying cover layer. This implies that often the lower screen has more aquifer space around it than the top screen which may lead to a somewhat higher efficiency for the bottom screen than for the top screen. For this reason both efficiencies are always evaluated and presented. We will see that the difference is actually very small.

The thermal efficiency is always computed over a full year and temperatures are considered relative to the mean of the injection temperatures of the warm and the cold screen, i.e. not relative to the initial groundwater temperature, although in our analyses these were actually the same. The thermal efficiency equals extraction temperature minus the reference temperature integrated over a full year divided by the injection temperature minus the reference temperature also integrated over a full year. This is true for both the warm and the cold screen. Each yielding its own value, which can be computed at any moment after the first simulation year to yield a continuous curve.

6.3. GRID RESOLUTION

The transport model has different methods to compute advection. The different advection methods were tested. However, it proved impossible to obtain consistent and plausible values when using the TVD and MOC methods for advection in a larger number of axi-symmetric models. The results were simply irregular, without a consistent pattern. Only the simplest method to compute advection, the finite difference method (abbreviated to FD) yielded plausible and consistent results in all cases that we tried. For this reason, the FD method had to be chosen as the only feasible method for the axisymmetric models at hand.

However, the FD method is highly sensitive for numeric dispersion, and, therefore, the outcomes are potentially strongly dependent on the size of the grid cells of the model. The influence of the grid resolution on the computed thermal efficiencies was therefore tested.

Our initial grid resolution was 1 m for the thickness of the layers within the aquifer and about 1 m for the column width near the well, slowly increasing with distance from the well. To investigate the impact of numerical dispersion, we tested our model with two finer grid resolutions, i.e. 0.50 m and 0.25 m. Further refinement was prohibitive given the enormous computation times and memory demand involved. The sensitivity analysis for the three grids took about 30 minutes, 2 hours and 10 hours computation time and the test with the 18 actual cases in chapter 7 took even 2.5 times as long. It was decided to accept the 0.25 m grid, also because the numerical dispersion should come in the neighborhood to the size of actual aquifer inhomogeneities, so that further refinement would not necessarily improve the results from a practical more real-world point of view.

The finer the grid, the higher were the attained thermal efficiencies, but the differences were quite limited. The higher thermal efficiencies for the finer grids are attributed to less numerical dispersion and, therefore, less mixing in the subsurface according to the model.

In the end we have done the simulations with all three grids so that the results may be directly compared as is done further down.

The actual vertical grid resolution that was applied in the sensitivity analysis was 5 m for the cover layer and the confining layer at the bottom and 1.0 0.5 and 0.25 m respectively for the aquifer layers.

The horizontal grid was compute using the sinspace function available in mfLab. It computes column width according the sine function where the beginning and end real world coordinates and the beginning and end sin-function arguments can be specified together with the desired number of points.

```
xGr = sinespace(0,500,51,pi/50,pi/2);  % Coarse grid
xGr = sinespace(0,500,101,pi/50,pi/2); % Medium grid
xGr = sinespace(0,500,201,pi/50,pi/2); % Fine grid
```

The only difference in the three calls that generate the coordinate of the column boundaries is the number of points. All three grids have the same outer radius of 500 m. To compute the coordinates it uses the sin function between pi/50 and pi/2. This implies that the grid size slowly increase near the well and becomes a constant near the outer boundary. The grid obtained by this sinespace function is generally better suited for axisymmetric models compared to logspace function.
The widths of the first 8 columns generated by the sinespace function are shown below:

```
1.3888  1.8312  2.2721  2.7110  3.1475  3.5812  4.0118  4.4390
0.5857  0.6979  0.8099  0.9217  1.0334  1.1448  1.2559  1.3668
0.2652  0.2934  0.3216  0.3498  0.3780  0.4062  0.4343  0.4624
```

The widths of the last 8 columns in the three grids are as follow:

```
14.6321 14.7300 14.8150 14.8871 14.9461 14.9921 15.0249 15.0447
 7.4863  7.4989  7.5098  7.5190  7.5266  7.5324  7.5366  7.5392
 3.7669  3.7685  3.7698  3.7710  3.7720  3.7727  3.7732  3.7736
```

The obtained efficiencies over simulations in the sensitivity analysis for the three grids were stored as three columns in the file that specifies the parameters used in the sensitivity analysis. This allows to compare the results by means of an Excel Pivot table. From the 130 models simulated for the sensitivity analysis for each of the grids, we selected the values for Qfrac=0.5, anisotropy = 2.0 and screen separations 3L, 4L and 5L where L is the screen length pertaining to each of the three system types GT15xx, GT20xx and Gt25xx which are 5, 7 and 10 m respectively.

Table 6. 1: Thermal efficiencies after 5 years computed for the three grids using Qfrac=0.5 (ratio of season average flow over installed pump capacity), Anisotropy=2.0 and screen separations 3L, 4L and 5L with L the screen length pertaining to each of the three SB-ATES systems

	Separation	Coarse Grid	Medium Grid	Fine Grid
GT15xx	3L	42%	45%	47%
GT20xx	4L	58%	61%	63%
GT25xx	5L	68%	71%	72%

The results, in Table 6. 1, show that the finer the grid the higher the efficiencies. But it also shows that the difference is small especially between the medium and the fine grid. Although it is not completely certain that the maximum of the efficiencies is computed with the 0.25 m resolution grid, it was accepted as our tool for further analysis. The rest of the results can be found in Appendix D.

6.4. VERIFICATION OF THE AXIAL- SYMMETRIC MODEL

To verify the model and be assured that the model will produce plausible and acceptable results, we run it with a subsurface that is vertically symmetrical, which means that the a confining layer at both the

top and bottom were given the same thickness of 25 m with a 30 m thick aquifer in between and the screens placed at the same distance from the top and the bottom of the aquifer, while the only boundary was fixed head and temperature at *r=1000* m from the wells. Further, the operation was also symmetrical in that the warm and cold screen operated at the same flow for the same length of season and had injection temperatures that differ equally but opposite from the reference temperature. Without viscosity and density effects operating in the model, the thermal efficiencies of the warm and the cold well must then approach to the same value.

The input data is given in Table 6. 2.

Table 6. 2: Input data for verification of axial symmetry of the model

	Top layer		***Aquifer***	***Bottom layer***
Horizontal hydraulic conductivity [m]	80		80	80
Anisotropy [-]	10000		8	10000
Thickness of the layers [m]	25		30	25
	Shallow filter screen		***Deep filter screen***	
Filter screen length [m]	5		5	
Pumping Discharge [m^3/h]	15		15	
	Top	***Bottom***	***Top***	***Bottom***
Depth of screens [m]	-27.5	-32.5	-47.5	-52.5

Fig. 6. 1 shows the thermal efficiency of the cold and the warm screen simulated by this axial-symmetric model. The efficiencies of both screens tend to the same value as required in this vertically symmetric model. Based on this result, the model was accepted suitable for further analysis.

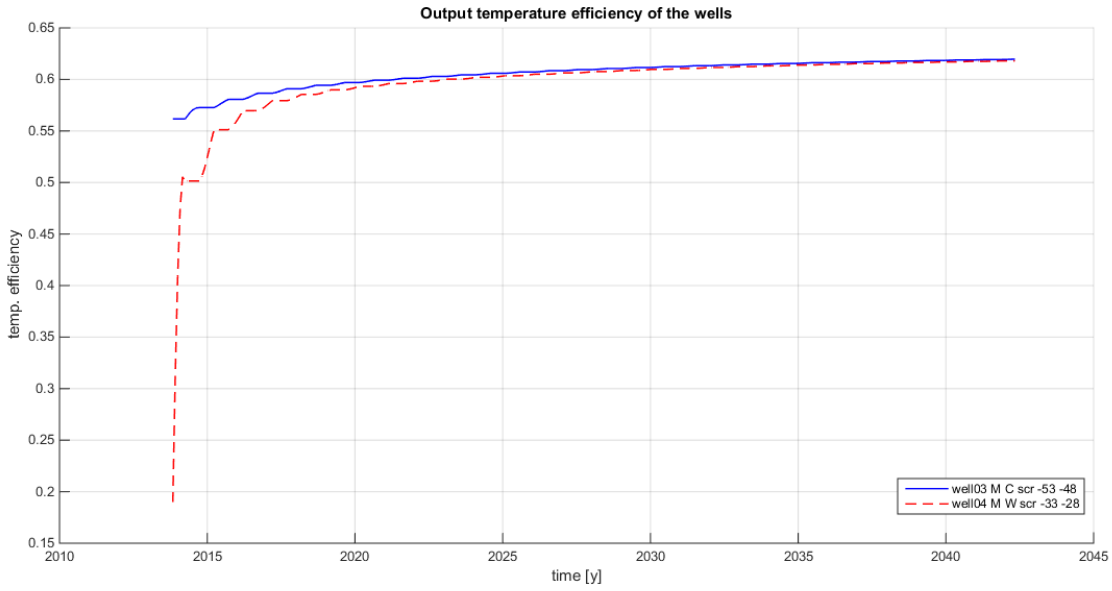

Fig. 6. 1: Verification of the axial-symmetry

6.5. SETUP OF THE SENSITIVITY ANALYSIS

The aim of the sensitivity analysis is to vary the relevant parameters such that from the result of a large number of simulations the optimal screen separation can be judged on the basis of the computed thermal efficiencies.

The idea is to generate curves showing efficiency versus screen separation for each of the three system types. We will generate these curves for three values of the anisotropy (2, 5 and 10) and for three values (0.25, 0.5 and 1.0) of Qfrac, the ratio of the seasonal average flow over the installed pump capacity that is implied for each system type, namely 15m3/h for GT15xx, 20 m3/h for GT20xx and 25 m3/h for GT25xx. This gives 9 separate figures each for a fixed combination of Qfrac and the anisotropy, where each figure has 3 pairs of efficiency-separation curves, one for each of the system types, and each pair has two lines, one for the cold screen and one for the warm screen. This gives in total 3 anisotropies x 3 Qfrac values x 3 system types x 5 separations = 135 axi-symmetrical wells each with its warm and cold screen. These models will be simulated simultaneously for a period of 5 years. The efficiency after 5 year simulation period is the sought result for further analysis.

Other variables will not be considered in the sensitivity analysis. For instance inhomogeneities and the effect of the distribution of the conductivities over the various sublayers. Hence the aquifer and the overlying and underlying confining layers will be homogeneous, yet anisotropic.

The influence of the conductivity of the confining layers is immaterial as it will be so low, we choose 0.001 m/d compared to the aquifer for which we choose 80 m/d that they do not influence the flow to any sensible extent. Of course, the confining layers interact with the aquifer through conduction. A homogeneous aquifer was use to simplify the analysis, i.e. to prevent too many degrees of freedom in the sensitivity analysis. The conductivity of this homogeneous aquifer is immaterial, as it does not influence the flow, which is completely driven by the prescribed injection and extraction flow of the screens. Of course, the distribution of hydraulic conductivities, both vertical and horizontal matter for the attainable thermal efficiency, yet we cannot take this influence into account in the sensitivity analysis. We will however test the results of the sensitivity analysis in chapter 7 by simulating the actual cases with their actual distribution of conductivities and comparing them with the results of the sensitivity analysis. We will then analyze and interpret any case that shows aberrant results.

We further ignore density and viscosity effects in the sensitivity analysis. This is generally done in practice as long as salinity is not involved as is the case with all case provided by Installect. We can investigate the influence of temperature induced viscosity and density by using SEAWAT instead of MT3D. This will be done in chapter 7 as well.

A last issue is irregular operations and mismatch between operations in successive seasons and years as well as an energy mismatch between the net storage of heat and cold between seasons. Irregular operations are beyond the scope of this thesis. They will always play a role in practice, but without concrete data from practice it seems not feasible to provide a useful and meaningful analysis here.

6.5.1. Defining a representative setting for the sensitivity analysis

To simplify the sensitivity analysis we had to generalize the subsurface over all cases to a cover layer followed by an aquifer followed by a confining layer at the bottom of the model. As explained above these layers were taken homogeneous in the sensitivity analysis. To prevent any interaction from upper an lower boundaries, the cover layer and the confining layer at the bottom of the system were taken 50 m thick, which is sufficient to prevent temperature changes in the aquifer to reach the top and the bottom of our system within the simulation period of 5 years.

The aquifer thickness was also taken the same for all 135 models in the sensitivity analysis, namely 70 m, which corresponds to the thickest aquifer encountered in any of the 18 case-studies provided by Installect.

The top screen was always placed immediately below the cover layer in the top of the aquifer. The position of the bottom layer depended on the separation. We ran all systems for 5 separations, indicated as 1L, 2L, 3L, 4L and 5L, where L is the screen length that pertains to the system type that is simulated, i.e. 5, 7 and 10 m respectively for the GT15xx, Gt20xx and the GT25xx systems. This means that the largest separation of GT25xx is 50 m so that with the top screen at the top of the aquifer, the bottom screen will touch the bottom of this 70 m deep aquifer. In all other case, the deep screen will soar above the bottom of the aquifer. This will cause some difference between the efficiencies of the two screens. Fig. 6. 2 gives a picture of the subsurface used in the sensitivity analysis.

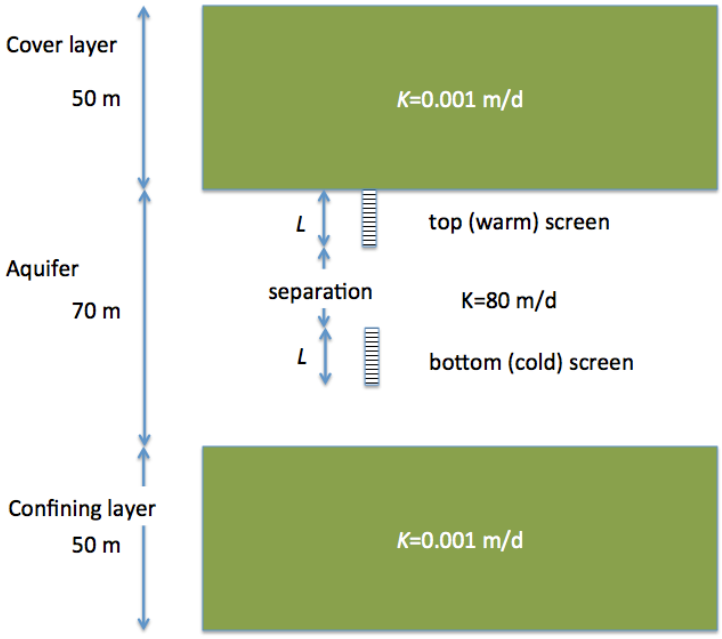

Fig. 6. 2: Geometry of the model use for the sensitivity analysis

6.6. RESULTS OF THE SENSITIVITY ANALYSIS

The results of the sensitivity analysis comprises the efficiency after 5 years simulation time, for all the wells and all the varied parameters, as it was explained earlier in this chapter. The results of the 135 cases that were simulated can be combined in a single figure consisting of 9 sub-figues as is shown in

Fig. 6. *3*. Herein is the anisotropy constant in each row of figures and the Qfrac in each column. For each combination of anisotropy and Qfrac there are three pairs of lines that show thermal efficiency versus screen separation. The green lines represent the results for the QT25xx systems, the read lines those for the Gt20xx systems and the blue lines those for the GT15xx systems. Each pair of lines has a drawn and a dashed line. The drawn line is for the cold screen and the dashed line for the warm screen.

It follows from the graphs that the efficiency of the warm and the cold screen are almost equal even though the lower cold screen generally has more aquifer space around it than the warm top screen, which always touches the bottom of the cover layer (see Fig. 6. 1).

The curves also reveal that the required separation distance for a given efficiency is almost the same for the different system types, especially for higher separations. This may seem strange, even unexpected at first, but it makes sense when one realizes that a GT25xx system with screen length 10 m and separation 30 m has more space to store heat than a GT20xx system with screen length 7 m and the same separation. This larger space accommodates storage of a larger volume. Just realize that the volume of a semi-spherical body (as a measure of the shape of the injected bubble) is $^2/_3 \pi r^3$, hence proportional to the third power of its radius. Therefore a bubble with a moderately larger radius stores a substantially larger volume.

As a main conclusion to be drawn from the graphs of the sensitivity analysis is that the required separation is virtually independent on the size of the system, this is the consequence of the graphs for the three systems falling on top of each other.

The required separation can now immediately be read form the presented graphs. For this we need to decide a criterion. The shape of the curves invite to separate a flat part in which the highest efficiency is almost reached from a steepening early part with clearly reduced efficiencies. Let us fix the criterion for now at 60%. Then for anisotropy 2.0 we need 24, 25 and 28 m separation respectively for the Qfrac values 0.25, 0.5 and 1.0. This invites using the same separation of say 25-27 m for all cases.

The situations with higher anisotropy require less separation. For anisotropy 10.0 the values would be 18, 19 and 20 m respectively for the mentioned Qfrac values. For the anisotropy 5.0 the values would be between these and the previous ones. However, it may be difficult to judge in practice what the exacted value of the vertical anisotropy is.

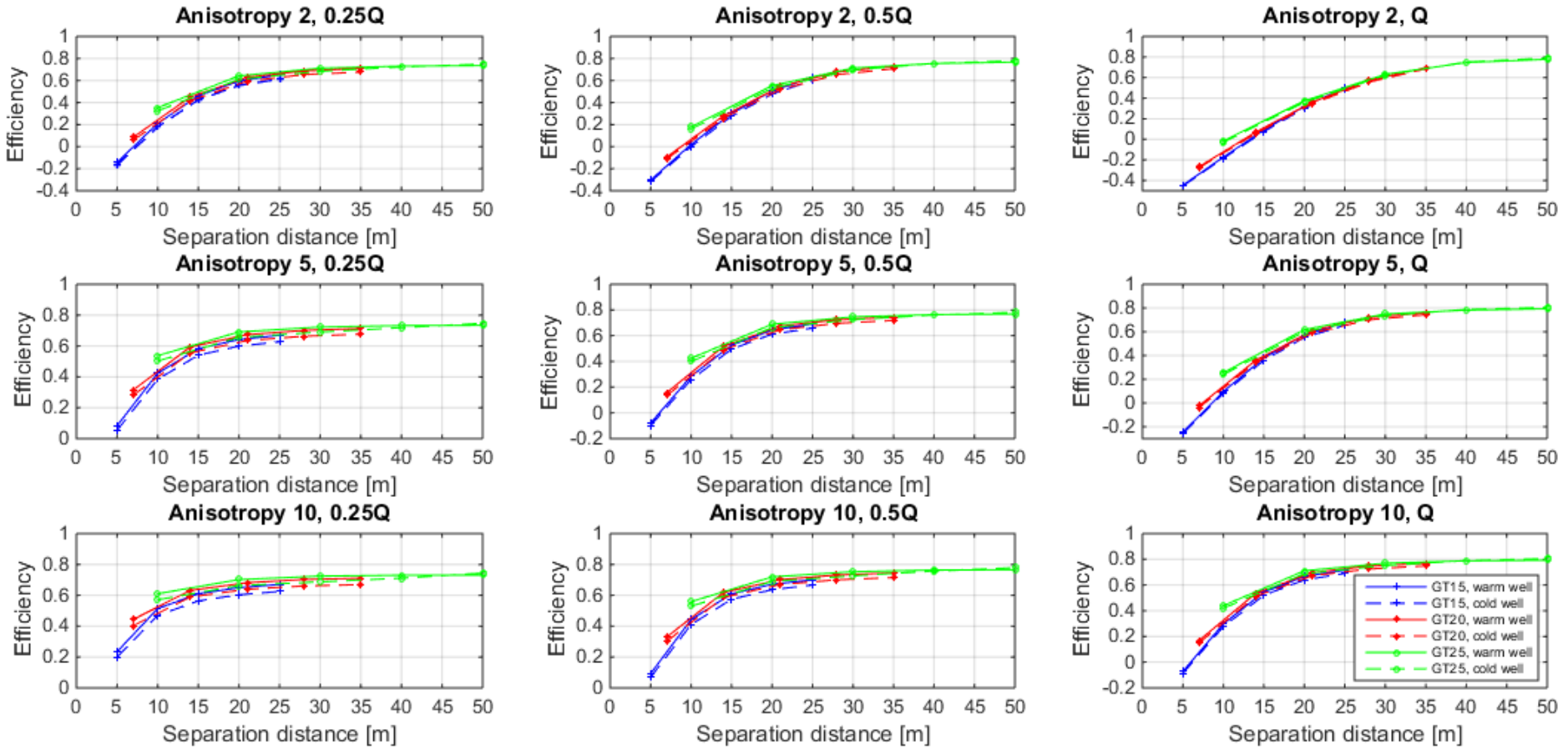

Fig. 6. 3: Sensitivity Analysis results

6.7. CONCLUSIONS

In this chapter, the sensitivity analysis and the evaluation of the sensitivity analysis were conducted to be obtain the optimum separation screen distance for SB-ATES systems. Three different grid resolutions were tested and the finest grid was selected to be used in the analysis as it gave the most accurate results. Three SB-ATES systems were examined, the GT15xx, GT20xx and GT25xx configurations. Each system type had a different full capacity and screen length. For each system type, nine cases were examined having different operational capacity and vertical anisotropy. In this analysis, 135 axial symmetric models were run and assessed simultaneously. The assessment of the cases was based on their thermal efficiency. The highest efficiency reached was independent on the system type when sufficient screen separation was applied. The anisotropy of the aquifer and the operation capacity were found to influence the performance of the configurations for shorter separation distances. For those shorter distances, the higher the anisotropy is, the more efficient the system becomes. But for large distances when interference is absent, a high anisotropy causes a loss of efficiency, because the bubbles will be more ellipsoid and therefore have a greater contact surface with the surrounding groundwater causing extra loss of energy. The Qfrac determines the size of the bubbles and therefore the higher its value the lower the efficiency is but only in cases of shorter distances, where interference is possible. In conclusion, the optimum separation distances when the anisotropy takes values of 2, 5 and 10 found to be at least 30m, 25m and 20m respectively.

CHAPTER 7

7. Evaluation of the sensitivity analysis results using real scale case-studies

The geo-hydrological setting used in the sensitivity analysis (chapter 6) was limited, as the influence of the actual distribution of the conductivities over the sublayers within the aquifer was not taken into consideration, instead chapter 7 deals with this parameter. The 18 case-studies for which an estimation of the horizontal hydraulic conductivity is available for each sublayer of the subsurface (these are the layers that can be found in the Soil-Profile Textbook, for which a grain size estimation was conducted during the drilling of the borehole) are being used to verify the applicability of the screen separation deduced by the sensitivity analysis in Chapter 6. As explained in Chapter 5, the conductivities were computed by applying the Kozeny-Carmen equation assuming a fixed porosity of 35%. Clearly, the results may still be a rough estimation of the conductivities because the Kozeny-Carmen equation does not consider specific ordering of the grains that depends on the sedimentation circumstances, neither grain shapes. Nevertheless, these estimated conductivities are our only concrete and independent information about the properties of the local subsurface. As all conductivities were estimated in the same uncertain way, one may presume that at least their relative magnitudes bear a reasonable relation with reality and so the use of the conductivities as estimated may reveal the impact of a non homogeneous aquifer on the thermal efficiency of an SB-ATES system.

In this chapter we will simulate the 18 case-studies provided by Installect for this study, applying their full conductivity distribution as explained and comparing the results to those of the sensitivity analysis in chapter 6, which was conducted with a homogeneous aquifer. Each case-study will be simulated for 3 values of anisotropy and 3 values of Qfrac exactly as was done in the sensitivity analysis.

It is expected that the output of the case studies will not deviate from the results of the sensitivity analyses (in Chapter 6). In the case of a small deviation, it will be due to the influence of the actual distribution of the conductivities over the aquifer layers. The cases with a substantial deviation will be further analyzed.

7.1. SETUP OF THE MODEL

The model setup in this analysis will be different for each of the cases. The sublayers, the position of the screens, the screen lengths and the screen separation pertaining to each of the

cases will be used without any modification. A problem arises regarding the bottom of the system, because the bottom of the aquifer was seldom reached by the borehole and, therefore, is considered unknown. It is expect the bottom screen position to be mostly defined by cost drilling rather than the actual depth of the aquifer, thus, we have assumed that there is 25 m of aquifer below the bottom of the lower screen in all the case-studies. Below the aquifer we have assumed a confining layer of 50 m thickness in all cases to allow exchange of heat with lower layers. This lower part of the aquifer was given the conductivity of the lowest aquifer layer for which a grain size value was available. The conductivity of the underlying confining layer was set to 0.001 m/d.

In the same way as in the sensitivity analysis, each case was simulated nine times, i.e. for anisotropy 2.0, 5.0 and 10.0 and for Qfrac 0.25, 0.5 and 1.0. All the models for the 18 case-studies were automatically simulated in a loop, each cycle of the loop simulated the nine models of each case-study.

7.2. RESULTS OF THE CASE-STUDIES

The results of these 18 cases are presented in Fig. 7. 1 together with the curves that were obtained in the sensitivity analysis.

Each case-study was simulated for 3 values of anisotropy and 3 values of Qfrac exactly as was done in the sensitivity analysis. In the 9 figures of the sensitivity analysis (Fig. 7. 1), the output of each case-study is presented by two points, on each figure, for the efficiency of the cold and warm well respectively. Furthermore, each actual case belongs to one of the three system types GT15xx, GT20xx and GT25xx. Therefore these dots are given the same system-type color as was used in the sensitivity analysis (blue for GT15xx, red for GT20xx and green for GT25xx) where a full dot is for the cold well and a hollow circle for the warm well.

In general the points representing the results for the case-studies coincide with the graphs obtained from the sensitivity analysis. Small differences can be attributed to the combined influence of the conductivity distribution and the actual screen length differing from the values used in the sensitivity analysis. Some of the results, however, show a large deviation with the sensitivity graphs

Regarding the cases with deviating results, there are some results that lie above the sensitivity curves and some that lie below it. Because the actual screen lengths do not deviate substantially from the standard values attributed to the system types, we will look for an explanation in terms of the conductivity distribution.

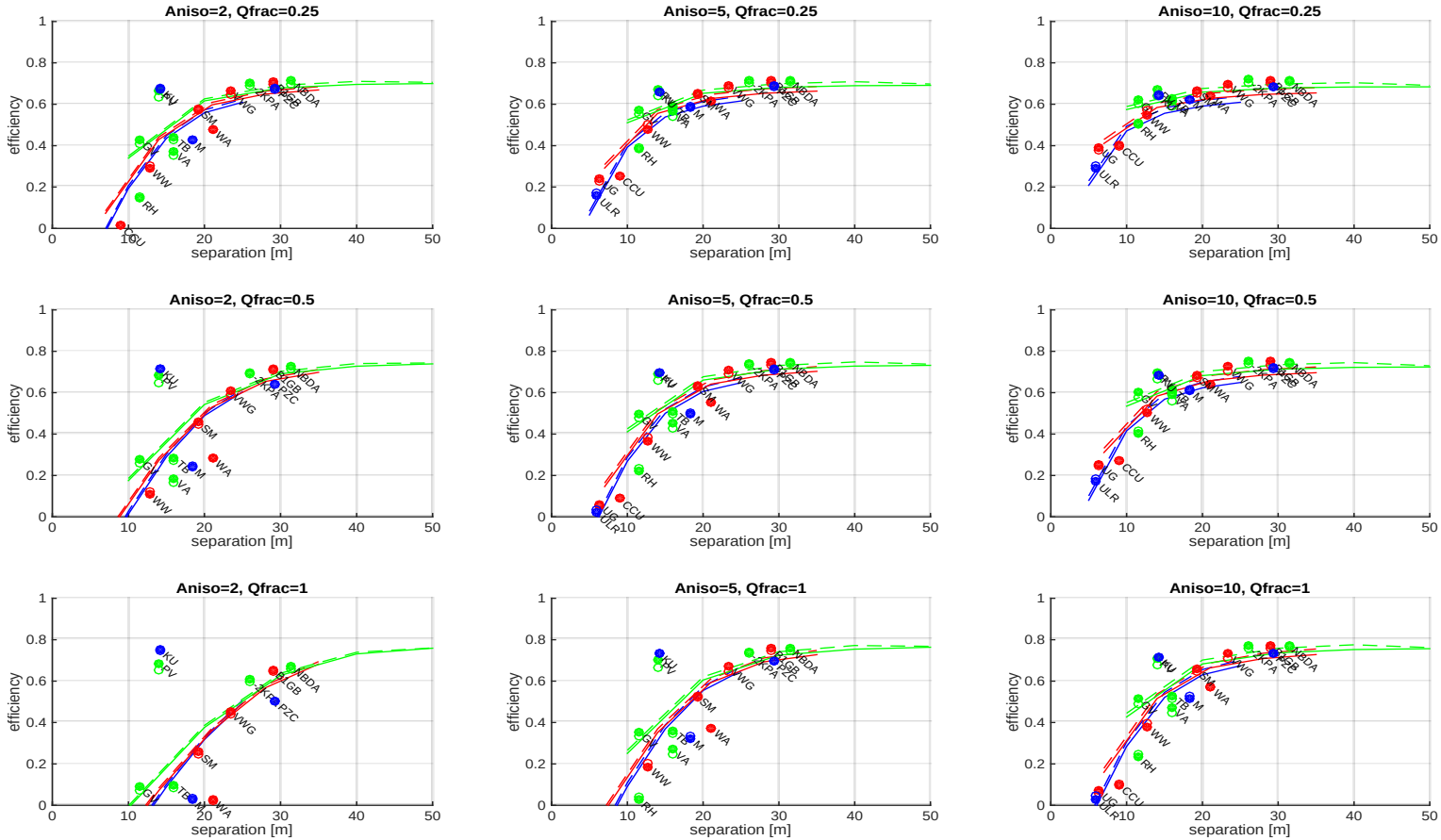

Fig. 7. 1: The efficiency after 5 years computed for the 18 actual cases (dots) for the same anisotropies and Qfrac values as the sensitivity analysis (graphs) where blue are the QT15xx systems, red the QT20xx systems and green the GT25xx systems. Full dots are the cold screens and hollow circles the warm screens. The actual cases are indicated with their name without their type prefix.

The most extreme cases are the GT15KU, GT25PV and GT20WA. Regarding the case-studies GT15KU and GT25PV, it can be noted that they perform better than the rest of the cases. This is due to the presence of clay layers between the filter screens. Specifically, the calibration for the case GT15KU showed a high anisotropy of 37.5 (Chapter 5, Table 5. 2), which means that clay layers are present which were overlooked during the drilling as it was concluded in Chapter 5, while regarding the GT25PV case-study the calibration showed a very low anisotropy less than 1 which is physical impossible with horizontal layers as encountered in the aquifers of the cases. The Kozeny-Carmen equation has attributed a low conductivity values in the layers presuming there is a clay layer.

In addition, the case-study with the lowest performance is the GT20WA. This case-study deviates from the sensitivity analysis results, having a lower performance than it was expected. This output is more pronounced in the case where the anisotropy equal to 2 and the system operates under full capacity. From the calibration an extremely low anisotropy value was obtained assuming the presence of a clay layer, however the performance of this specific case-study does not compensate with the calibration results (Chapter 5, Table 5. 2). Looking at the soil profile data, the filter screens are located in soil layers with lower permeability than the layers that are present between the filter screens (conductivities higher than 100m/d between the filter screens). Thus, it can be assumed that the measured capacity test drawdowns underestimate the situation presuming the presence of a clay layer, the calibration raised the vertical conductivity of all the layers through reducing the anisotropy, assuming clay layers.

7.3. EVALUATION OF THE RESULTS

Now that we have interpreted what causes the deviations from the sensitivity graphs for the three deviating systems we can illustrate the effects on the hand of the homogeneous model that was used for the sensitivity analysis (chapter 6). Hereby, the standard sensitivity situation is compared to one in which there is a resistant layer half way between the two screens and one in which a portion of the zone between the two screens has a conductivity that is substantially higher than that of the two zones around the screens in a vertical sense.

Along the process we will also demonstrate that the overall efficiency does not depend on the mean hydraulic conductivity of the aquifer. To check this, we will simulate a homogeneous aquifer with the distinct values of its hydraulic conductivity, i.e. with 20 and 80 m/d.

Fig. 7. 2 gives the simulated efficiency for four homogeneous models, the only difference between the models is the horizontal conductivity of the aquifer, which was 10, 20, 40 and 80 m/d respectively. The Fig. 7. 2 shows that the thermal efficiencies can be expected the same, irrespective of the overall conductivity of the aquifer, as expected; the deviation of the curves can be considered negligible. The efficiency of the cold well (drawn lines) is somewhat higher than that of the warm well (dashed lines) because the cold well has its bottom at some distance above

the bottom of the aquifer, whereas the upper part of the warm well touches the bottom of the cover layer.

The small deviations can be fully attributed to the small fraction of the flow that passes through the over and underlying confining layers, with conductivity 0.001 m/d that does not change between the layers. This effect is, in fact, negligible.

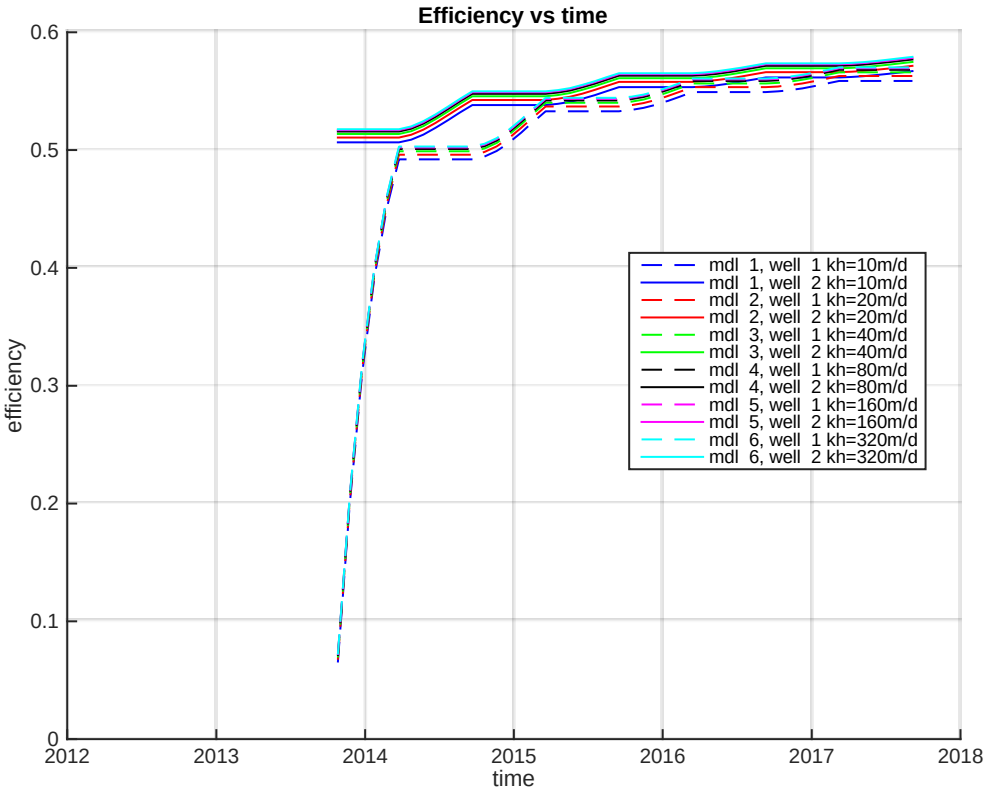

Fig. 7. 2: Thermal efficiency for four well as described where the only difference is the conductivity in the homogeneous aquifer (10, 20, 40 and 80 m/d respectively). The system is a Q20xx system with 7 m screen length and 21 m separation (3L) with anisotropy 2 and Qfrac 0.50. The aquifer is 70 m thick, both confining layers are 50 m thick. Head and temperature boundary fixed at r=500 m. Grid resolutions 0.1 m, longitude dispersivity also 0.25m, transversal dispersivity 0.1 of the horizontal one in both directions. Advection method finite differences. The time axis of the graph spans the 2nd through the 5th year of the simulation.

The second test shows the impact of a thin layer with a low conductivity between the two screens. The aquifer is homogeneous with 80 m/d horizontal conductivity except for one meter of thickness layer (kClay) halfway between its top and bottom with a conductivity of only 1 m/d. The results are shown in Fig. 7. 3.

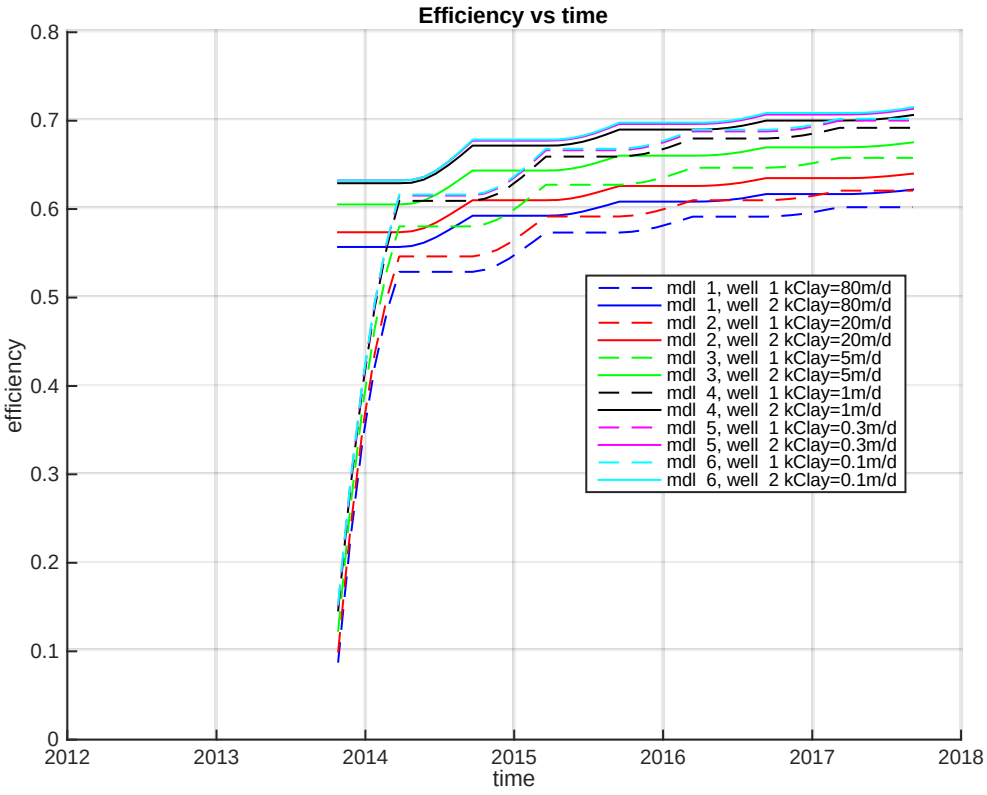

Fig. 7. 3: Thermal efficiency in homogeneous aquifer of 50 m thickness with a conductivity of 80 m/d with an 1 m thick layer of lower conductivity (kClay) in its center. GT25 systems, 10 m screen length at top and bottom of the aquifer. Anisotropy 2, Qfrac 0.5, medium resolution model. The time axis of the graph spans the 2nd through the 5th year of the simulation.

In Fig. 7. 3 the aquifer is homogeneous with conductivity of 80 m/d, but a 1 m of thickness layer halfway the two screens has a different, lower conductivity as shown in the legend of the Fig. 7. 3. The results show that the efficiency rises to lower the resistance of this thin layer, which was expected. Nevertheless, it should be clear that such a layer does not have an effect when the distance between the two screens is so large that they don't interfere with each other. In the current situation the distance is 3L, i.e. aquifer 50 m, screen length 10 m at top and bottom, which leaves 30 m separation screen distance. The non-interference separation is about 5 L as can be read from the sensitivity graphs (Fig. 7. 1).

The next test is the effect of a zone in the aquifer between the screens that has a higher conductivity than the zones at the top and bottom of the aquifer in which the two screens reside. Again we have an aquifer having 50 m of thickness but now it is divided in three horizontal zones of thickness 15, 10 and 15 m respectively. The conductivity of the zones (the layers where the screens are placed with a layer thickness of 15 m) is 10 m/d while the zone in the middle has a

varying conductivity among the tested models. The results are presented in Fig. 7. 4 the legend of Fig. 7. 4 includes the varying conductivity of the middle zone (kZone) for each model.

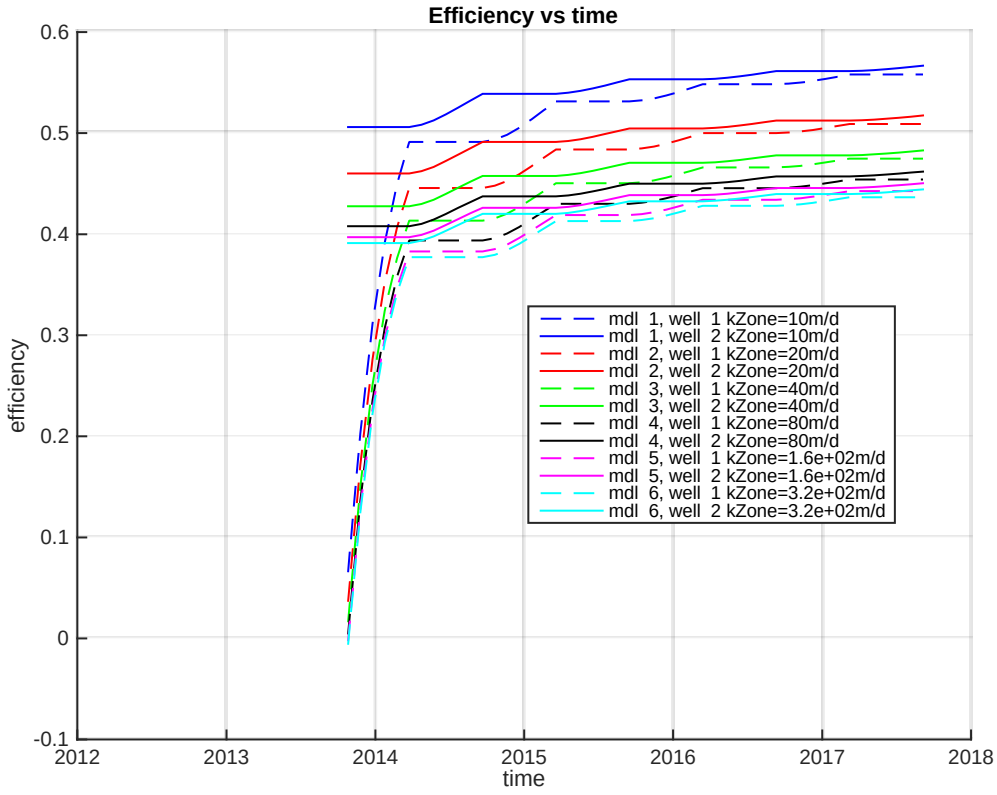

Fig. 7. 4: Thermal efficiency in homogeneous aquifer of 50 m divided in 3 horizontal zones of thickness 15, 10 and 15 m respectively. The 10 m thick zones at the top and bottom of the aquifer have the same conductivity of 10 m/d in all models, the 10 m zone in the middle has a different higher conductivity as indicated in the legend. GT25xx systems, 10 m screen length at top and bottom of the aquifer. Anisotropy 2, Qfrac 0.5, medium resolution model. The time axis of the graph spans the 2nd through the 5th year of the simulation.

Fig. 7. 4 shows that the higher the conductivity in the central zone is, the lower the thermal efficiency becomes. There are two reasons for this behavior, one is the fact that with a more conductive intermediate zone, the stored water will be squeezed into that zone and spreads out radially more in that zone than it does in the zones at the elevations of the screens. The stored warm and cold water will thus be pushed closer together causing more interference and hence less efficiency. The second reason is that a small high conductive zone generates a bubble of larger radial extent than in the homogeneous case. This more pancake-like form results in a larger exchange surface with and hence more heat loss into the adjacent less conductive zones. This heat, or coldness when the cold screen is concerned, can to a large extent not be retrieved. In fact, this hydrogeological setting increases the total outer surface of the stored bubbles.

7.4. THE IMPACT OF TEMPERATURE INDUCED VISCOSITY AND DENSITY

In the analysis of the former chapters, we ignored viscosity and density variation caused by the temperature differences entailed with thermal energy storage, as it is generally done in practice when designing ATES systems. However, it is not guaranteed that they can be neglected.

In this paragraph, we will investigate these effects on the hand of an example where we compare the temperature distribution and the resulting efficiency with and without considering the effect of viscosity and density changes that temperature differences induce. To simulate these effects, we have to use SEAWAT instead of MT3DMS. SEAWAT enables updating viscosity and density after every transport step during the simulation, whereas MT3DMS requires all flows to be computed and stored independently by MODFLOW and afterwards MT3DMS uses this information. Furthermore it can either compute the relation between temperature and viscosity or density, or between salinity and density.

For the comparison, we apply the same model as before, it consists of two confining zones of 30 m thickness with an aquifer of 50 m thickness in between. The system which was simulated is a GT25xx configuration, with Qfrac = 0.5 and anisotropy 2.0. The associate screens are 10 m long and are placed immediately below the cover layer and immediately above the underlying confining layer, so that there is 3L or 30 m separation distance between the two screens. To reduce the computational complexity, we used the medium resolution model (grid size near the well and layer thickness 0.5 m, paragraph 6. 3) with longitudinal dispersivity 0.25 m and one tenth of this for the two transversal dispersivities. The compared cases will be simulated simultaneously for presentation purposes.

We test the impact on the performance by adapting the injection temperatures of a series of models that are simulated together. The injection temperatures will be ΔT above and below the reference temperature for the warm and cold screen respectively. In the six models ΔT will be 2, 4, 6, 8, 10 and 12^0C, where ΔT stands for the injection temperature difference between the warm and the cold screen. The reference temperature (groundwater temperature) is half this value.

In the next test both the density and viscosity are made active. Notice that the ΔT in the legend of the next figure is the difference between the temperature of the warm and the cold screen. The density used by SEAWAT is given in the list file:

$$\rho = 1000 - 0.1370(T - 8.4)$$

The viscosity is given by the Voss formula as described in the SEAWAT manual:

$$\mu(T) = 239.5 \cdot 10^{-7} \cdot 10^{(248.37T + 133.15)}$$

The results are shown in Fig. 7. 5.

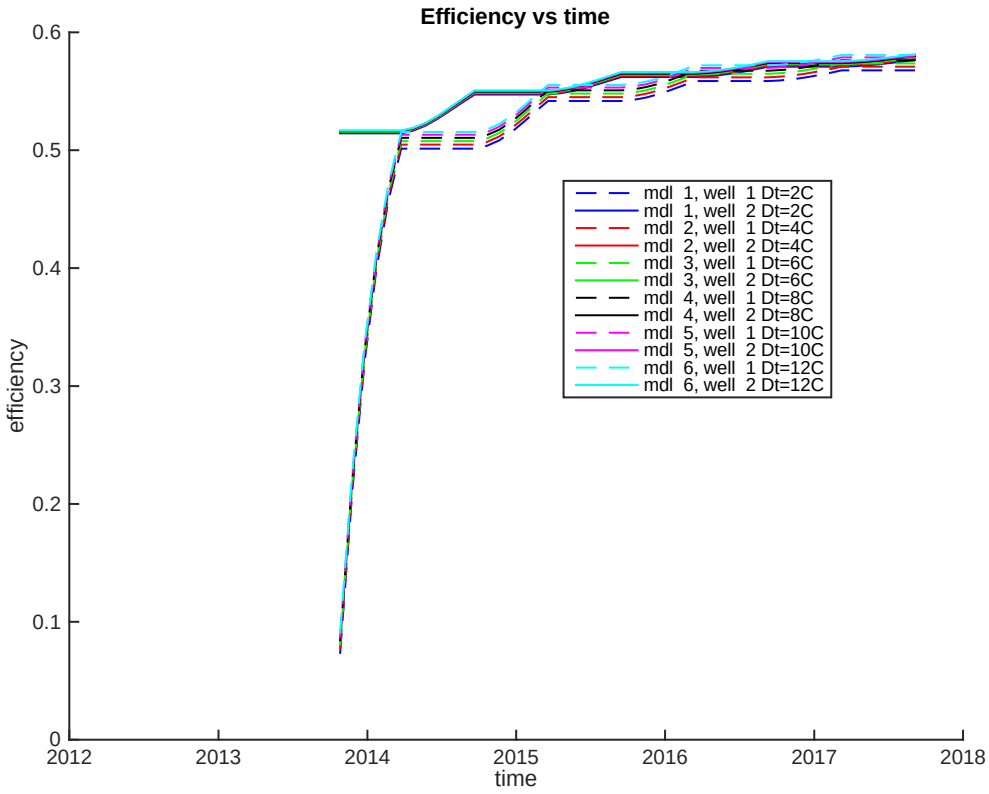

Fig. 7. 5: Thermal efficiency in homogeneous aquifer of 40 m with 40 m/d. The injection temperature of the different models is 1, 2, 3, 4, 5, 6 ^{0}C above and below the reference temperature of 12 C. GT25 systems, 10 m screen length at top and bottom of the aquifer. Anisotropy 2, Qfrac 0.5, medium resolution model.

As can be concluded from Fig. 7. 5, the combined influence of temperature induced density and viscosity is minor for the temperature range applied in SB-ATES systems. Therefore, it is acceptable to ignore the effects in the design of such systems as we did in this work.

7.5. CONCLUSIONS

In this chapter the evaluation of the sensitivity analysis was conducted using 18 cases-studies. The actual geological conditions were used during the elaboration, taking into account the hydraulic conductivity distribution among the layers. The model results show that most of the case-studies were in good agreement with the homogeneous case of the sensitivity analysis (Chapter 6). Small deviations can be explained due to the use of different screen lengths and the effects of conductivity distribution. However, three cases substantially deviated from the homogeneous case of the sensitivity analysis. Two of them had higher performance than it was

expected while the other one the efficiency was low. The results of the first 2 case-studies can be explained by the presence of a clay layer between the screens while the results of the last case indicate the presence of a high permeable layer between the screens. These effects were verified by modeling two different cases with the model that was used in chapter 6. The only different was that in the first case a layer with low conductivity between the screens was introduced in the model while in the latter, a layer with high conductivity was used between the screens. The output of the model shows that in the case of a clay layer the efficiency increases while when there is a high permeable layer, the performance of the SB-ATES system drops. Additionally, it was proven that the performance of the systems is independent of the mean hydraulic conductivity of the aquifer when the anisotropy is constant. Finally, the effect of density and viscosity was investigated on the efficiency of the SB-ATES systems. It was found that the combined water temperature induced density and viscosity is minor for the temperature range applied in SB-ATES systems.

CHAPTER 8

8. Conclusions and Recommendations

8.1. CONCLUSIONS

This MSc thesis derived an optimal separation distance between the screens that are vertically placed within the same borehole of SB-ATES systems.

This was done by simulating a large number of systems with an axi-symmetrical flow and transport model, i.e. MODFLOW with MT3DMS or SEAWAT. Axial symmetry does not allow simulation of random spatial heterogeneity or ambient flow. It allows simulation of systems consisting of many sublayers with different horizontal and vertical conductivities and also, when necessary, the impact of density and viscosity can be included.

We did not analyze systems under the influence of density flow caused by differences in salinities (brackish and saltwater), but we showed that the impact of temperature-related density and viscosity is negligible for SB-ATES systems for injection temperature differences between the warm and cold screen of at least up to 12^0C.

The necessary separation distance between the two screens of single-borehole ATES systems was determined for three standard SB-ATES configurations. Their names are GT15xx, GT20xx and GT25xx, where the numbers indicate the installed pump capacity in m^3/h. These systems have a mean screen length of 5, 7 and 10 m respectively, varying somewhat according to local circumstances.

The necessary separation distance was determined by simulating the systems in a sensitivity scheme, in which Qfrac (ratio of the mean seasonal flow over the installed pump capacity implied by the system type), vertical anisotropy and screen separation were varied for each of the three system types. The results were presented as thermal efficiency after 5 years of operation versus vertical screen separation. Curves for 3 different anisotropies and 3 values of Qfrac for the 3 system types were presented. The efficiency of the warm and cold screens was computed separately. These curves indicate that the necessary separation to reach virtually the maximum possible efficiency is practically independent of system type. This is due to the volume that can be stored in the aquifer zone that is determined by the two screens and their separation distance; this zone is substantially larger for systems with greater screen lengths than for smaller systems even when their separation distance is the same.

The optimal separation can be read from the sensitivity curves, in Chapter 6. For an anisotropy of 2, the value may be set to 25, 30 and 35 m for Qfrac is 0.25, 0.5 and 1.0, irrespective of the system type.

The 18 actual cases, with their specific conductivity distribution, the actual screen length and screen positions, were simulated to verify the results of the sensitivity analysis. The thermal efficiency between the results of the sensitivity analysis and the actual cases is generally small with a few exceptions. The small differences are attributed to differences in screen length while the few cases with a large difference were analyzed separately:

The two cases with a substantially higher efficiency than expected from the sensitivity analysis were shown to be due to the presence of one or two thin low-conductive layers between the screens.

The one case with a substantially lower efficiency than expected from the sensitivity analysis was due to the presence of a higher conductive zone between the zones in which the screens were placed.

A thin resistant layer like a clay or peat layer between the two screens will have an impact only if the screen separation is relatively small, in this case the impact will be positive.

A more conductive zone between the two screens will reduce the efficiency of the SB-ATES system as both the interference increases and the size of the contact surface between the stored warm and cold bubbles and the surrounding groundwater increases relative to their volume, which causes higher losses to adjacent zones in the subsurface from which energy recovery is to large extent impossible.

The capacity tests yield very little information about the hydraulic conductivities of the subsurface due to the reciprocity principle, which causes that the capacity test on the second screen yields exactly the same information as the one on the first screen and vice versa. Further, due to the simultaneous injection and extraction on screens that are close together during the capacity tests, the head changes that they cause, reaches a steady-state condition within minutes. The result is that all head measurements during the test, which were taken between the first measurement at 15 minutes and 60 minutes, yield the same information.

The capacity tests allow calibration of only one hydraulic parameter, for which the overall vertical anisotropy was chosen. This so-determined factor is a very crude parameter, but it can be used to conclude whether there are separating layers between the screens that went overlooked during the drilling of the borehole (determined anisotropy << 2), or whether clay layers that were deduced from the samples taken during drilling actually produce no or little vertical resistance (determined anisotropy >> 10).

The final and highest thermal efficiency attainable for the SB-ATES systems is reached within 5 years. Under the circumstances that were valid in the simulations, i.e. equally long seasons with equal heat and cold demand, no ambient groundwater flow and no heterogeneities other than implemented through the hydraulic dispersivity (and numerical dispersion), we attained thermal efficiencies up to about 75% for the larger GT25xx systems and up to about 70% for the smaller GT15xx systems.

A higher anisotropy and a lower Qfrac increase the efficiencies in about the same way. These factors become immaterial beyond a certain separation distance, as can be immediately seen from the sensitivity curves in chapter 6.

The efficiencies as a function of screen separation seem almost independent of system type. This is because larger systems (type GT25xx versus GT15xx) have larger screens (10 m versus 5 m) and, therefore, larger space to store warm or cold water, even when the two have the same vertical separation. This available space increases with the second to the third power of the distance between the middle of the two screens, depending on the flatness of the bubble, which is caused by anisotropy or a certain distribution of the conductivities of the sublayers in the aquifer.

We had to simulate the heat transport using the finite difference method (the FD method) for the computation of advection, because the VTD and MOC methods did not give plausible and consistent results in our axisymmetric models. Because the FD method is subject to numerical dispersion, we had to reduce the cell size and layer thickness to the limit that was still manageable on a PC with 8 GB of memory and a computational time less than a day. This resolution was 25 cm for the layer thickness in the aquifer and 25 cm for the width of the cells near the well. We compared the results to those of other grids that had 50 cm and 100 cm resolution. As the difference between the results in terms of attained efficiency for the two 25 and 50 cm grid resolutions was small, we accepted the finest grid for the interpretation of the sensitivity analysis (Chapter 6) and the evaluation of the sensitivity analysis with real-scale systems (chapter 7). The impact of specific subdivisions of the aquifer and the impact of temperature-induced density and viscosity changes were analyzed using the medium grid having reduced computational time, as only the comparison mattered and not the absolute values.

In designing SB-ATES systems it is safe to assume little vertical anisotropy within the aquifer, unless there is independent information that the anisotropy is higher. We presumed that a safe lowest value would be 2.0, as the anisotropy of any layered system is larger than one. Hydrologists generally estimate vertical anisotropies of sandy aquifers to be less than about 10, but clear independent data is rare, even from pumping tests.

8.2. RECOMMENDATIONS

- *Requirements for a better design of an SB – ATES system*

The capacity test yields very little information about the hydraulic conductivities of the subsurface. This may be improved by placing separate piezometers at some horizontal distance from the well.

It is recommended to compare the total transmissivity that was obtained from the conductivities that were derived from the grain sizes, determined during the drilling, with that of the national database of the subsurface at TNO, i.e. REGIS, to determine to what extent these values may be trusted.

Sampling during drilling should be done at least every m. This is also an official requirement.

Whenever possible, porosity values should be determined to more accurately compute conductivities with the Kozeny-Carmen equation. Currently, only a fixed value of 35% was used due to lack of more information.

The optimized value for the vertical anisotropy obtained by calibration of the capacity tests should be used to signal the presence of thin overlooked clay layers between the screens or a more conductive zone between the screens. Thin clay layers will generally be advantageous, while a higher conductive zone between the screens will generally reduce the thermal efficiency.

- *Recommendations for future research*

The main focus of this study is the optimal vertical separation distance between the screens. However, we had to ignore other factors like general spatial heterogeneity and ambient groundwater flow. It is recommended to apply full 3D modeling to assess those effects.

It is recommended to complete the information obtained from the borehole with that of the subsurface present for the location in the TNO database REGIS. This would allow to more accurately be estimated the depth of the aquifer and the confining layers below the end of the borehole.

An app could be developed that accepts the energy demand and the subsurface profile in terms of grain sizes, and would compute from it the optimal screen length, screen separation, screen placement and even automatically download and include additional data from the TNO-database in the design computations.

REFERENCES

[1] Batu V. (1998), Aquifer hydraulics, a comprehensive guide to hydro geologic data analysis, John Wiley &Sons, book

[2] Bridger, D. W., and D. M. Allen (2005), Designing aquifer thermal energy storage systems, Ashrae J, 47(9).

[3] Calje, R. J. (2010), Future use of aquifer Thermal Energy Storage below the historic center of Amsterdam Delft University of Technology, Delft.

[4] Desbarats, A. J. (1994), Spatial Averaging of Hydraulic Conductivity under Radial Flow Conditions, Math Geol, 26(1), 1-21.

[5] Dickinson, J. S., N. Buik, M. C. Matthews, and A. Snijders (2009), Aquifer thermal energy storage: theoretical and operational analysis, Geotechnique, 59(3), 249-260.

[6] Edzer J. Pebesma (2014), Gstat user's manual, Dept. of Physical Geography, Utrecht University

[7] Ferguson, G. (2007), Heterogeneity and thermal modeling of ground water, Ground Water, 45(4), 485-490.

[8] Fitts, C. R. (2002), Groundwater Science, Academic Press, Amsterdam.

[9] Hansen, T.M. and K. Mosegaard, (2011), VISIM user guide, DTU Informatics, Technical University of Denmark, Lyngby, Denmark

[10] Hansen, T.M. and K. Mosegaard, (2007), VISIM: sequential simulation for linear inverse problems, DTU Informatics, Technical University of Denmark, Lyngby, Denmark

[11] Helsel, D. R., R. M. Hirsch, and Geological Survey (U.S.) (2002), Statistical methods in water resources, in Techniques of water-resources investigations book 4, chapter A3, edited, U.S. Geological Survey.

[12] Huang, S. Y., J. C. Wen, T. C. J. Yeh, W. X. Lu, H. L. Juan, C. M. Tseng, J. H. Lee, and K. C. Chang (2011), Robustness of joint interpretation of sequential pumping tests: Numerical and field experiments, Water Resour Res, 47.

[13] Johns, R. A., L. Semprini, and P. V. Roberts (1992), Estimating Aquifer Properties by Nonlinear Least-Squares Analysis of Pump Test Response, Ground Water, 30(1), 68-77.

[14] Kitanidis, P. K. (1997), applications to hydrogeology Introduction to geostatistics, 246 blz. pp., Cambridge University Press, Cambridge, UK.

[15] Kranz, S., and J. Bartels Simulation and data based identification of parameters affecting season ATES efficiency, Rep.

[16] Kruseman, G. P., N. A. d. Ridder, and International Institute for Land Reclamation and Improvement (1990), Analysis and evaluation of pumping test data, 2nd. ed ed., 377 blz. pp., International Institute for Land Reclamation and Improvement, Wageningen.

[17] Lamarche, L., S. Kajl, and B. Beauchamp (2010), A review of methods to evaluate borehole thermal resistances in geothermal heat-pump systems, Geothermics, 39(2), 187-200.

[18] Langevin, C. D., and Geological Survey (U.S.) (2008), SEAWAT Version 4 a computer program for simulation of multi-species solute and heat transport, in Techniques and methods Book 6, Chapter A22, edited, pp. vi, 39

[19] Langevin, C. D., and W. Guo (2006), MODFLOW/MT3DMS-based simulation of variable-density ground water flow and transport, Ground Water, 44(3), 339-351.

[20] Langevin, C. D., W. B. Shoemaker, W. Guo, and Geological Survey (U.S.). (2003), Modflow-2000 : the U.S. Geological Survey modular ground-water model--documentation of the SEAWAT-2000 version with the variable-density flow process (VDF) and the integrated MT3DMS transport process (IMT), v, 43 p. pp.

[21] Langevin C.D. (2008), Modeling Axisymmetric flow and transport, Ground Water, 46(4), 579-590.

[22] Lienhard, John H. (2011), Heat transfer textbook, Dover Publications

[23] Li, K. Y., S. Y. Yang, and H. D. Yeh (2010), An analytical solution for describing the transient temperature distribution in an aquifer thermal energy storage system, Hydrol Process, 24(25), 3676-3688.

[24] Olsthoorn T. and Nienhuis P. (2011), Alle meerlaagsoplossingen van Gijs Briggeman in Matlab en Octave, Rep.

[25] Rosen, M. A. (1999), Second-law analysis of aquifer thermal energy storage systems, Energy, 24(2), 167-182.

[26] Technische documentatie GT & GeoWP-SKID (broncapaciteit 10- t/m 15 m3/h), GeoComfort

[27] Technische documentatie GT & GeoWP-SKID (broncapaciteit 20- t/m 30 m3/h), GeoComfort

[28] Walter, Donald A. (2008), Use of numerical models to simulate transport of sewage-derived nitrate in a coastal aquifer, central and Western Cape Cod, Massachusetts, U.S. Geological Survey, 2007-5259

[29] Ward, C. H., Cherry, J.A. and Scard, M.R. (1997), Subsurface restoration, Sleeping Bear Press

[30] Wasantha La A. M. (2002), Numerical errors in groundwater and overland flow models, Water Resour Res, 36(5), 1237-1247.

[31] Yang, S. Y., and H. D. Yeh (2008), An analytical solution for modeling thermal energy transfer in a confined aquifer system, Hydrogeol J, 16(8), 1507-1515.

[32] Zlotnik, V. A., and B. R. Zurbuchen (2003), Field study of hydraulic conductivity in a heterogeneous aquifer: Comparison of single-borehole measurements using different instruments, Water Resour Res, 39(4).

[33] Swiss Standard SN 670 010b, Characteristic Coefficients of soils, Association of Swiss Road and Traffic Engineers.

[34] Das, B. Taylor & Francis (2008), Advanced Soil Mechanics, London & New York.

[35] N.V.O.E. (2006). Nederlandse Vereniging voor Ondergrondse Energieopslagsystemen-Richtlijnen Ondergrondse Energieopslag. Woerden: NVOE.

APPENDIX A

Design characteristics

Appendix A includes the design characteristics of all the case studies. These characteristics were introduced to the numerical model, making the simulation of the cases feasible. This information was obtained from soil profile data which was provided from Installect Advies. The cross-section of the boreholes with a detailed description of the soil layers can be found in “Soil – Profile Textbook” which accompanies this report.

Table D - 1: Design characteristics of SB -ATES layout

Case ID	Well Length [m]	Number of Aquifers		Top depth of the filter screen [m]	Bottom depth of the filter screen [m]	Number of piezometers	ID number of piezometer	Top depth of the piezometer [m]	Bottom depth of the piezometer [m]
GT15ULR	55	2	Shallow Aquifer	-28	-33.0	2	1	-28.73	-29.73
			Deep aquifer	-46	-51.0		2	-47.19	-48.19
GT25VA	102	2	Shallow Aquifer	-25	-35	2	1	-25.54	-26.54
			Deep aquifer	-88	-98		2	-88.51	-89.51
GT25GV	68	2	Shallow Aquifer	-34.84	-44.5	2	1	-35.04	-36.04
			Deep aquifer	-56.02	-65.1		2	-56.22	-57.22
GT25TB	89	2	Shallow Aquifer	-41.89	-51.5	2	1	-41.89	-42.89
			Deep aquifer	-77.38	-87.0		2	-77.38	-78.38
B1GB	82	2	Shallow Aquifer	-29	-40.0	2	1	-31	-32
			Deep aquifer	-69	-78.7		2	-69.25	-70.25
GT20VWG	114	2	Shallow Aquifer	-70.38	-80.0	2	1	-70.38	-71.38
			Deep aquifer	-103.37	-113.0		2	-103.4	-104.37
GT20UG	64	2	Shallow Aquifer	-36.5	-45.0	2	1	-40.4	-41.4
			Deep aquifer	-51.36	-61.0		2	-51.56	-52.56
GT15PZC	67	2	Shallow Aquifer	-25.13	-30.0	2	1	-25.35	-26.35
			Deep aquifer	-59.29	-64.1		2	-59.5	-60.5
GT15KU	53	2	Shallow Aquifer	-26	-30.8	2	1	-26.2	-27.2
			Deep aquifer	-44.99	-49.8		2	-45.19	-48.19
GT25RH	51	2	Shallow Aquifer	-24	-29.7	2	1	-25	-26
			Deep aquifer	-41.21	-46.0		2	-41.21	-42.21
GT25-2KPA	160	2	Shallow Aquifer	-100.28	-115.28	2	1	-110	-111
			Deep aquifer	-141.28	-158.28		2	-151.4	-152.4
GT20WW	54	2	Shallow Aquifer	-44.67	-49.5	2	1	-27.3	-28.3
			Deep aquifer	-27.09	-31.9		2	-44.9	-45.9
GT25NBDA	129	2	Shallow Aquifer	-67.16	-82.0	2	1	-67.55	-68.55
			Deep aquifer	-113.38	-123.0		2	-113.4	-114.38

GT25PV	60	2	Shallow Aquifer	-23	-33.0	2	1	-25.5	-26.5
			Deep aquifer	-47	-57.0		2	-47.5	-48.5
GT15M	56	2	Shallow Aquifer	-25.01	-28.0	2	1	-25.01	-26.01
			Deep aquifer	-46.35	-51.2		2	-48.35	-49.35
GT20SM	59	2	Shallow Aquifer	-23.39	-30.68	2	1	-23.5	-24.5
			Deep aquifer	-49.88	-57.0		2	-49.88	-50.88
GT20WA	81	2	Shallow Aquifer	-47.27	-52.1	2	1	-47.49	-48.49
			Deep aquifer	-73.17	-78.0		2	-73.39	-74.39
GT20CCU	55	2	Shallow Aquifer	-27.17	-32.0	2	1	-27.2	-28.2
			Deep aquifer	-41	-45.6		2	-40.8	-41.8

APPENDIX B

Capacity Test Data

Appendix B includes the capacity test data that was used to calibrate the model. Two pumping tests were available for each case-study. One test regards the shallow aquifer and the other was conducted to the deep aquifer. For each case study, the drawdowns at the borehole and at the piezometers' location are presented. Further Information about the location of the piezometers is available in the Soil – Profile Textbook which includes the cross section soil profiles of all the cases studies.

APPENDIX B:
CAPACITY TEST DATA

Table E- 1: Capacity Test Data for GT20WW Case Study

Deep Aquifer

Pumping Rate [m³/h]: 41.30

Time [min]	Flow [m³]	Drawdown at the source [m]	Drawdown at the piezometer 1 (Shallow) [m]	Drawdown at the piezometer 2 (Deep) [m]
0	5950.35	1.75	1.91	1.92
5				5.32
15	5960.70	1.92	2.07	5.37
30	5971.01	1.95	2.10	5.40
45		1.96	2.11	5.41
60	5991.65	1.97	2.11	5.42

Shallow Aquifer

Pumping Rate [m³/h]: 44.19

0	5999.51	1.78	1.95	1.95
5		3.69	3.70	2.09
15	6010.80	3.72	3.73	2.16
30		3.74	3.77	
45	6032.80	3.78	3.79	2.17
60	6043.70	3.79	3.79	2.18

Table E- 2: Capacity Test Data for GT25-2KPA Case Study

Deep Aquifer

Pumping Rate [m³/h]: 25.62

Time [min]	Flow [m³]	Drawdown at the source [m]	Drawdown at the piezometer 1 (Shallow) [m]	Drawdown at the piezometer 2 (Deep) [m]
0	2712878.00	4.68	4.85	4.72
5		4.68	4.85	5.57
10		4.68	4.85	5.58
15		4.68	4.85	5.58
30	2725735.00	4.68	4.85	5.58
60	2738496.00	4.68	4.85	5.58

Shallow Aquifer

Pumping Rate [m³/h]: 25.78

0	2739446.00	4.68	4.85	4.72
5		5.85	6.02	4.72
10		5.85	6.02	4.72
15		5.86	6.03	4.72
30	2752337.00	5.86	6.03	4.72
60	2765228.00	5.86	6.03	4.72

Table E- 3: Capacity Test Data for GT25VA Case Study

Deep Aquifer

Pumping Rate [m^3/h]: 26.58

Time [min]	Flow [m^3]	Drawdown at the source [m]	Drawdown at the piezometer 1 (Shallow) [m]	Drawdown at the piezometer 2 (Deep) [m]
0	1881.10	2.52	2.52	2.52
5		2.52	2.52	3.78
10		2.52	2.52	3.82
15		2.52	2.52	3.80
20		2.52	2.52	3.78
30	1894.38	2.52	2.52	3.79
40		2.52	2.52	3.79
50		2.52	2.52	3.80
60	1907.68	2.52	2.52	3.79

Shallow Aquifer

Pumping Rate [m^3/h]: 25.78

0	1912.60	2.52	2.52	2.56
5		4.51	4.48	2.56
10		4.51	4.46	2.56
15		4.52	4.46	2.56
20		4.54	4.46	2.56
30	1927.50	4.57	4.53	2.56
40		4.58	4.53	2.56
50		4.58	4.53	2.56
60	1942.54	4.57	4.53	2.56

Table E- 4: Capacity Test Data for GT15M Case Study

Deep Aquifer

Pumping Rate [m^3/h]: 35.61

Time [min]	Flow [m^3]	Drawdown at the source [m]	Drawdown at the piezometer 1 (Shallow) [m]	Drawdown at the piezometer 2 (Deep) [m]
0	131089.92	1.82	2.10	1.98
10		2.02	2.30	4.24
30		2.04	2.32	4.25
60	131125.53	2.05	2.32	4.25

Shallow Aquifer

Pumping Rate [m^3/h]: 37.93

0	131127.00	1.90	2.18	2.06
10		3.95	4.12	2.26
30		3.95	4.12	2.26
60	131164.93	3.98	4.14	2.26

Table E- 5: Capacity Test Data for GT25NBDA Case Study

Deep Aquifer

Pumping Rate [m³/h]: 25.04

Time [min]	Flow [m³]	Drawdown at the source [m]	Drawdown at the piezometer 1 (Shallow) [m]	Drawdown at the piezometer 2 (Deep) [m]
	23858.25	2.70	2.64	3.07
5		2.71	2.64	3.48
10		2.71	2.64	3.48
15		2.71	2.64	3.48
30	23870.75	2.70	2.64	3.48
60	23883.29	2.71	2.64	3.48

Shallow Aquifer

Pumping Rate [m³/h]: 24.89

	23832.80	2.68	2.63	3.06
5		3.55	3.48	3.08
10		3.58	3.49	3.08
15		3.59	3.50	3.08
30	23845.61	3.59	3.50	3.08
60	23857.69	3.59	3.50	3.08

Table E- 6: Capacity Test Data for GT25TB Case Study

Deep Aquifer

Pumping Rate [m³/h]: 31.52

Time [min]	Flow [m³]	Drawdown at the source [m]	Drawdown at the piezometer 1 (Shallow) [m]	Drawdown at the piezometer 2 (Deep) [m]
	57672.30	1.80	1.79	1.79
5		1.85	1.86	2.65
10		1.86	1.86	2.66
15	57680.05	1.86	1.86	2.67
30	57688.05	1.86	1.86	2.67
60	57703.82	1.87	1.87	2.67

Shallow Aquifer

Pumping Rate [m³/h]: 31.61

	57705.00	1.80	1.79	1.79
5		3.96	3.85	1.87
10		3.97	3.86	1.86
15	57712.89	3.97	3.87	1.86
30	57720.77	3.97	3.88	1.86
60	57736.61	3.97	3.89	1.86

Table E- 7: Capacity Test Data for B1GB Case Study

Deep Aquifer

Pumping Rate [m³/h]: 31.44

Time [min]	Flow [m³]	Drawdown at the source [m]	Drawdown at the piezometer 1 (Shallow) [m]	Drawdown at the piezometer 2 (Deep) [m]
0	3672.55	2.42	2.43	2.43
5		2.47	2.45	3.38
10		2.48	2.48	3.41
15	3682.60	2.48	2.48	3.42
30	3692.35	2.50	2.50	3.42
45		2.52	2.51	3.45
60	3711.85	2.52	2.52	3.45

Shallow Aquifer

Pumping Rate [m³/h]: 31.96

0	3713.14	2.46	2.46	2.46
5		4.00	3.90	2.50
10		4.02	3.92	2.52
15	3723.73	4.02	3.92	2.53
30	3733.35	4.04	3.95	2.55
45		4.04	3.96	2.55
60	3755.10	4.04	3.97	2.57

Table E- 8: Capacity Test Data for GT20CCU Case Study

Deep Aquifer

Pumping Rate [m³/h]: 24.32

Time [min]	Flow [m³]	Drawdown at the source [m]	Drawdown at the piezometer 1 (Shallow) [m]	Drawdown at the piezometer 2 (Deep) [m]
0	802665.00	2.28	2.28	2.28
5		2.39	2.39	4.38
10		2.39	2.39	4.38
20		2.39	2.39	4.38
30	814823.00	2.39	2.39	4.38
60	826981.00	2.39	2.39	4.38

Shallow Aquifer

Pumping Rate [m³/h]: 24.38

0	829932.00	2.28	2.28	2.28
5		3.40	3.37	2.40
10		3.42	3.40	2.40
20		3.45	3.40	2.40
30	841706.00	3.47	3.45	2.40
60	854316.00	3.48	3.45	2.40

Table E- 9: Capacity Test Data for GT20VWG Case Study

Deep Aquifer

Pumping Rate [m³/h]: 19.73

Time [min]	Flow [m³]	Drawdown at the source [m]	Drawdown at the piezometer 1 (Shallow) [m]	Drawdown at the piezometer 2 (Deep) [m]
0	20219.78	2.46	2.46	2.98
5		2.48	2.48	3.45
10		2.48	2.48	3.45
15		2.49	2.48	3.45
30	20229.12	2.49	2.48	3.45
60	20239.51	2.52	2.49	3.45

Shallow Aquifer

Pumping Rate [m³/h]: 21.01

0	20240.57	2.50	2.46	2.98
5		3.00	2.96	2.99
10		2.99	2.96	3.00
15		2.99	2.97	3.00
30	20251.05	2.99	2.97	3.00
60	20261.58	2.99	2.97	3.00

Table E- 10: Capacity Test Data for GT20UG Case Study

Deep Aquifer

Pumping Rate [m³/h]: 32.26

Time [min]	Flow [m³]	Drawdown at the source [m]	Drawdown at the piezometer 1 (Shallow) [m]	Drawdown at the piezometer 2 (Deep) [m]
0	21139.75	2.49	2.54	2.48
5	21142.44	2.74	2.79	3.62
10	21145.13	2.80	2.86	3.67
15	21147.82	2.84	2.90	3.71
30	21155.88	2.89	2.96	3.77
60	21172.01	2.96	3.02	3.82

Shallow Aquifer

Pumping Rate [m³/h]: 26.15

0	21190.75	2.49	2.54	2.52
5	21192.93	5.60	5.51	2.82
10	21195.09	5.67	5.57	2.86
15	21197.25	5.69	5.59	2.89
30	21203.78	5.78	5.66	2.92
60	21216.90	5.80	5.68	2.95

Table E- 11: Capacity Test Data for GT25RH Case Study

Deep Aquifer

Pumping Rate [m³/h]: 28.44

Time [min]	Flow [m³]	Drawdown at the source [m]	Drawdown at the piezometer 1 (Shallow) [m]	Drawdown at the piezometer 2 (Deep) [m]
0	70922.79	2.60	2.60	2.60
5		3.11	3.08	4.37
10		3.13	3.11	4.38
20		3.13	3.14	4.39
30	70932.19	3.14	3.14	4.41
45		3.14	3.14	4.41
60	70951.23	3.14	3.14	4.41

Shallow Aquifer

Pumping Rate [m³/h]: 40.13

0	70954.89	2.60	2.60	2.60
5		4.27	4.21	3.16
10		4.30	4.21	3.17
20		4.30	4.22	3.19
30	70974.55	4.30	4.25	3.20
45		4.30	4.25	3.20
60	70995.02	4.30	4.25	3.20

Table E- 12: Capacity Test Data for GT20SM Case Study

Deep Aquifer

Pumping Rate [m³/h]: 20.74

Time [min]	Flow [m³]	Drawdown at the source [m]	Drawdown at the piezometer 1 (Shallow) [m]	Drawdown at the piezometer 2 (Deep) [m]
	2139.85	2.15	2.15	2.15
5		2.17	2.16	2.78
10		2.17	2.17	2.80
15		2.17	2.17	2.80
30	2150.26	2.17	2.17	2.81
60	2160.59	2.17	2.17	2.81

Shallow Aquifer

Pumping Rate [m³/h]: 20.94

	2160.87	2.15	2.15	2.15
5		2.81	2.80	2.16
10		2.81	2.80	2.17
15		2.82	2.81	2.17
30	2171.25	2.82	2.82	2.17
60	2181.81	2.82	2.82	2.17

Table E- 13: Capacity Test Data for GT15KU Case Study

Deep Aquifer

Pumping Rate [m³/h]: 38.76

Time [min]	Flow [m³]	Drawdown at the source [m]	Drawdown at the piezometer 1 (Shallow) [m]	Drawdown at the piezometer 2 (Deep) [m]
	1789.11	1.21	1.21	1.21
5		1.31	1.32	3.92
10		1.32	1.32	3.93
15	1798.79	1.33	1.33	3.93
30	1808.49	1.33	1.33	3.93
60	1827.87	1.33	1.33	3.94

Shallow Aquifer

Pumping Rate [m³/h]: 41.62

	1831.13	1.21	1.21	1.21
5		3.43	3.31	1.33
10		3.44	3.33	1.34
15	1841.54	3.45	3.34	1.35
30	1851.94	3.46	3.34	1.35
60	1872.75	3.46	3.34	1.35

Table E- 14: Capacity Test Data for GT15ULR Case Study

Deep Aquifer

Pumping Rate [m³/h]: 15.58

Time [min]	Flow [m³]	Drawdown at the source [m]	Drawdown at the piezometer 1 (Shallow) [m]	Drawdown at the piezometer 2 (Deep) [m]
	3693.24	1.78	1.78	1.78
5		1.80	1.80	2.86
10		1.81	1.81	2.88
15	3697.12	1.81	1.81	2.89
30	3701.01	1.82	1.82	2.90
60	3708.82	1.83	1.83	2.90

Shallow Aquifer

Pumping Rate [m³/h]: 15.03

	3709.22	1.78	1.78	1.78
5		2.30	2.30	1.82
10		2.33	2.33	1.82
15	3712.97	2.35	2.33	1.82
30	3716.84	2.36	2.34	1.85
60	3724.25	2.36	2.34	1.86

Table E- 15: Capacity Test Data for GT25GV Case Study

Deep Aquifer

Pumping Rate [m³/h]: 27.99

Time [min]	Flow [m³]	Drawdown at the source [m]	Drawdown at the piezometer 1 (Shallow) [m]	Drawdown at the piezometer 2 (Deep) [m]
	9494.92	2.65	2.63	2.65
5		2.72	2.75	3.37
15	9501.20	2.74	2.75	3.38
30	9508.92	2.75	2.80	3.40
45		2.77	2.80	3.42
60	9522.91	2.78	2.79	3.45

Shallow Aquifer

Pumping Rate [m³/h]: 32.72

	9523.72	2.65	2.63	2.64
5		3.00	2.95	2.75
15	9531.92	3.02	2.99	2.76
30	9540.10	3.04	3.00	2.76
45		3.05	3.03	2.79
60	9556.44	3.07	3.03	2.82

Table E- 16: Capacity Test Data for GT25PV Case Study

Deep Aquifer

Pumping Rate [m³/h]: 32.97

Time [min]	Flow [m³]	Drawdown at the source [m]	Drawdown at the piezometer 1 (Shallow) [m]	Drawdown at the piezometer 2 (Deep) [m]
	69701.930	1.67	1.67	1.67
5		1.70	1.70	2.63
10	69707.480	1.75	1.75	2.64
15		1.75	1.75	2.65
30	69718.500	1.75	1.75	2.66
60	69734.900	1.76	1.76	2.67

Shallow Aquifer

Pumping Rate [m³/h]: 33.69

	69756.740	1.67	1.67	1.67
5		3.12	3.12	1.72
10	69762.600	3.13	3.13	1.75
15		3.13	3.13	1.75
30	69773.700	3.15	3.15	1.75
60	69790.430	3.15	3.15	1.76

Table E- 17: Capacity Test Data for GT20WA Case Study

Deep Aquifer

Pumping Rate [m³/h]: 32.14

Time [min]	Flow [m³]	Drawdown at the source [m]	Drawdown at the piezometer 1 (Shallow) [m]	Drawdown at the piezometer 2 (Deep) [m]
	94672.51	1.26	1.26	1.26
5	94675.35	1.34	1.32	3.28
10	94677.89	1.35	1.32	3.33
15	94680.57	1.37	1.36	3.34
30	94688.59	1.38	1.38	3.35
60	94704.65	1.39	1.39	3.38

Shallow Aquifer

Pumping Rate [m³/h]: 30.46

	94722.82	1.26	1.26	1.26
5	94725.43	4.02	3.92	1.33
10	94727.97	4.04	3.93	1.33
15	94730.40	4.04	3.94	1.33
30	94738.08	4.05	3.96	1.34
60	94753.28	4.07	3.97	1.35

Table E- 18: Capacity Test Data for GT15PZC Case Study

Deep Aquifer

Pumping Rate [m³/h]: 36.90

Time [min]	Flow [m³]	Drawdown at the source [m]	Drawdown at the piezometer 1 (Shallow) [m]	Drawdown at the piezometer 2 (Deep) [m]
0	3285.90	1.51	1.51	1.51
5				2.60
10				2.61
15	3295.10			2.61
30				2.61
45				2.61
60	3322.80	1.51	1.51	2.61

Shallow Aquifer

Pumping Rate [m³/h]: 39.38

0	3326.83	1.53	1.53	1.53
5		3.18	3.18	
10		3.19	3.19	
15	3336.54	3.19	3.19	1.54
30		3.20	3.20	
45		3.21	3.21	1.55
60	3366.21	3.21	3.21	1.56

APPENDIX C

Estimation of hydraulic conductivities, implementing Kozeny - Carmen Bear equation

Appendix C includes the hydraulic conductivities of each soil layer, using the Kozeny – Carmen Bear equation. The equation can be found in Chapter 3. As can be seen from the graphs in this appendix, each case consists from multiple layers. These layers were derived from soil profile data, which can be found in Soil – Profile Textbook. It should be mentioned that the implementation of Kozeny – Carmen equation was an important step of the automatic calibration. These conductivities were used as inputs to generate the average vertical anisotropy rate values.

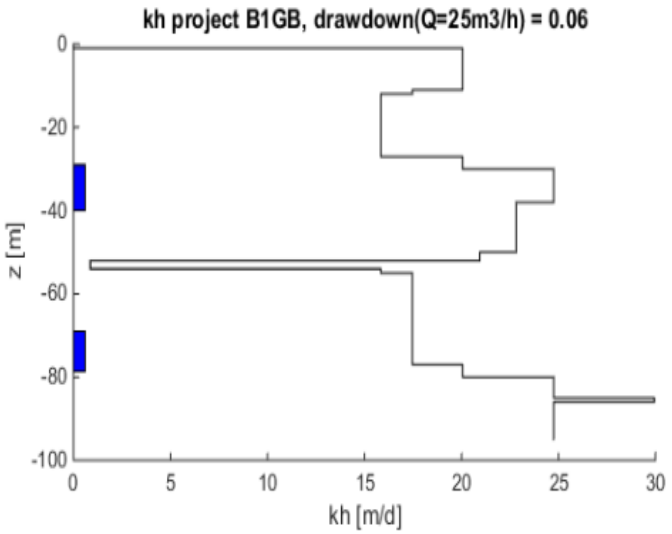

Fig. A- 1: Case B1GB

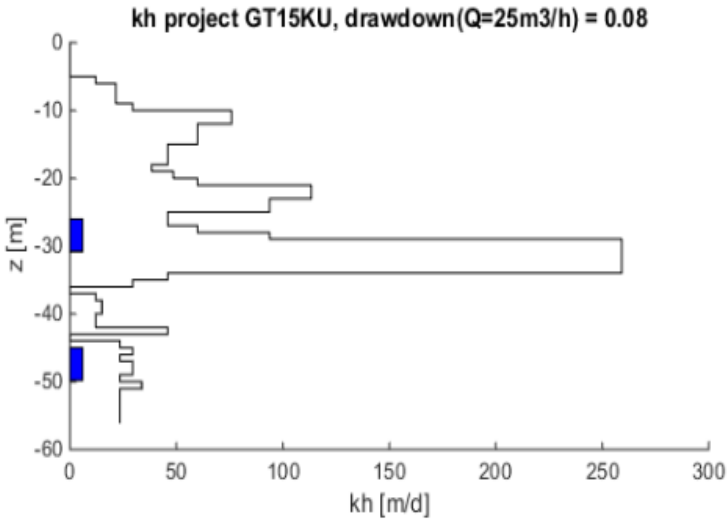

Fig. A- 3: Case GT15KU

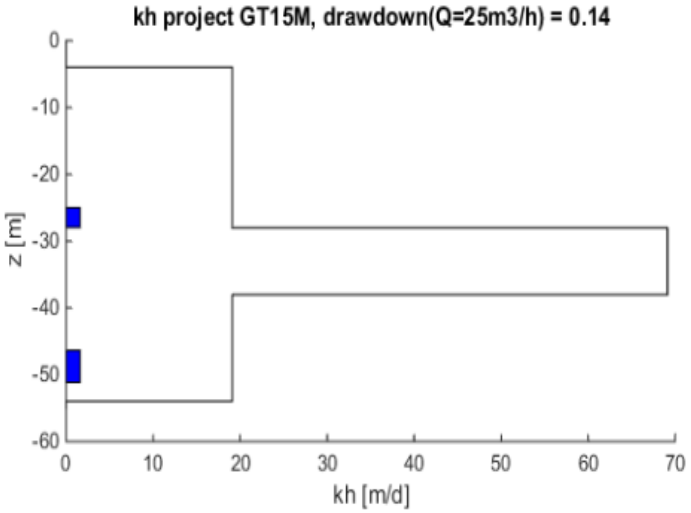

Fig. A- 2: Case GT15M

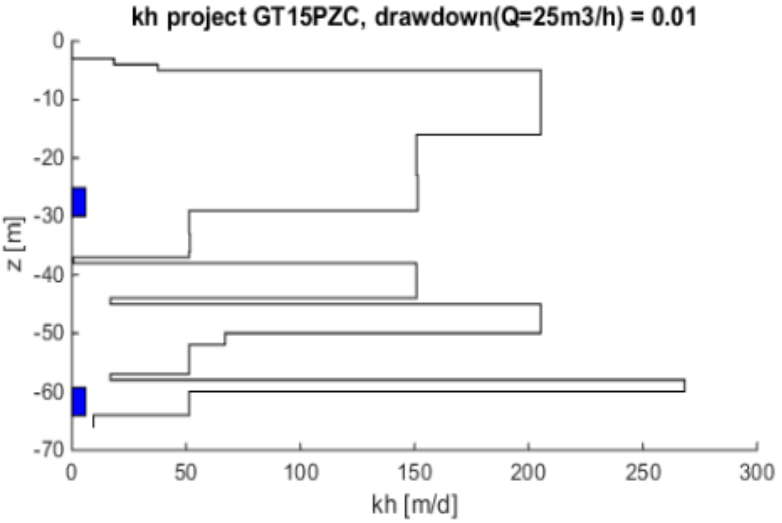

Fig. A- 4: Case GT15PZC

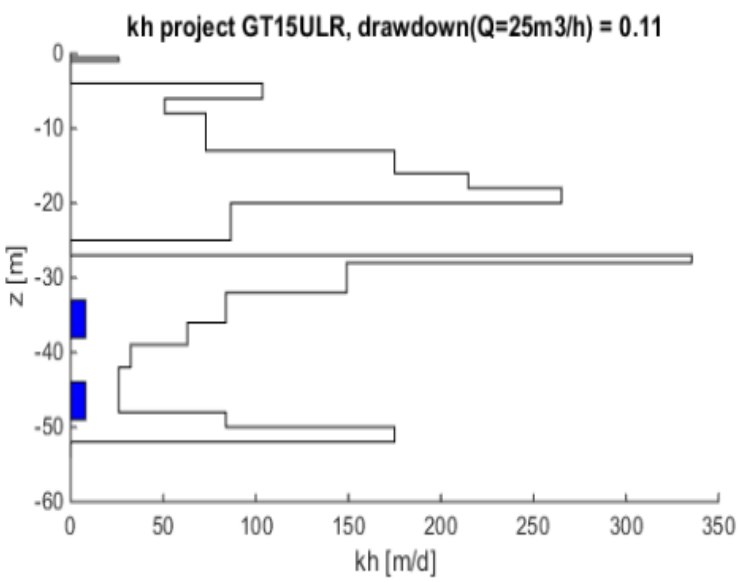

Fig. A- 5: Case GT15ULR

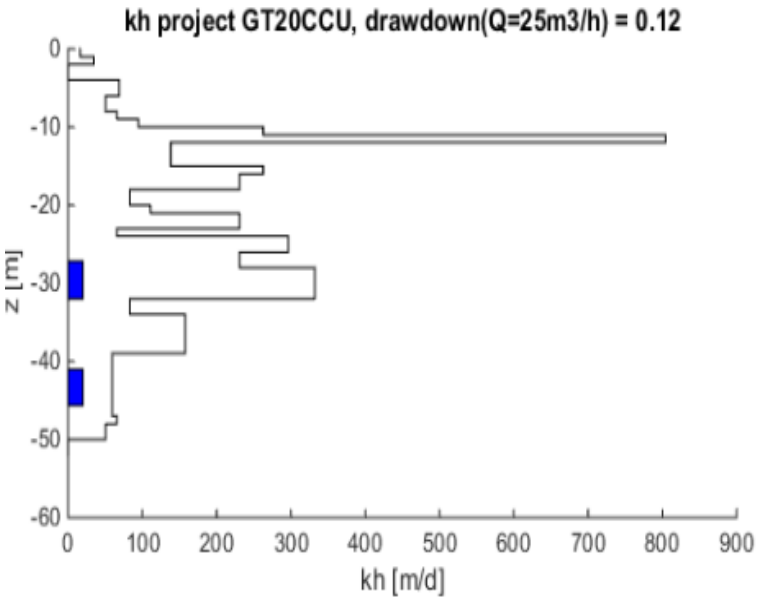

Fig. A- 7: Case GT20CCU

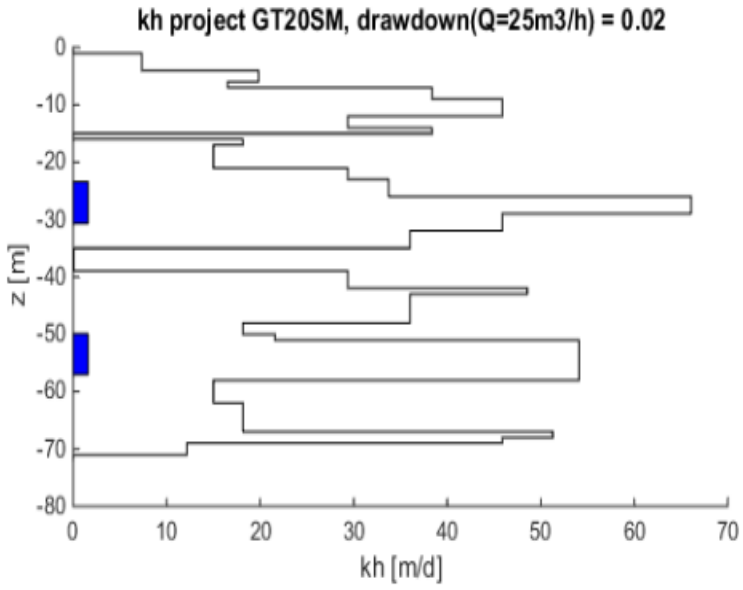

Fig. A- 6: Case GT20SM

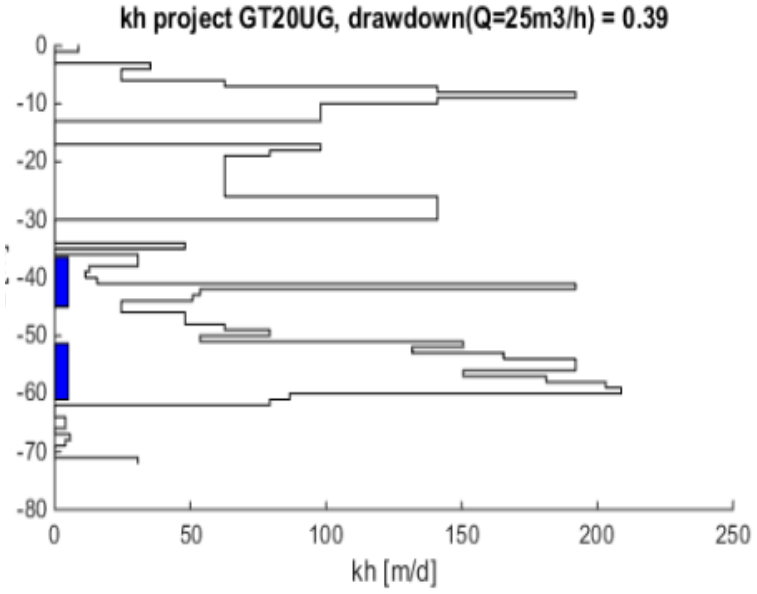

Fig. A- 8: Case GT20UG

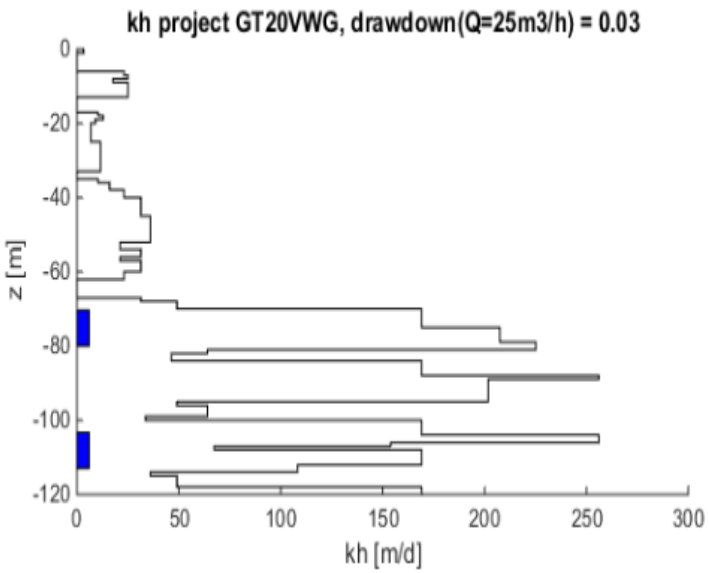

Fig. A- 9: Case GT20VWG

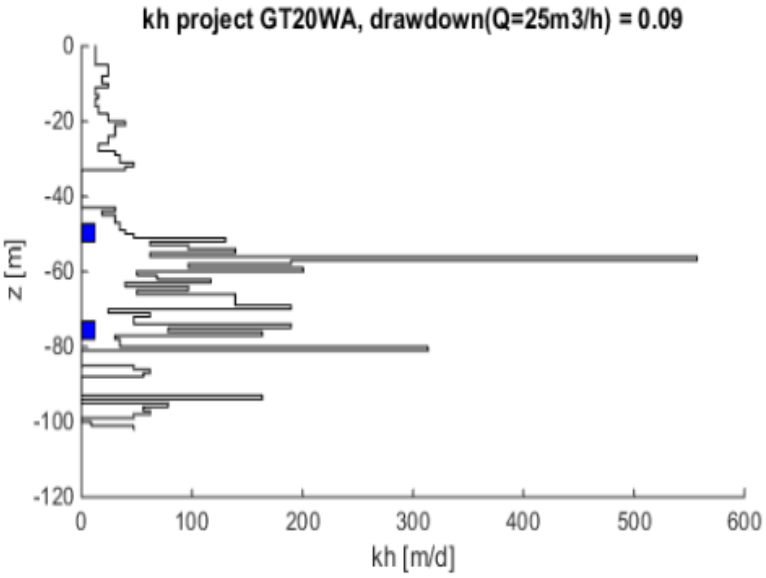

Fig. A- 11: Case GT20WA

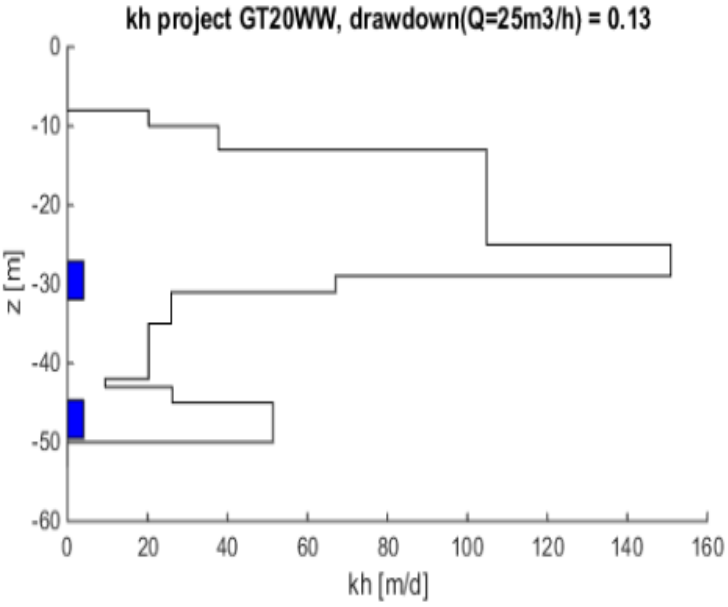

Fig. A- 10: Case GT15WW

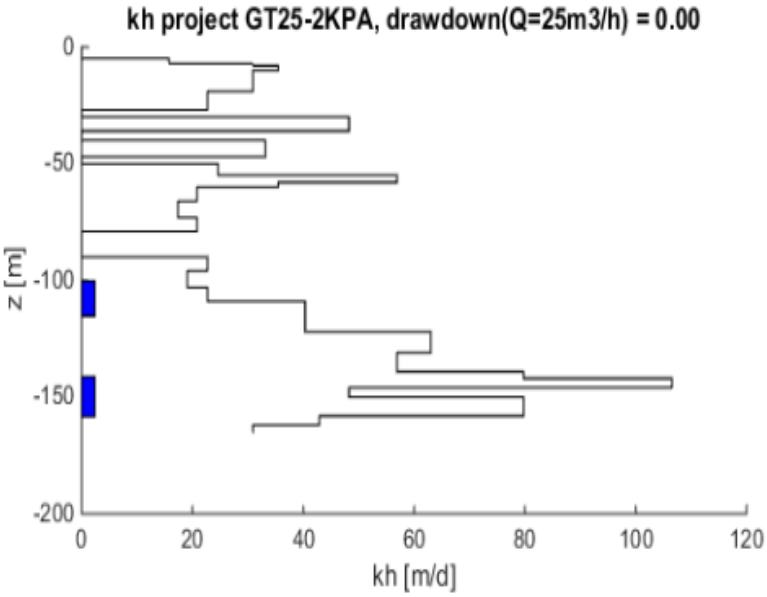

Fig. A- 12: Case GT25-2KPA

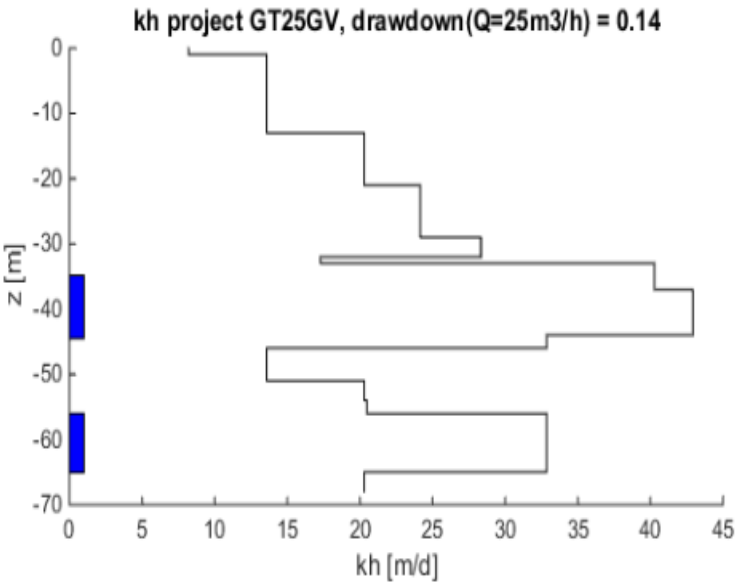

Fig. A- 13: Case GT25GV

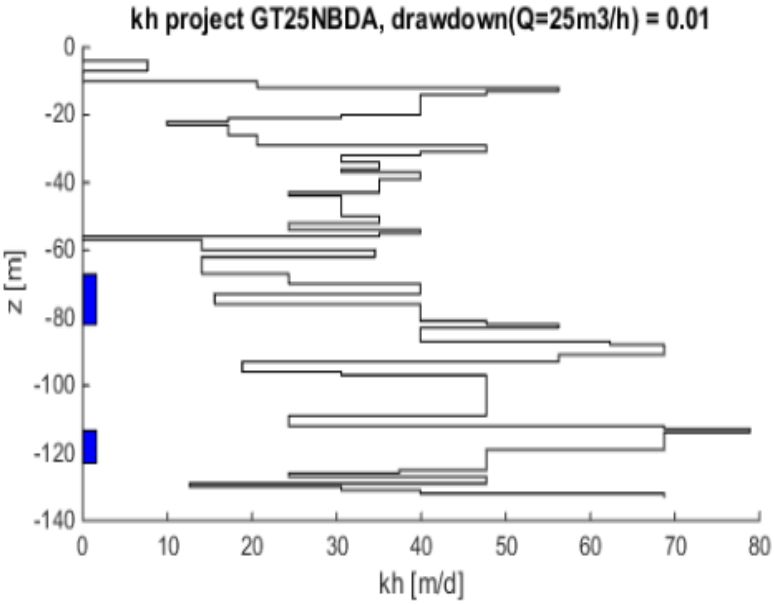

Fig. A- 15: Case GT25NBDA

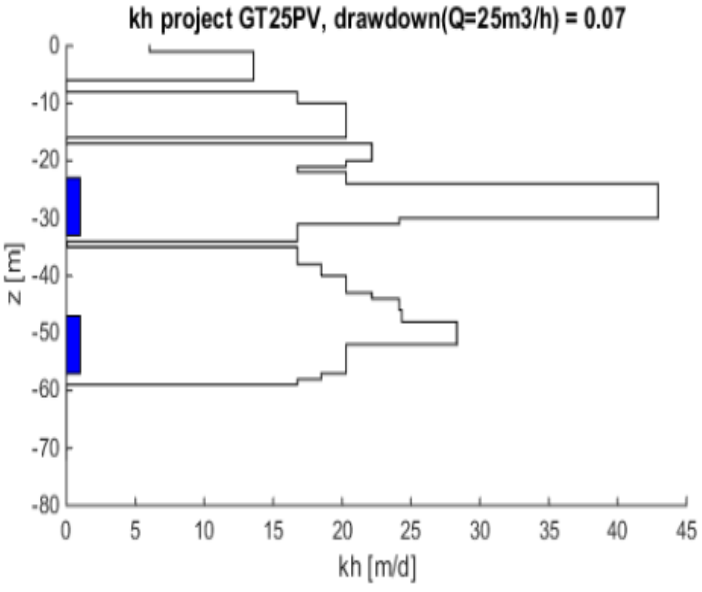

Fig. A- 14: Case GT25PV

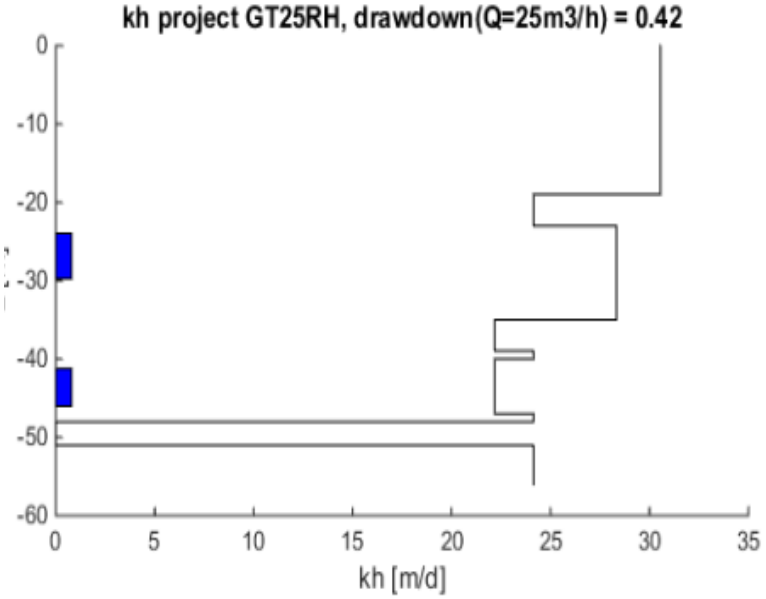

Fig. A- 16: Case GT25RH

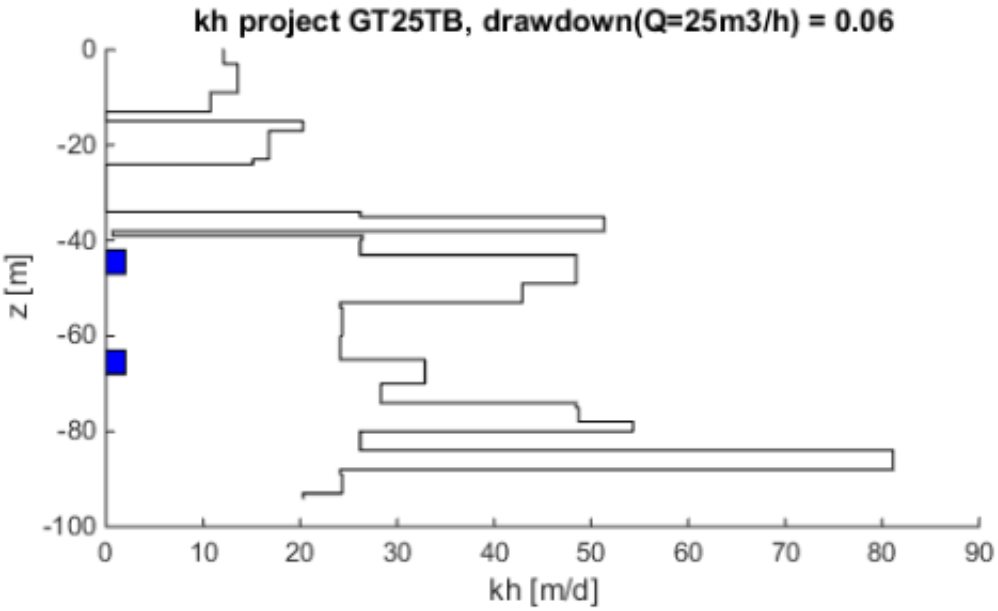

Fig. A- 17: Case GT25TB

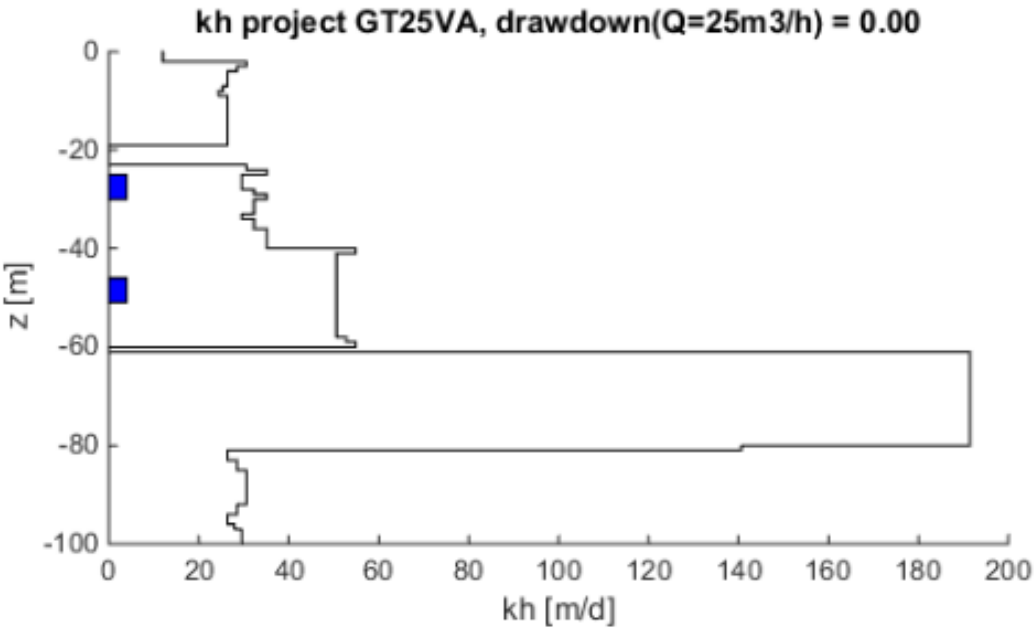

Fig. A- 18: Case GT25VA

APPENDIX D

Results of the sensitivity analysis, using different grid resolutions

In Appendix D the results of the sensitivity analysis (Chapter 6) are presented. The tables include each configuration separately as well as the tree different grid resolutions that they were tested 0.25, 0.50 and 1.00 m).

GT15								
Capacity fraction (Q)			0.25Q		0.5Q		1Q	
Anisotropy	**Separation**	**Grid**	**Warm Well**	**Cold Well**	**Warm Well**	**Cold Well**	**Warm Well**	**Cold Well**
2	5	0.25	-14.38%	-16.61%	-30.32%	-31.69%	-44.57%	-45.29%
		0.5	-14.79%	-17.04%	-30.61%	-31.94%	-44.76%	-45.48%
		1	-15.42%	-17.65%	-31.08%	-32.41%	-45.09%	-45.80%
	10	0.25	21.07%	17.91%	2.05%	0.01%	-17.26%	-18.44%
		0.5	20.41%	17.24%	1.54%	-0.48%	-17.56%	-18.75%
		1	19.21%	16.03%	0.71%	-1.31%	-18.11%	-19.32%
	15	0.25	46.14%	42.46%	30.06%	27.55%	8.97%	7.44%
		0.5	45.37%	41.68%	29.35%	26.84%	8.52%	6.96%
		1	43.92%	40.20%	28.13%	25.62%	7.67%	6.06%
	20	0.25	59.51%	55.63%	50.54%	47.77%	31.96%	30.19%
		0.5	58.86%	54.96%	49.75%	46.97%	31.39%	29.56%
		1	57.60%	53.65%	48.33%	45.56%	30.26%	28.37%
	25	0.25	65.19%	61.28%	62.87%	59.99%	50.01%	48.09%
		0.5	64.72%	60.80%	62.15%	59.25%	49.35%	47.38%
		1	63.81%	59.83%	60.82%	57.93%	48.06%	46.03%
5	5	0.25	8.28%	5.35%	-7.93%	-9.83%	-24.44%	-25.53%
		0.5	7.68%	4.74%	-8.40%	-10.26%	-24.76%	-25.86%
		1	6.67%	3.75%	-9.19%	-11.02%	-25.33%	-26.40%
	10	0.25	42.35%	38.48%	28.55%	25.87%	9.64%	7.98%
		0.5	41.55%	37.69%	27.78%	25.12%	9.11%	7.42%
		1	40.11%	36.24%	26.47%	23.83%	8.14%	6.46%
	15	0.25	58.28%	54.05%	52.73%	49.64%	37.94%	35.91%
		0.5	57.66%	53.43%	51.90%	48.81%	37.22%	35.14%
		1	56.50%	52.24%	50.40%	47.34%	35.89%	33.80%
	20	0.25	64.20%	59.93%	64.38%	61.16%	57.33%	55.09%
		0.5	63.79%	59.52%	63.74%	60.51%	56.55%	54.27%
		1	63.01%	58.71%	62.53%	59.32%	55.10%	52.81%
	25	0.25	66.95%	62.73%	69.14%	65.95%	67.79%	65.50%
		0.5	66.66%	62.44%	68.69%	65.49%	67.14%	64.81%
		1	66.10%	61.85%	67.83%	64.64%	65.89%	63.54%
10	5	0.25	23.44%	19.90%	9.31%	6.96%	-7.14%	-8.61%
		0.5	22.54%	19.06%	8.72%	6.37%	-7.60%	-9.08%
		1	21.39%	17.97%	7.69%	5.38%	-8.42%	-9.86%
	10	0.25	51.40%	46.98%	44.25%	41.10%	29.78%	27.64%
		0.5	50.60%	46.25%	43.45%	40.28%	29.04%	26.88%
		1	49.39%	45.08%	42.00%	38.86%	27.72%	25.57%
	15	0.25	61.04%	56.40%	60.95%	57.48%	54.56%	52.06%
		0.5	60.56%	55.97%	60.32%	56.83%	53.75%	51.22%
		1	59.76%	55.19%	59.11%	55.64%	52.23%	49.71%
	20	0.25	64.97%	60.38%	67.17%	63.68%	66.64%	64.03%

		0.5	64.65%	60.10%	66.76%	63.25%	66.00%	63.36%
		1	64.10%	59.55%	65.94%	62.43%	64.77%	62.13%
	25	0.25	67.08%	62.52%	70.08%	66.67%	71.56%	68.99%
		0.5	66.85%	62.34%	69.79%	66.35%	71.13%	68.52%
		1	66.43%	61.93%	69.19%	65.75%	70.25%	67.63%

GT20								
Capacity fraction (Q)			0.25Q		0.5Q		1Q	
Anisotropy	**Separation**	**Grid**	**Warm Well**	**Cold Well**	**Warm Well**	**Cold Well**	**Warm Well**	**Cold Well**
2	7	0.25	8.56%	5.90%	-9.34%	-11.04%	-26.64%	-27.60%
		0.5	8.04%	5.37%	-9.73%	-11.41%	-26.90%	-27.87%
		1	7.17%	4.47%	-10.38%	-12.07%	-27.35%	-28.34%
	14	0.25	45.01%	41.73%	28.01%	25.79%	7.04%	5.68%
		0.5	44.30%	41.01%	27.38%	25.15%	6.63%	5.24%
		1	42.97%	39.63%	26.29%	24.06%	5.88%	4.45%
	21	0.25	62.90%	59.45%	54.35%	51.87%	36.13%	34.54%
		0.5	62.30%	58.83%	53.61%	51.12%	35.58%	33.94%
		1	61.14%	57.60%	52.28%	49.78%	34.51%	32.81%
	28	0.25	68.77%	65.35%	67.85%	65.34%	57.27%	55.66%
		0.5	68.39%	64.95%	67.22%	64.71%	56.63%	54.99%
		1	67.64%	64.14%	66.05%	63.55%	55.40%	53.72%
	35	0.25	70.96%	67.75%	72.81%	70.70%	69.66%	68.56%
		0.5	70.70%	67.49%	72.38%	70.28%	69.06%	67.95%
		1	70.18%	66.96%	71.56%	69.52%	67.88%	66.79%
5	7	0.25	31.52%	28.14%	15.74%	13.51%	-2.36%	-3.75%
		0.5	30.84%	27.46%	15.22%	12.97%	-2.78%	-4.20%
		1	29.64%	26.23%	14.25%	11.97%	-3.52%	-4.94%
	14	0.25	59.37%	55.53%	51.80%	49.08%	35.93%	34.11%
		0.5	58.74%	54.89%	51.09%	48.33%	35.28%	33.42%
		1	57.56%	53.66%	49.72%	46.92%	34.10%	32.22%
	21	0.25	67.33%	63.49%	67.50%	64.67%	60.92%	58.92%
		0.5	66.96%	63.11%	66.95%	64.08%	60.20%	58.15%
		1	66.26%	62.35%	65.86%	62.95%	58.86%	56.79%
	28	0.25	70.13%	66.35%	72.39%	69.64%	72.05%	70.07%
		0.5	69.90%	66.10%	72.04%	69.26%	71.50%	69.48%
		1	69.43%	65.60%	71.34%	68.52%	70.44%	68.41%
	35	0.25	71.34%	67.66%	74.39%	71.87%	75.91%	74.35%
		0.5	71.18%	67.50%	74.15%	71.63%	75.55%	73.98%
		1	70.85%	67.15%	73.65%	71.14%	74.81%	73.29%
10	7	0.25	44.37%	40.38%	33.04%	30.25%	16.89%	15.04%
		0.5	43.67%	39.68%	32.37%	29.56%	16.32%	14.45%
		1	42.42%	38.41%	31.16%	28.36%	15.32%	13.44%

	14	0.25	63.21%	58.89%	61.86%	58.66%	53.55%	51.27%
		0.5	62.77%	58.45%	61.22%	57.99%	52.80%	50.47%
		1	61.95%	57.58%	60.00%	56.77%	51.40%	49.07%
	21	0.25	68.19%	63.96%	70.19%	67.02%	69.71%	67.35%
		0.5	67.94%	63.70%	69.83%	66.61%	69.14%	66.73%
		1	67.45%	63.17%	69.08%	65.86%	68.02%	65.59%
	28	0.25	70.26%	66.06%	73.16%	70.07%	74.74%	72.48%
		0.5	70.09%	65.90%	72.92%	69.80%	74.39%	72.08%
		1	69.77%	65.54%	72.42%	69.30%	73.66%	71.35%
	35	0.25	71.10%	66.98%	74.49%	71.54%	76.83%	74.85%
		0.5	70.98%	66.86%	74.32%	71.36%	76.59%	74.60%
		1	70.74%	66.61%	73.96%	71.02%	76.07%	74.12%

GT25								
Capacity fraction (Q)			**0.25Q**		**0.5Q**		**1Q**	
Anisotropy	**Separation**	**Grid**	**Warm Well**	**Cold Well**	**Warm Well**	**Cold Well**	**Warm Well**	**Cold Well**
2	10	0.25	35.37%	32.48%	17.98%	16.03%	-1.49%	-2.68%
		0.5	34.78%	31.88%	17.47%	15.52%	-1.82%	-3.04%
		1	33.70%	30.74%	16.63%	14.66%	-2.44%	-3.70%
	20	0.25	64.23%	61.14%	55.27%	53.05%	37.39%	35.99%
		0.5	63.66%	60.55%	54.60%	52.37%	36.89%	35.45%
		1	62.58%	59.38%	53.40%	51.16%	35.91%	34.42%
	30	0.25	71.22%	68.43%	71.36%	69.55%	63.21%	62.35%
		0.5	70.92%	68.12%	70.83%	69.03%	62.62%	61.76%
		1	70.30%	67.48%	69.84%	68.10%	61.46%	60.61%
	40	0.25	73.06%	72.28%	75.47%	75.54%	74.65%	75.15%
		0.5	72.87%	72.13%	75.14%	75.24%	74.16%	74.65%
		1	72.49%	71.79%	74.51%	74.68%	73.18%	73.68%
	50	0.25	73.58%	74.88%	76.68%	77.92%	77.79%	78.95%
		0.5	73.44%	74.74%	76.44%	77.67%	77.43%	78.55%
		1	73.15%	74.42%	75.96%	77.22%	76.67%	77.76%
5	10	0.25	53.74%	50.27%	42.47%	40.04%	25.59%	23.97%
		0.5	53.10%	49.62%	41.89%	39.41%	25.09%	23.42%
		1	51.94%	48.39%	40.77%	38.23%	24.16%	22.46%
	20	0.25	69.12%	65.65%	68.90%	66.34%	61.81%	60.00%
		0.5	68.78%	65.29%	68.39%	65.78%	61.16%	59.30%
		1	68.13%	64.56%	67.36%	64.70%	59.94%	58.05%
	30	0.25	72.31%	69.03%	74.69%	72.47%	75.01%	73.66%
		0.5	72.13%	68.84%	74.41%	72.17%	74.57%	73.20%
		1	71.76%	68.44%	73.84%	71.59%	73.69%	72.35%
	40	0.25	73.23%	71.87%	76.38%	76.16%	78.26%	78.74%
		0.5	73.12%	71.79%	76.21%	76.00%	78.00%	78.47%

		1	72.88%	71.60%	75.83%	75.69%	77.43%	77.97%
	50	0.25	73.43%	74.70%	76.86%	78.15%	79.32%	80.56%
		0.5	73.33%	74.61%	76.73%	78.00%	79.13%	80.34%
		1	73.13%	74.39%	76.44%	77.70%	78.70%	79.92%
10	10	0.25	61.07%	57.11%	55.90%	52.96%	44.01%	41.93%
		0.5	60.55%	56.58%	55.27%	52.29%	43.39%	41.26%
		1	59.60%	55.56%	54.09%	51.09%	42.23%	40.09%
	20	0.25	70.20%	66.33%	71.96%	69.03%	71.06%	68.87%
		0.5	69.97%	66.09%	71.62%	68.64%	70.52%	68.29%
		1	69.54%	65.59%	70.93%	67.92%	69.47%	67.21%
	30	0.25	72.47%	68.73%	75.33%	72.66%	77.01%	75.23%
		0.5	72.34%	68.60%	75.15%	72.45%	76.73%	74.92%
		1	72.10%	68.32%	74.75%	72.06%	76.13%	74.35%
	40	0.25	73.06%	71.14%	76.37%	75.71%	78.79%	79.01%
		0.5	72.97%	71.09%	76.25%	75.61%	78.61%	78.85%
		1	72.80%	70.95%	75.98%	75.41%	78.22%	78.54%
	50	0.25	73.16%	74.43%	76.61%	77.90%	79.32%	80.56%
		0.5	73.08%	74.36%	76.51%	77.78%	79.19%	80.41%
		1	72.93%	74.18%	76.29%	77.57%	78.90%	80.12%